Guidelines for Structural Health Monitoring

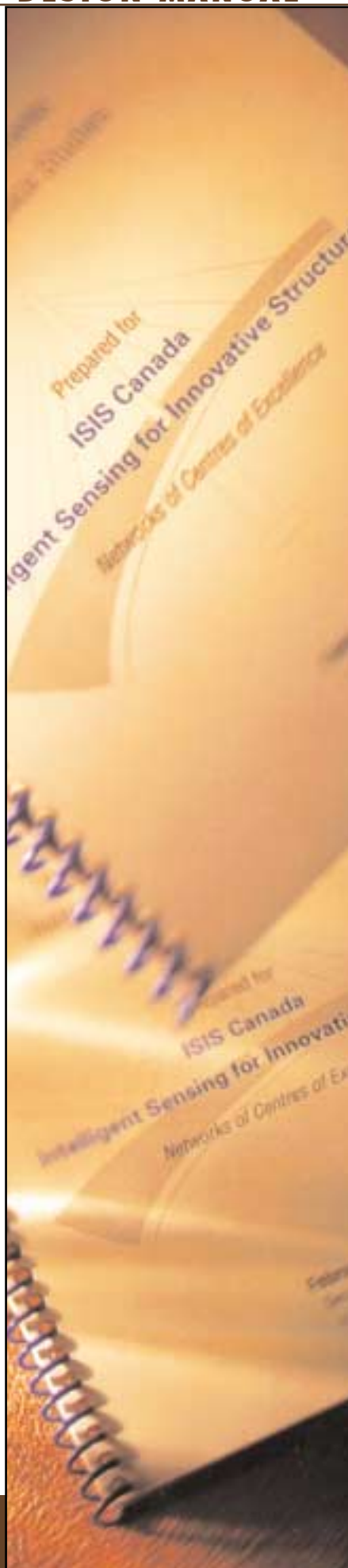

Design Manual No. 2
September 2001

ISIS CANADA
The Canadian Network of Centres of Excellence on Intelligent Sensing for Innovative Structures
Le réseau canadien de Centres d'excellence sur les innovations en structures avec systèmes de détection intégrés

www.isiscanada.com

Guidelines for Structural Health Monitoring

Design Manual No. 2
September 2001

ISIS CANADA
The Canadian Network of Centres of Excellence on Intelligent Sensing for Innovative Structures
Le réseau canadien de Centres d'excellence sur les innovations en structures avec systèmes de détection intégrés

Guidelines for Structural Health Monitoring
Design Manual No. 2
ISBN 0-9689006-0-7

September 2001

ISIS Canada, Intelligent Sensing for Innovative Structures, A Canadian Network of Centres of Excellence,
227 Engineering Building, University of Manitoba, Winnipeg, Manitoba, R3T 5V6, Canada
E-mail: central@isiscanada.com http://www.isiscanada.com

To purchase additional copies, refer to the order form at the back of this document.

Acknowledgements

This document has been prepared by:

Baidar Bakht	JMBT Structures Research Inc.
Jag Humar	Carleton University
Javad Jalali	Dalhousie University
Aftab Mufti	University of Manitoba
John Newhook	University of Calgary
Saidur Rahman	University of Manitoba

Technical Committee:

Emin Aktan	Drexel University
Roger Cheng	University of Alberta
Kenneth Neale	Université de Sherbrooke
Emile Shehata	Wardrop Engineering Inc.
Gamil Tadros	SPECO Engineering Ltd
Roderick Tennyson	University of Toronto Institute for Aerospace Studies
Carlos Ventura	University of British Columbia

Peer Review:

Emile Shehata	Wardrop Engineering Inc.
Wayne Klaiber	Iowa State University
Roger Till	Michigan Department of Transportation

(These individuals reviewed only those sections of the manual consistent with their expertise)

Technical Editor:	Leslie Jaeger	Dalhousie University
Design and Production: J	Charleen Choboter	ISIS Canada
Editor:	Jamie Zukewich	ISIS Canada

Author:	**Aftab Mufti**	**University of Manitoba**

ISIS Canada is a member of the Networks of Centres of Excellence (NCE) program, administered and funded by the Natural Sciences and Engineering Research Council (NSERC), the Canadian Institutes of Health Research (CIHR) and the Social Sciences and Humanities Research Council (SSHRC), in partnership with Industry Canada.

TABLE OF CONTENTS

Figures

Tables

PREFACE

In Canada, more than 40% of the bridges currently in use were built over 30 years ago. A significant number of these structures are in urgent need of strengthening, rehabilitation or replacement. Many bridges, as well as other types of structures, are deficient due to the corrosion of steel reinforcement and consequent break down of the concrete - a result of Canada's adverse climate and extensive use of de-icing salts. In addition, many structures are functionally obsolete because they no longer meet current standards. The expensive cycle of maintaining, repairing and rebuilding infrastructure has led owners to seek more efficient and affordable solutions in the use of fibre reinforced polymers (FRPs). These lightweight, high-strength composite materials are resistant to corrosion, durable and easy to install. Glass and carbon FRPs are already increasing infrastructure service life and reducing maintenance costs.

The evolution of FRPs in civil engineering is accompanied by the evolution of fibre optic sensors (FOS) for structural health monitoring (SHM). The recent emergence of structural health monitoring is primarily due to the fact that innovative designs using new materials necessitate a requirement for long-term monitoring. Accurate monitoring is key to securing the confidence of infrastructure owners in the use of FRPs in civil engineering structures. The ability to assess the behaviour of concrete structures reinforced, strengthened or repaired with carbon and/or glass FRPs will accelerate the material's widespread use.

In the past, structures were monitored by transporting measuring devices to the site each time a set of readings was required. By using FOSs for structural health monitoring, an extensive amount of data can be collected and processed without ever visiting the site. In situations of rehabilitation and repair, fibre optic sensors can be attached to or mounted on existing concrete structures where composite materials are used as reinforcing wraps. They can be used to measure and monitor a variety of components, conditions, and environments.

Within the *ISIS Canada Network of Centres of Excellence*, much research has been conducted to develop advanced technologies to facilitate remote monitoring. A wireless transmission system has been developed as well as an economical, portable microchip data acquisition system that accommodates transmission via radio fequency, Internet or via satellite. Wireless, remote monitoring is emerging as the preferred method of SHM.

The durability and reliability of SHM systems have been demonstrated for five years in ISIS demonstration projects located across Canada. The data collected so far have been used to develop an archive and retrieval system for use by Network researchers. In one ISIS demonstration projet, a camera has been installed and synchronized with a computer that records strain measurements, permanently stores photos, and records trucks that exceed weight limits. In addition, a web page facilitates interactive access to data and downloading of information from a database. A software program is also available for intelligent processing of data. Several years worth of data are now available on the durability and performance of SHM systems.

The content of this manual focuses on Structural Health Monitoring as a diagnostic tool and the various components that comprise a SHM system. This manual is one in a series of manuals that cover the use fibre optic sensors for monitoring structures, reinforcing concrete structures with fibre reinforced polymers, and strengthening concrete structures with externally-bonded fibre reinforced polymers. This design manual will be expanded and updated periodically as other technologies are developed and validated.

1 INTRODUCTION

1.1 Scope of the Manual

The basic purpose of this Manual is to expose the benefits of Structural Health Monitoring (SHM) to structural engineers who are not fully cognizant of this field of engineering. This manual will also be useful to engineers who are already involved in some aspect of SHM, and would like to expand their knowledge about other aspects.

In order to keep the Manual readable and user friendly, the main body is kept free of daunting details. For example, details pertaining to sensors and data acquisition systems are provided in Appendices A and B. Similarly, details of algorithm for vibration-based damage detection, involving many equations, are in Appendix C.

A special feature of this Manual is that the authors, all directly involved with ISIS Canada, have hands-on knowledge of the subject. Other areas for consideration, such as continuous monitoring and remote acquisition of data, will be dealt with in future editions of the manual, as experience with this new technology unfolds.

1.2 Basic Concepts

Structural Health Monitoring (SHM) is a relatively new term for civil engineering applications, and a single definition has yet to be standardized. For the purpose of this guideline, SHM will be defined both by its objectives, and by the physical system and sensors required to achieve these objectives. The guideline will focus mainly on SHM as applied to bridges, but the concepts are applicable to civil engineering structures generally.

The objective of SHM is to monitor the in-situ behaviour of a structure accurately and efficiently, to assess its performance under various service loads, to detect damage or deterioration, and to determine the health or condition of the structure. The SHM system should be able to provide, on demand, reliable information pertaining to the safety and integrity of a structure. The information can then be incorporated into bridge maintenance and management strategies, and improved design guidelines. The immediacy and sensitivity of SHM can allow for short-term verification of innovative designs, early detection of problems, avoidance of catastrophic failures, effective allocation of resources, and reduced service disruptions and maintenance costs. The physical diagnostic tool of SHM is the comprehensive integration of various sensing devices and ancillary systems, including:

- a sensory system
- a data acquisition system
- a data processing system
- a communication system
- a damage detection and modelling system

Although SHM is a relatively new term in civil engineering, the use of instruments to assess the health (i.e. integrity of structures) is not new. Bridge field testing using various measuring instruments is a very old activity, as shown in Figure 1.1.

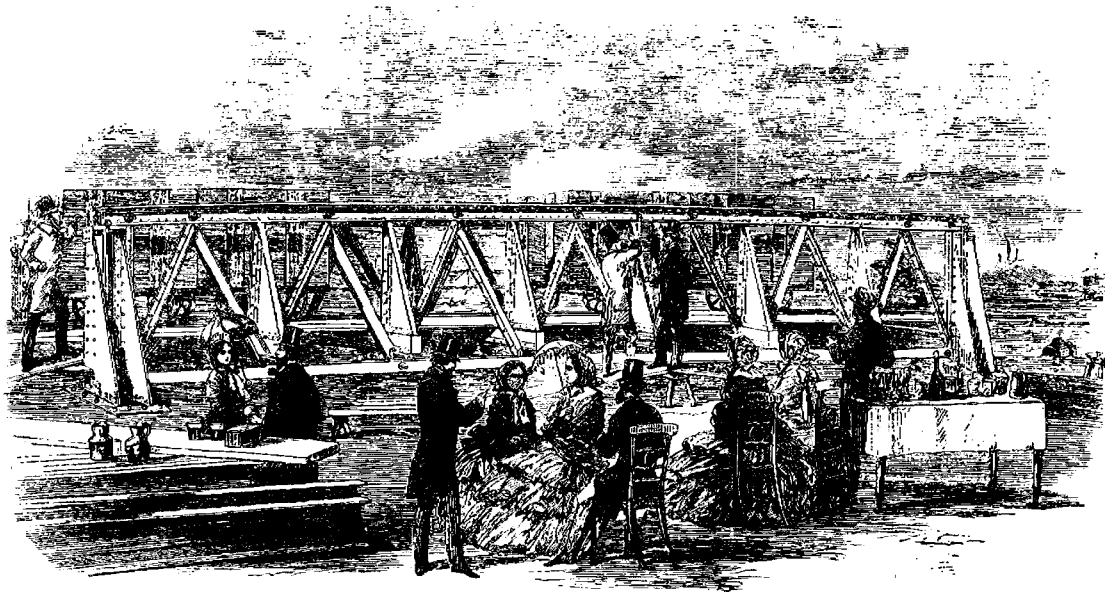

Figure 1.1 Testing of a steel truss in England for a railway bridge in India in the 19th century
(print courtesy of R.A. Dorton)

Similarly, the basic instruments that comprise a SHM system have been in use for a long time in structural engineering laboratories around the world. Further, bridge codes and bridge owners have established evaluation and inspection guidelines that have been in practice for many years. Indeed, the objectives of SHM are consistent with the objectives of many of these long-standing practices. Structural health monitoring is, in fact, an augmentation of current practice, not only through the use of leading-edge technology in sensing, instrumentation, communications and modeling, but also through effective integration of these technologies into an intelligent system.

The driving force behind implementing SHM comes from recognizing the limitations of conventional visual inspections and evaluations using conservative codes of practice. Conventional means are not sufficient to determine the structural adequacy of many older bridges and buildings, for example those constructed in earthquake prone areas (Chase 1999). The development of an integrated SHM system is also justified by the fact that North American infrastructure currently includes a very large number of aged bridges whose capacity to sustain modern traffic loads is questionable.

Just as consumers demand state-of-the-art technology in products and services, bridge owners and users will demand advanced technology, such as SHM, in civil engineering infrastructure management. The intention of this manual, therefore, is to provide a framework for consolidating various basic instruments and technologies into an integrated system that can be utilized to advantage for maintenance of bridges, buildings, power plants, offshore platforms, and other significant structures.

1.3 Analogy

One way of gaining an appreciation of Structural Health Monitoring (SHM) is to draw an analogy with the human body. Just as a doctor checks the health of his patients, today's engineers need to be able to check on the prevailing condition of bridges and structures.

The doctor uses specialized equipment to check a patient's blood pressure, and thereby monitor that patient's health. The engineer utilizes specialized sensors imbedded in a structure to take a reading on the structural health of that facility. If a patient's blood pressure is too high, the doctor prescribes corrective medicine. Similarly, in SHM, if the data flowing form the sensors indicates excessive stress on the structure, the engineer can take appropriate measures to correct the situation. In both cases immediate action prevents catastrophic consequences.

Annual check-ups by your doctor are now a routine form of preventative maintenance. Similarly, SHM of infrastructure will be commonplace in the not too distant future to provide check-ups as preventative maintenance. It is an emerging technology that is destined to be of great value to those responsible for the safety and well being of civil engineering structures.

1.4 Subsystems and Classification of Structural Health Monitoring

For ease of description, the SHM system has been divided into the following four subsystems, which are sub-divided further in Figure 1.2.

- static field testing
- dynamic field testing
- periodic monitoring
- continuous monitoring

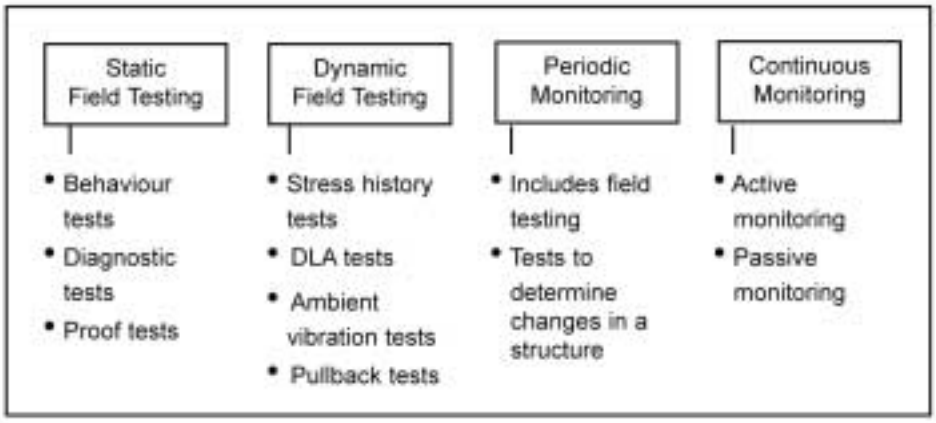

Figure 1.2 Subsystems of a Structural Health Monitoring system

The main difference between the SHM under consideration and other kinds of structural monitoring, is that SHM, besides detecting damage in a structure, can also determine the strength of a structure. The damage-detection capabilities of the four subsystems of SHM can be classified as follows, in ascending order of complexity of the system (Sirkorsky 1999). In Level I, a SHM system can detect only the presence of damage. In Level II, the capabilities of the monitoring system are extended to determine the location of damage. In

Level III the severity of damage is also quantified. In Level IV, the most comprehensive SHM system, the evaluation of the safety of the structure is also included.

It is noted that there are several other classification systems for SHM, with no precisely defined demarcation. Indeed, all classifications overlap.

1.5 Advantages of Structural Health Monitoring

In order to remain competitive in the current global economic environment, it is necessary to minimize service disruptions to civil engineering structures because of routine maintenance or repairs following extreme events, such as earthquakes or hurricanes.

By providing instant information about issues such as serviceability, safety and durability, a SHM system can help civil engineers cope with these types of disruptions. Monitoring and evaluating the integrity of large civil structures, while they are in service, optimizes resources for repair, rehabilitation, or replacement of the structures. SHM can also be useful in evaluating the life-cycle costs of structural components.

The potential direct benefits of a SHM system are numerous, including:

- real-time monitoring and reporting
- reducing down time
- improving safety and reliability, while reducing maintenance costs

As noted by Chang (1999) and Aktan (1999), reduction of down time and improvement in reliability enhances the productivity of the structure. Finally, the results provide information about the behaviour of the structure on the inside, thus SHM can be used to improve the design of future structures.

2 COMPOSITION OF STRUCTURAL HEALTH MONITORING

An ideal SHM system should be capable of providing information on demand about any significant damage occurring in the structure. Information about the health of the structure can be obtained directly through a local network, or transmitted automatically to a remote location. Clearly, the development of such a system involves the use of expertise in many disciplines, such as structures, materials, damage detection, sensors, data collection and intelligent processing, computers and communication.

SHM systems are comprised of a number of subsets:

- acquisition of data
- communication of data
- intelligent processing of data
- storage of processed data
- diagnostics
- retrieval of data

These subsets are discussed in the following sections in sequential order. As illustrated in Figure 2.1 and discussed later, the flow of information between some subsets can take more than one path.

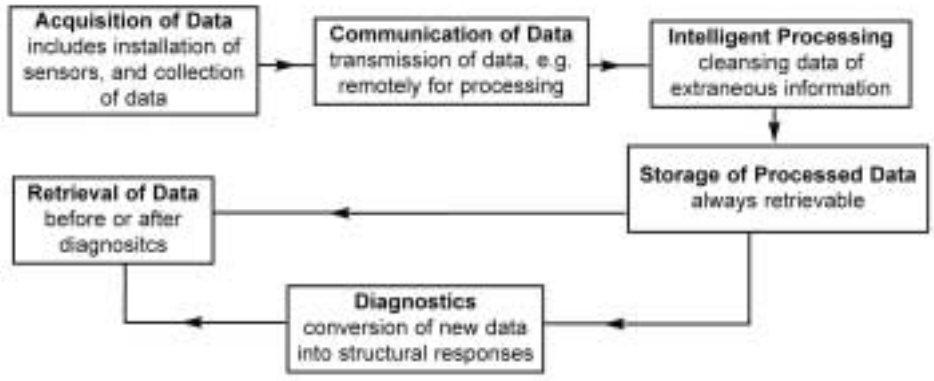

Figure 2.1 Subsets of a Structural Health Monitoring system

2.1 Acquisition of Data

The first subset in a SHM system involves the acquisition of data. The first task in this subset is the preparation of a plan for the installation of various sensing devices that can measure absolute values of, or changes in, one or more of the following:

- strains
- deformations
- accelerations
- temperatures
- moisture
- acoustic emissions
- time
- electric potential
- load
- other attributes of a structure

The sensors should be clearly selected for their ability to provide required information about the health of the structure. A list and description of various sensors is given in Appendix A. A number of types of sensing devices are commercially available; these include electrical resistance strain gauges, vibrating wire strain gauges, deflection transducers, accelerometers, anemometers, fibre optic gauges, etc. Many of these sensors, however, are not always suitable for all subsystems of SHM. For example, some of the commercially available strain gauges are unsuitable for long-term monitoring, because they are not free from drifting. An electrical resistance strain gauge that has a shifting glue interface with the structure may be suitable for obtaining a response under loads applied for only a short duration, but highly unsuitable for long-term monitoring. There is a research need, therefore, to develop an inventory of reliable and economic sensors for tracking the response of a structure on a continuing basis.

In addition to sensors that have been available commercially for a long time, there are many new sensor technologies that are in different stages of development, including more advanced fibre optics sensors, di-electric measurement sensors, and piezo-electric sensors. Many of these newer sensors are meant for application in the aerospace and automotive industries (Chang 1999). However, efforts are currently underway, through the auspices of ISIS Canada, to extend the application of these sensors to civil engineering applications. For example, fibre optic sensors (FOSs) with gauge lengths of 1 to 20 m have recently been developed (Tennyson and Mufti 2000) and used to monitor the performance of fibre reinforced polymer (FRP) repairs on deteriorated columns (Lee 1998). The Long Gauge FOSs, ideally suited to detect the fracture of long steel members in tension and to monitor crack growth in bridge decks, are now economical for a wide variety of civil engineering applications. Similarly, distributed sensors comprising a large number of different sensors in one measuring unit are being used to monitor important large civil engineering structures, such as the Confederation Bridge in Canada (Tadros 1997 and Mufti et al. 1997).

The collection of data from various sensors installed on a structure, a very important component of a SHM system, is becoming increasingly complex. Fortunately, specialised expertise is now available to deal with this task. A general rule-of-thumb regarding the volume of data is that the amount of data should not be so scanty as to jeopardize its usefulness, nor should it be so voluminous as to overwhelm interpretation. A low sampling rate leads to the former, and an unnecessarily high rate to the latter.

Much of the data collected during continuous monitoring activities may be substantially compressed by recording only changes in readings. For example, the strain readings from a bridge component may remain essentially the same when no traffic is on the structure or even when only light vehicles are crossing the structure. To avoid excessive data files, it may not be necessary to store this information in its entire form. A simple algorithm which reviews the data and writes to a file that the reading was "value A" between "time 1" and "time 2" can replace megabytes of redundant data. Furthermore, the SHM activity may require that only data exceeding a specified threshold value needs to be recorded; all other data can be discarded. Another option is to only keep peak values of readings for each event, such as a heavy truck passing over a bridge. This technique may be suitable for fatigue assessments that are based on overloads, but is not suitable for frequency analysis. It is possible that a combination of data acquisition algorithms may be required so that only peak values are recorded as a general operating mode, and continuous data is recorded for discrete periods of time, if a threshold value is exceeded. Selection of the most appropriate data acquisition algorithm is an important component of SHM and will affect both the volume of stored data and the type of diagnostic information that can be obtained.

The usual conduit for transferring data from a sensor to the data acquisition system is the lead wire, the length of which may have an adverse influence on the level of noise collected with the actual data. Care should be exercised to ensure that the length of the lead wires is within the limits that are compatible with the data acquisition system. Proximity of transmission devices, such as those found in a radio station, have been known to corrupt the recorded data. Sources of extraneous information should be detected during the early stages of monitoring, and avoided wherever possible. Further advice about the acquisition of data is in Appendix B.

In the case of a large number of sensors, the handling of the lead wires is not only difficult but also prone to errors in the correlation between individual sensors and the collected data. These difficulties can be overcome, to a certain extent, by wireless communication between the sensors and the data acquisition system.

2.2 Communication of Data

Here, the term 'communication of data' refers to the conveyance of data from the data acquisition system to the location where the data is processed. During static field testing, this communication is often seen in its most basic form, when the collected data is printed and the hard copy is physically handed over to the test engineer. At the most sophisticated end of the communication continuum, the collected data is transmitted remotely, either through telephone lines or by a wireless mode. The selection of a suitable communication system is an essential component of a SHM subsystem.

2.3 Intelligent Processing of Data

The data retrieved directly from sensors is likely to contain extraneous information that is not only useless, but also uneconomical to store. The source of the extraneous information can be a transmitting device, high-tension electric wires, or telephone lines among others. It is important for interpretation that the collected data be cleansed or intelligently processed. Efficient and good processing techniques make interpretation easier, faster and more accurate.

Processing of data is also important when multiple sensory systems are used in the same SHM project. For example, a bridge may be monitored using a combination of FOSs, potentiometers, electronic gauges, accelerometers and video input. Many of these sensors may have quite separate signal conditioning and demodulation systems for acquiring the raw data from the respective sensors. The only common link between the systems is a central computer which processes and stores data. It is important that this computer be able to process the data from all inputs and relate it to a common reference such as a time stamp. In this manner, the readings from one sensor can be related to those of the other sensors. Ideally, this processing should be performed prior to the storage of data.

A further consideration for processing of data is correction for thermal effects. Some sensors can be thermally compensated while other sensors rely on reference gauges in order to isolate changes in readings due to thermal changes from those induced by other types of loads. Data should be consistently processed so that all readings either include thermal effects or are free from thermal effects. The latter is more common.

2.4 Storage of Processed Data

The term 'storage of data' is being used here for the storage of data that has been cleansed by intelligent processing and is available for diagnostics. The medium used for this storage should be such that the data remains retrievable even after many years. In addition, the data files should contain enough information about the details of format to understand the meaning of the myriad of numbers.

In certain cases, it may be appropriate to discard raw data after it has been converted into quantities that relate directly to a bridge response. For example, files containing plots of spectral densities versus frequencies of vibration might be preferred over the volumes of data gathered from a dynamic test. Discarding the large amount of raw data in favour of the processed information has both positive and negative aspects. In today's rapidly changing world, it is virtually impossible to predict the makeup of the administrative system used by the owners of significant structures. It is quite likely that the lack of commitment for continuation might render the raw data useless for future generations. On the other hand, the loss of the data might lose future opportunities for re-interpretation.

2.5 Diagnostics

The most important subset of a SHM system deals with diagnostics, or the interpretation of the collected and cleansed data. In this subset of SHM, the abstract data numbers are converted into quantities that relate directly to the responses of a structure. For example, the deflection measurements might be converted into quantities of flexural stiffness, strains into stresses, or accelerations into plots of spectral densities against frequencies. The conversion of raw data into response indicators always depends upon basic assumptions, which are rarely perfect. Unfortunately, no comprehensive procedure is currently available for overcoming difficulties in the interpretation of observed data. However, in order to provide an appreciation of the problem, details of some case histories and difficulties in the interpretation of observed data are discussed in Section 3.

2.6 Retrieval of Data

As noted earlier, the raw data collected from sensors must be intelligently processed, including conversion to quantities that relate directly to structural responses. A decision has to be made about the kind of data that is deemed fit for retrieval. In the case of static field-testing, the observed data is not too voluminous and can be stored along with the interpreted responses. There is usually too much data from dynamic field tests to be stored in its entirety; quite often it is considered sufficient to record only the interpreted data. A decision about the storage of data suitable for retrieval depends not only on the significance of the data, but also on the confidence of its interpretation.

3 STATIC FIELD TESTING

Since the history of field-testing bridges is far more extensive than field-testing of other structures, it was decided to devote this section to bridge field-testing. It is emphasised that many of the principles inherent in bridge testing are common to all structures; therefore, this section will also be useful in the testing of structures other than bridges. The static field tests provide information about the capacity of bridges to sustain live vehicle loads.

3.1 Introduction

Static field-testing of bridges is not a new activity and has been in practice for centuries. Early in the 20th century, a bridge would be tested under uniformly distributed loads simulating actual traffic. If it did not collapse or show excessive deflections under the test loads, the bridge was considered to be sound. It was customary in some European countries to demonstrate the load-worthiness of important bridges by testing them before opening them to traffic. For these tests, the bridge was loaded by the equivalent of service loads, and its response was monitored mainly through manual deflection measurements. Effectively, these early tests related the health of a bridge only to its stiffness in flexure.

Some of the equipment and technology required for modern static field-testing of bridges has been available for some time. Until recently, however, use was limited to laboratory testing and occasional field tests that were usually undertaken by university scholars as special research projects. In the early 1970s, in Ontario, the Structures Research Office of the Ministry of Transportation (MTO) introduced routine testing of highway bridges, with a prime objective to assess load carrying capacities of bridges. Since the inception of this program, more than 250 bridges have been tested in Ontario. Most of these tests show that the actual load-carrying capacity of bridges is much higher than can be rationalized analytically. A comprehensive bridge-testing program was also established in the United States by the Florida Department of Transportation. In addition to a limited number of governmental bridge testing facilities, several commercial specialist teams in North America can now assess the health of bridges through testing.

The purpose of this section is to introduce static field-testing as an effective means of assessing the absolute health of a structurally suspect bridge. Technical literature contains details of many case histories, some of which are referenced in this Section. It is noted that the references are generally limited to case histories that the authors of the section have been involved with directly.

3.2 Types of Static Tests

In a broad sense, bridge tests are either static or dynamic. For the purpose of bridge testing, static loads are considered to be those loads that are brought onto or placed on the bridge very slowly, so as not to induce dynamic effects in the bridge. In the case of testing with vehicles, vehicle loads are considered to be static when vehicles are brought onto the bridge at a crawling speed. Static field tests can be subdivided into behaviour tests, diagnostic tests and proof tests. Dynamic load tests, as the term implies, are carried out with moving loads that excite the dynamic response of the bridge.

3.2.1 Behaviour Tests

Behaviour tests are carried out either to study the mechanics of bridge behaviour or to verify certain methods of analysis. The objective in the latter case is to verify that analytical methods can be used with confidence for the design and evaluation of similar bridges. Applied loading during such tests is usually kept at, or below, the level of maximum service loads, i.e. legally permitted maximum loads. A behaviour test provides information regarding how the load is distributed among various components of a bridge. The test does not furnish direct information about the capacity of various components to sustain loads.

Recent examples of behaviour tests are those conducted by Bakht et al. (1999) and Bakht and Mufti (1999). One of these sets of tests was conducted on six sawn timber stringer bridges in Nova Scotia. The principle objective was to determine load distribution characteristics of the bridges. The second set of behaviour tests was conducted in British Columbia on two concrete plank bridges with shear keys. The purpose of these tests was to calibrate an analytical method, and then assess the magnitude of shear stresses in shear keys for all concrete plank bridges on forestry roads in British Columbia. Contrary to earlier apprehensions, it was found that the stresses in the welds of the shear keys were quite low and, therefore, there is no concern about fatigue resistance.

3.2.2 Diagnostic Tests

It is quite rare for the behaviour of a bridge component to be unaffected by its interaction with other components in the bridge. The presence of such interaction in certain types of bridges can be analysed with confidence. However, there are certain conditions where a realistic assessment of the interaction remains a subject for speculation. The effect of the interaction may be either detrimental or beneficial to the behaviour of the component concerned. In the case of a detriment, the effect might manifest itself in the form of visible distress in the component. In the case of a benefit, the beneficial action may never be utilized. A diagnostic test is the surest way to establish the source of the distress, or enhancement, of the load-carrying capacity of a component.

While there is no clear-cut distinction between behaviour and diagnostic tests, the former term is customarily used for a test that is carried out mainly to verify a certain method of analysis. The latter term denotes a test that is carried out to diagnose the effects of component interaction. For example, the behaviour test may be conducted to verify a certain method of transverse load distribution analysis of slab-on-girder bridges. The diagnostic test may be conducted to establish the rotational restraint conditions at the ends of a bridge column.

Through a large number of tests, it has been confirmed that diagnostic testing can be used with advantage: to locate the sources of distress that might exist in a bridge due to inadvertent component interaction, and to determine the positive effects of interaction. The source of distress in many cases can be eliminated by simple remedial measures. Beneficial interaction, on the other hand, can be used to advantage in establishing the enhanced load-carrying capacity of a bridge.

Examples of diagnostic tests include those reported by Bakht and Csagoly (1979, 1980), Bakht and Jaeger (1987, 1990 a).

3.2.3 Proof Tests

A proof test is carried out to establish the safe load-carrying capacity of a bridge. During this test, the structure is subjected to exceptionally high static loads that cause larger responses in the bridge than the responses that are induced by statically-applied maximum service loads. A definition of the proof load, together with the process of obtaining the operating loads from proof test loads, is given in Section 3.6.

It should be emphasized that subjecting a bridge to a sufficiently high proof load is not always a confirmation of the load carrying capacity of a bridge. Supporting analysis based on sound reasoning is absolutely essential for determining why the bridge carried the loads applied to it, and for establishing whether there is reason to believe that it can be relied upon accordingly for the foreseeable future.

Because of the very high loads applied to the bridge in proof testing, there is always the possibility that the bridge may be permanently damaged by the test. However, it should be pointed out that the possibility of incurring permanent damage with the test is extremely small, providing the test is planned and executed carefully and methodically. Of the more than 250 bridge tests conducted in Ontario, not a single bridge suffered any damage because of testing. Notwithstanding the lengthy accident-free record of bridge testing in Ontario, a bridge test, in particular a proof test, should only be undertaken by qualified professionals and only after the owners of the bridge have confirmed that they are prepared to accept the risk of damage to the structure as a result of the test.

A well-planned proof test is carried out with gradually increasing loads, ensuring that the loads are not allowed to increase beyond the limit of linear elastic behaviour.

There are very few published examples of proof tests conducted outside Ontario; examples of those conducted in Ontario are reported by Bakht (1981, 1988), Bakht and Csagoly (1979), Bakht and Mufti (1992 a and c).

3.3 Equipment for Testing

Static bridge testing, a subsystem of an overall SHM system, generally requires the same equipment as other subsystems. The equipment requirements for SHM are discussed in Section 2 and elsewhere in this manual. Loading for proof testing in particular, however, deserves further explanation, which is provided here and also in Section 3.6.

A good loading system applicable to various types of static field testing should preferably have the following characteristics:

- It should be representative of actual vehicular loads on the bridge.
- It should be easy to manoeuvre so that it can be brought on and off a bridge quickly.
- It should be easily transportable.
- Its load should be adjustable so that it can be increased or decreased conveniently.
- After it has been placed on the bridge, its weight distribution should be repeatable and capable of quick stabilization.
- For proof testing, it should be capable of being moved by remote control as well as manually.

The foregoing desirable attributes clearly disqualify ballast loading similar to that used in pile testing. Trucks laden with gravel and water tanks are also unsuitable for proof testing. In order to apply concentrated loads at the top surface of a bridge deck, a portable hydraulic jack system that will react against the frame of a heavily loaded truck should be utilized. The MTO has two heavy-duty test vehicles, one with a hydraulic jack attached to its underside.

3.4 Case Histories

In a general way, an actual bridge behaves like the typical conceptual bridge used in design or analysis. However, there are some aspects of bridge behaviour that do not enter into design considerations. Even an experienced bridge designer may remain unaware of certain aspects of bridge behaviour. Similarly, even an expert analyst may not be able to replicate actual bridge behaviour through mathematical models. There is no better way to understand the shortcomings of the mathematical models used for the design or evaluation of bridges than to compare the analytical predictions with the observed behaviour of structures.

As noted earlier, the Structures Research Office of the MTO has, for many years, conducted a program of bridge field testing that includes both static and dynamic tests. Many lessons have been learned from the results of this testing program. It has become obvious that design analysis, as customarily practised, can be in error in a number of different ways. Indeed, it is fair to say that virtually every bridge test had a surprise in store, revealing a significant aspect of bridge behaviour that had been previously ignored in the evaluation analysis of the bridge (Bakht and Jaeger, 1990b).

The discrepancies between analytical and measured responses are discussed in this Section, with the help of specific examples. As could be foreseen, these discrepancies were not due to inadequacies of the methods of analysis, but rather to the presence of behavioural factors that could not be included in the mathematical modelling because of difficulties in idealization. Various case histories presented below confirm this contention.

3.4.1 Girder Bridges

Tests on girder bridges show consistently that the girders are usually much stiffer in flexure than is predicted by calculations. In dynamic tests, this unaccounted-for flexural stiffness manifests itself in the form of measured frequencies that are greater than the calculated ones. In most static tests, the measured deflections and longitudinal strains in the bridge girders were much smaller than the calculated ones, again indicating that the bridge is stiffer in flexure than assumed.

Results from tests on three bridges with steel girders are presented in the following section demonstrating that even highly rigorous methods of analysis cannot be relied upon, unquestioningly, to predict the actual response of a bridge.

3.4.1.1 Bridge with Timber Decking

The Lord's Bridge is the first example presented. It is outfitted with rolled steel girders and a nail-laminated timber decking with the wood laminates laid transversely. As described by Bakht and Mufti (1992a), the bridge is 6.25 m wide and has a single span that is apparently simply-supported. The girders are 10.2 m long with a bearing length of 0.53 m at each end, resting directly on timber crib abutments. There are no mechanical devices to transfer interface shear between the girders and the timber decking, although there are 100 x 200 mm nailing strips bolted to the top flanges of the girders where the decking is nailed. Details of this bridge are shown in Figure 3.1.

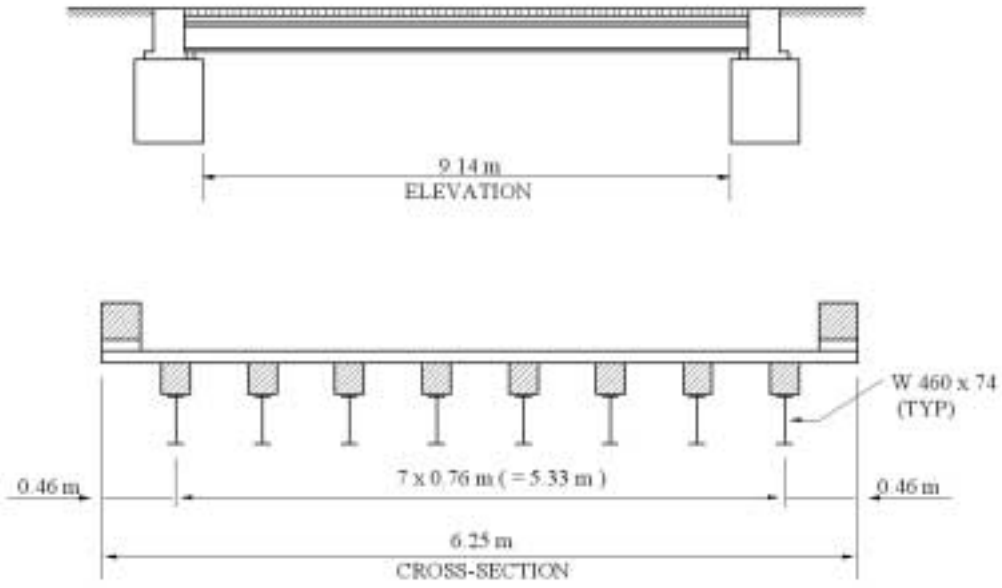

Figure 3.1 Details of the Lord's Bridge

The bridge was tested with a test vehicle under several load levels and different longitudinal and transverse positions. The girders responded in a linear elastic manner, even up to the highest load level. For two of the load cases, the longitudinal position of the vehicle was the same, but the eccentric transverse positions were the mirror images of each other. For these two load cases at the highest test load level, the distribution factors for mid-span deflections are plotted in one of the sketches of Figure 3.2. Viewing the cross-section of the bridge from two different ends so that the two transverse distribution profiles overlap each other offers an easy comparison. It is noted that the distribution factor for deflection is the ratio of the actual and average girder deflections at the transverse section under consideration.

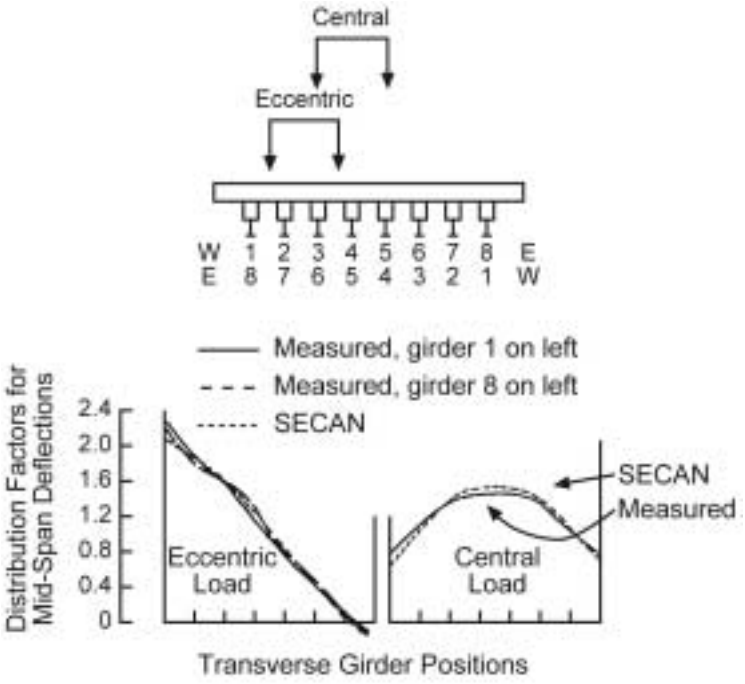

Figure 3.2 Distribution coefficients for mid-span deflections

If the geometrically symmetrical bridge was also symmetrical with respect to its structural response, the distribution factors of the two mirror-image load cases noted above would have led to transverse distribution profiles that lie exactly on top of each other. As can be seen in Figure 3.2, the two profiles were fairly close to each other but were not exactly the same, indicating that the two transverse halves of the bridge did not respond in the same way to corresponding loads. The two sets of distribution factors obtained from measured deflections in Figure 3.2 were also compared with those obtained from deflections given by SECAN, a computer program based on semi-continuum analysis of girder bridges (Jaeger and Bakht, 1989). It can be seen that the analytical values of the non-dimensionalized deflections were not any more different from the two sets of observed values than the latter were from each other. This confirms that, for the bridge under consideration, the semi-continuum method used for analysis was able to predict the pattern of transverse distribution of load fairly accurately.

The same accuracy of prediction, however, cannot be claimed in the case of absolute values of girder deflections. This is because of uncertainty in quantifying the following parameters. As noted earlier, the girders for the Lord's Bridge are 10.2 m long with an unusually long bearing length of 0.53 m at each end. It is customary to assume that the nominal point-support for a girder lies midway along the bearing length, in which case the nominal span of each girder would be 9.67 m. It can be demonstrated, for the case under consideration, that the vertical pressure under the supported length of a girder should have its peak away from the midway point of the bearing length and toward the free edge of the abutment. Determination of the exact location of this peak requires detailed knowledge of the modulus of subgrade reaction of the timber crib abutment. Clearly, this factor is not easily quantifiable, making the task of determining the effective span very difficult. The clear span of the girder, being 9.14 m, is clearly the lower bound of the effective span of the girder.

The transverse modulus of elasticity of the wood deck, which is operative in the longitudinal direction of the bridge, is extremely small compared to the longitudinal modulus. Even if the transverse laminated deck were made composite with the girders, the contribution of the deck to the longitudinal strength and stiffness of the composite section would normally be negligible. Consequently, no attempt is usually made to provide shear connectors in such bridges. There are some holding down devices to connect the deck to the girders through the nailing strips; these devices, by transferring some interface shear, make the girders partially composite with the nailing strips and the decking. From measured girder strains, it was discovered that despite the absence of shear connectors, the decking and the nailing strips of the Lord's Bridge were partially composite with the girders. The degree of composite action was found to vary from girder to girder and was clearly not quantifiable.

The Lord's Bridge was analysed using two different sets of idealizations. In one idealization, the girders were assumed to be non-composite with a simply-supported span of 9.67 m. In the other idealization, full composite action was assumed between the girders and the timber components, comprising the nailing strips and the decking. The girders were assumed to have the lower bound span of 9.14 m. In Figure 3.3 the measured deflections, for the same load case for which the distribution factors are plotted in Figure 3.2, are bracketed entirely with very large margins by the analytical results corresponding to the two idealizations.

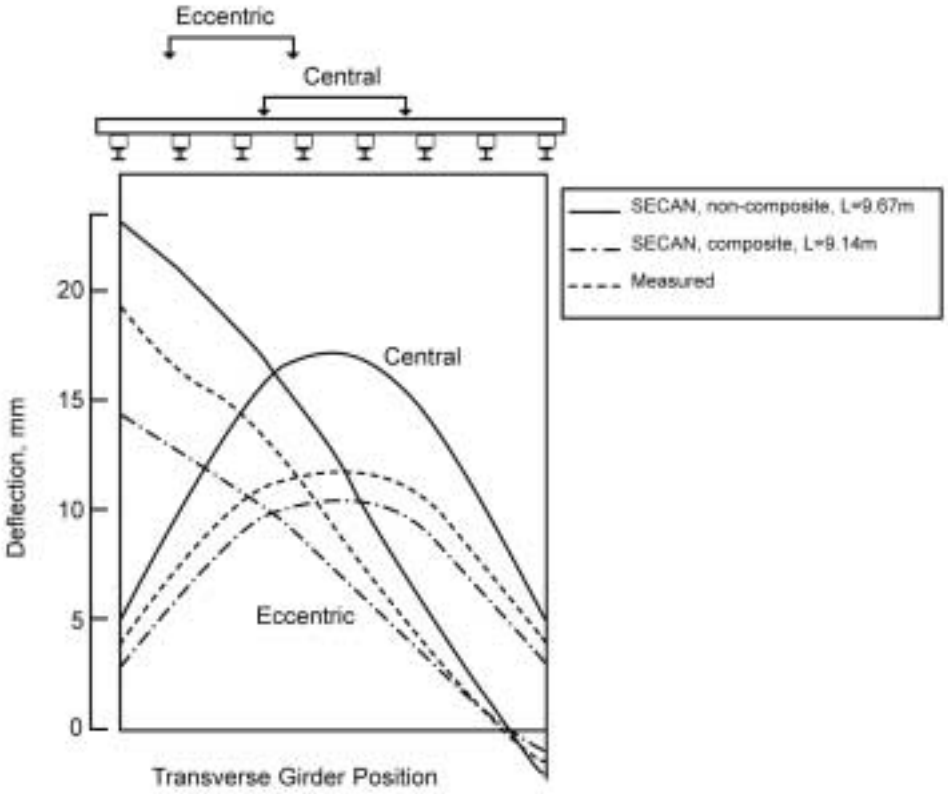

Figure 3.3 Mid-span deflections

3.4.1.2 A Non-Composite Slab-On-Girder Bridge

The unquantifiable and random nature of the bearing restraint forces, and of the degree of composite action in the absence of mechanical shear connection, is illustrated by the results obtained from a test on the Belle River Bridge. This bridge is a slab-on-girder bridge with steel girders and an apparently non-composite concrete deck slab (Bakht, 1988). The nominal span of the bridge is 16.3 m and the width is 9.1 m.

The transverse load distribution analysis of slab-on-girder bridges without mechanical shear connectors is made difficult, to the point of becoming initially impossible, by the uncertain degree of the composite action. It is tempting to believe that the actual load distribution pattern of such bridges can be bracketed by two sets of analyses, one corresponding to full composite action and the other to no composite action at all, with the former analysis always leading to safe-side estimates of the maximum load effects in the girders. In reality, a deterministic analysis, no matter how advanced, might fail completely to safely predict such maximum load effects. The assertion is illustrated in Figure 3.4 with the help of the results from tests on the Belle River Bridge.

Transverse profiles of the distribution factors for mid-span girder moments in the bridge are plotted in Figure 3.4, for a transversely symmetrical load case. One of these profiles corresponds to moments computed from observed girder strains, both at the mid-span and near the abutments, with the latter providing information regarding the bearing restraint forces. The other two transverse profiles were obtained from the results of the semi-continuum method of analysis for the two bounds of the composite action. It is noted that no attempt was made to model the bearing restraint in these analyses.

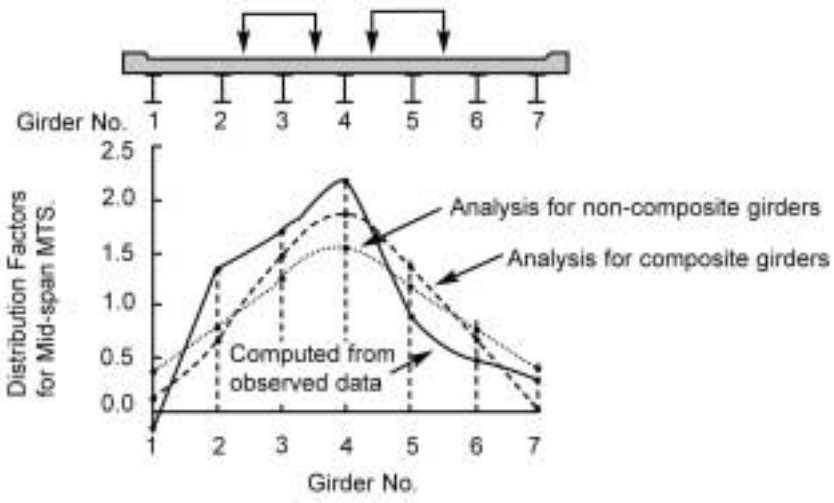

Figure 3.4 Distribution factors for mid-span moments

In Figure 3.4, the pattern of transverse distribution of actual moments was similar, but only in a general way, to the two analytical patterns. It was also quite irregular. Unlike the analytical patterns, the actual pattern was far from being symmetrical. In fact, the actual distribution factor for maximum girder moments was about 10 percent larger than the corresponding analytical factor for the fully non-composite bridge. The very high distribution factor and significant departure from symmetry was probably caused by the middle girder accidentally becoming much stiffer than the adjoining girders, through

composite action by bond. From the results plotted in Figure 3.4, there can be little doubt that, for the kind of bridge under consideration, even the most rigorous deterministic analysis was, at best, only a fairly close approximation.

Bearing restraint forces in the girders of the Belle River Bridge were computed from observed girder strains near the abutments. From these bearing restraint forces and approximately calculated girder reactions at the supports, it was concluded that the effective coefficient of friction between the girder flange and supports varied between 0.66 and 0.95. The former limit relates to loading by single vehicles and the latter to two side-by-side vehicles. Such effective coefficients of friction may be on the high side, but are not uncommon in bridges in which the girders rest directly on highly rusted steel bearing plates.

Bearing restraint forces computed from measured girder strains are plotted in Figure 3.5 for the same load case that the distribution factors for mid-span girder moments are plotted in Figure 3.4. The bearing restraint forces are shown as positive when they tend to push the abutment away from the girders.

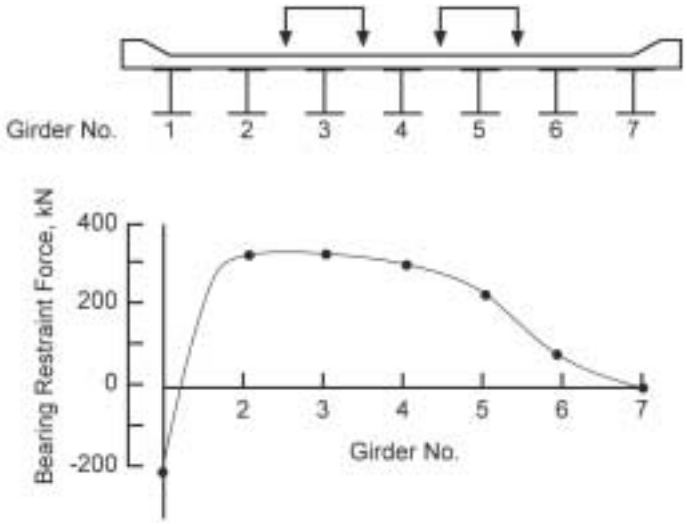

Figure 3.5 Distribution factors for mid-span moments

In Figure 3.5, the bearing restraint forces in all the girders, except one, were positive. At the location of the left-hand outer girder, the bearing restraint force was not only negative, but also fairly large in magnitude. It was postulated that this unusual response was the result of a relatively soft pocket in the backfill behind the abutment, in the vicinity of the left-hand outer girder.

In light of the uncertainties discussed above, it is fair to say that for the kind of bridge under consideration, no deterministic analysis can be expected to predict the actual behaviour of the bridge.

3.4.1.3 A New Medium Span Composite Bridge

The examples presented in 3.4.1.1 and 3.4.1.2 are relatively short span bridges with no mechanical shear connectors where the girders rest either directly on the abutments or on fairly rusty steel bearing plates. In such bridges, there may be difficulties in assessing the degree of composite action and the magnitude of bearing restraint forces. Further, because of the spans themselves being short, even small errors in the estimation of the effective span can have a relatively large influence on the computed responses of the bridge. Consequently, it can be concluded that difficulties in predicting the realistic response of a bridge occur only in the kinds of bridges discussed earlier. It is shown below that errors in predicting bridge behaviour can also extend to medium-span bridges in which mechanical shear connectors ensure virtually full composite action, and in which the girders are supported by elastomeric bearings that apparently permit free longitudinal movement of the girders.

The cross-section of the single-span North Muskoka River Bridge is shown in Figure 3.6. This bridge comprises five steel girders and a composite deck slab; its span and width are 45.7 and 14.6 m, respectively. Both ends of every girder rest on laminated elastomeric bearings, each measuring 560 **x** 335 mm in plan view and 64 mm in thickness. The design shear rate for each bearing is about 30 kN/mm.

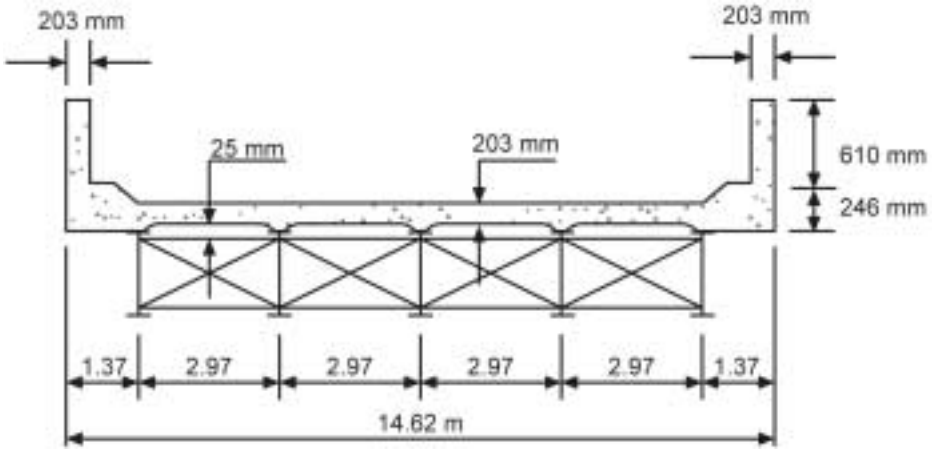

Figure 3.6 Cross-section of the North Muskoka River Bridge

A dynamic test showed the North Muskoka River Bridge to be about 20 percent stiffer in flexure than could be rationalized by even a very detailed analysis in which all those aspects of bridge behaviour that could conceivably enhance flexural rigidity were taken into account. To determine the cause for the apparent discrepancy, a diagnostic static test was subsequently conducted. For this latter test, all the girders were instrumented with strain measuring devices to measure longitudinal strains at three transverse sections of the bridge, with one section near the mid-span and the other two near each abutment (Bakht and Jaeger 1990a).

If the elastomeric bearings had permitted free longitudinal movement of the girders, under live loads, then the strains in the bottom flanges near the bearings would have been tensile and very small. This was not the case. The test loads induced fairly large compressive strains in the bottom flanges near the elastomeric bearings. Bearings restraint forces, which were computed as an approximation from observed strains for different case loads, are plotted in Figure 3.7. It is interesting to note that under transversely-symmetrical loads, the corresponding bearing restraint forces were not exactly the mirror image of each other, as should have been the case for an ideally symmetrical structure. Bearing restraint forces as high as 175 kN, which can be seen in Figure 3.7, are considerably larger than a functioning elastomeric bearing would be expected to develop. Nevertheless, such large forces were actually present, despite the fact that the bearings were apparently in excellent and functioning condition.

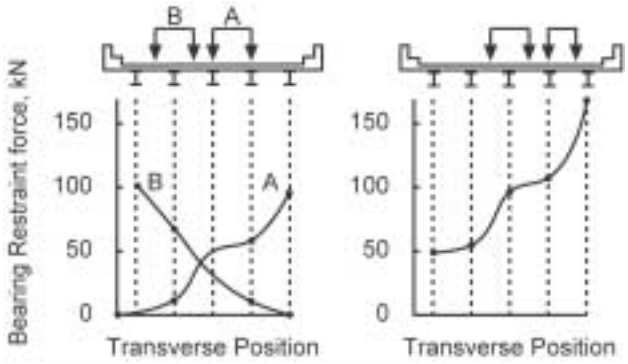

Figure 3.7 Bearing restraint forces in the North Muskoka River Bridge

At the time of the test, it was found that the bearing restraint in the North Muskoka River Bridge reduced the mid-span deflections due to test loads, by about 12 percent. This reduction is considerably smaller than the 20 percent reduction observed in the previous test on the same bridge. The first test was conducted on a relatively cool day in October and the second on a very hot day in June. It was hypothesized that the elastomeric bearings became stiffer in the colder temperature during the first test, thereby generating higher restraint forces that consequently caused the bridge to become effectively stiffer than indicated in the results of the second test.

Test results on the North Muskoka River Bridge demonstrate the significant influence of the restraining effects of elastomeric bearings which may change with load level and temperature. To be able to analyse bridges with these bearings more accurately, it is essential to include their effective shear stiffness in the mechanical model.

3.4.2 Steel Truss Bridges

Simply-supported steel truss bridges are usually simple to analyse because of the limited number of paths that a load can take, i.e. because of their low degree of structural redundancy. Tests show, however, that even these bridges have certain aspects of behaviour that may surprise bridge engineers. The more significant surprises are presented in the following section.

3.4.2.1 Interaction of the Floor System with the Bottom Chord

Bakht and Jaeger (1987) have described tests on two truly pin-connected steel truss bridges that were similar in dimensions. The bottom chord strains of one through-truss bridge plotted in Figure 3.8 (a), were found to be smaller, by a factor of about 15, than the strains that would have occurred if the chord had sustained all of the live load force. The obvious conclusion drawn from this observation is that if the bearings of the truss are functioning, the floor system must be acting with the bottom chord to sustain the tensile forces. The observation has been made so many times that it is almost a cliché to say that, in pony-truss and through-truss bridges, the floor system takes a large portion of the tensile force of the truss bottom chords. Nevertheless, a surprising feature was observed in the test results as shown in Figure 3.8 (b).

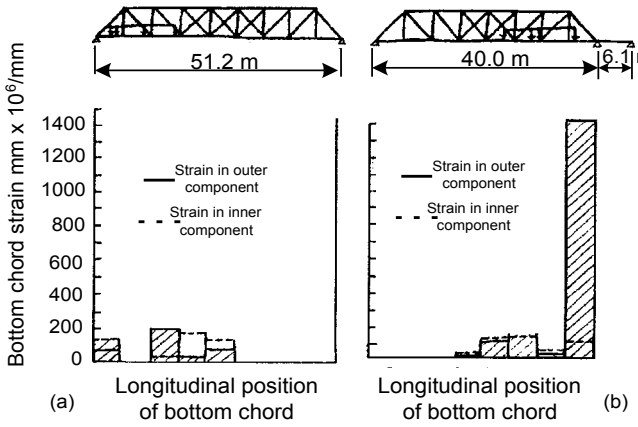

Figure 3.8 Strains along the bottom chords of the trusses of two bridges

The surprising feature relates to the bottom chord strains in the panel closest to the right hand support of the bridge. In Figure 3.8 (b), the strains in this panel are about 15 times larger than the strains in the adjacent panel. Since the two panels have components of the same section, it is obvious from simple statics that the bottom chord force in the two panels should be nearly the same.

The fact that the total strains in the bottom chords of the two panels were significantly different from each other suggests that the floor system did not participate with the bottom chord in the end panel. Bakht and Jaeger (1987) explained this behaviour as follows. All stringers of the floor system of the bridge, shown in Figure 3.8 (b), are connected to the truss nodes in such a way that the bottom chord between adjacent nodes cannot deform without engaging the stringers. As shown in this figure, the bridge had a small approach span that is formed by extending the stringers of the floor system beyond the pier, i.e. the intermediate support. Because of this extension, the floor system did not have a floor beam at the end node, like it does for all other nodes. Accordingly, the bottom chord in the end panel was called upon to sustain all the tensile force of the truss by deforming independently of the stringers. It is obvious that the beneficial interaction between the floor system and the bottom chords of trusses cannot always be taken for granted.

3.4.2.2 Component Interaction

The beneficial effect of component interaction in truss bridges is often disregarded as insignificant. Confirmation that the effect of interaction is not always small was provided by a test on a 100 m span deck-truss type of arch bridge. The bridge had a large number of transverse floor beams of the same cross-section, the strengths of which were investigated by a diagnostic test. The bottom flanges of these beams were instrumented with strain measuring devices attached to their respective mid-spans. As shown in Figure 3.9, it was found that under similar loading, the four beams closest to one of the truss supports showed considerably higher strains than the other two instrumented floor beams. The reason for this unexpected behaviour became obvious after an inspection of the cross-frames under the various floor beams. The configurations of the various cross-frames are shown in Figure 3.10. It can be seen in this figure that the cross-frames under the four floor beams closest to the truss support had an X-type of bracing which permitted these floor beams to span between the trusses, as was assumed in the pre-test analysis, and as was probably assumed in the design calculations. The measured strains were considerably smaller than they would have been otherwise because of the integral nature of these latter floor beams with the cross-frames. This could be an advantage in the rehabilitation of the bridge.

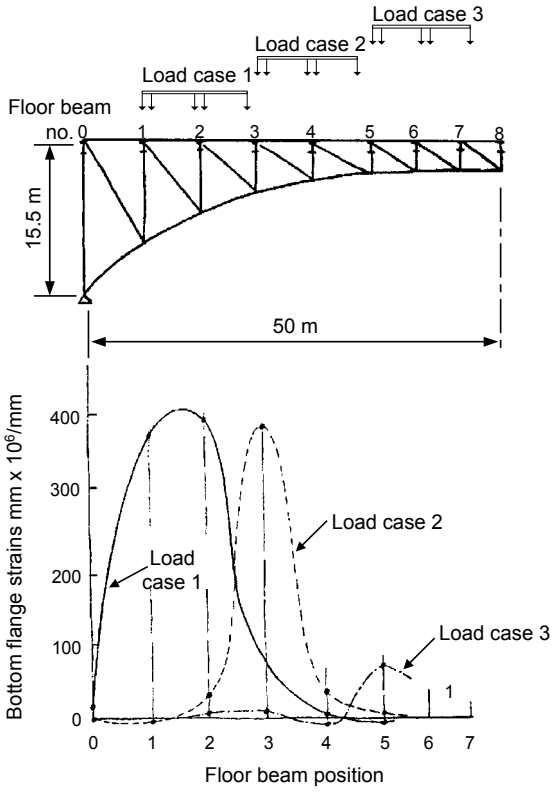

Figure 3.9 Strains in the bottom flanges of floor beams at mid-span

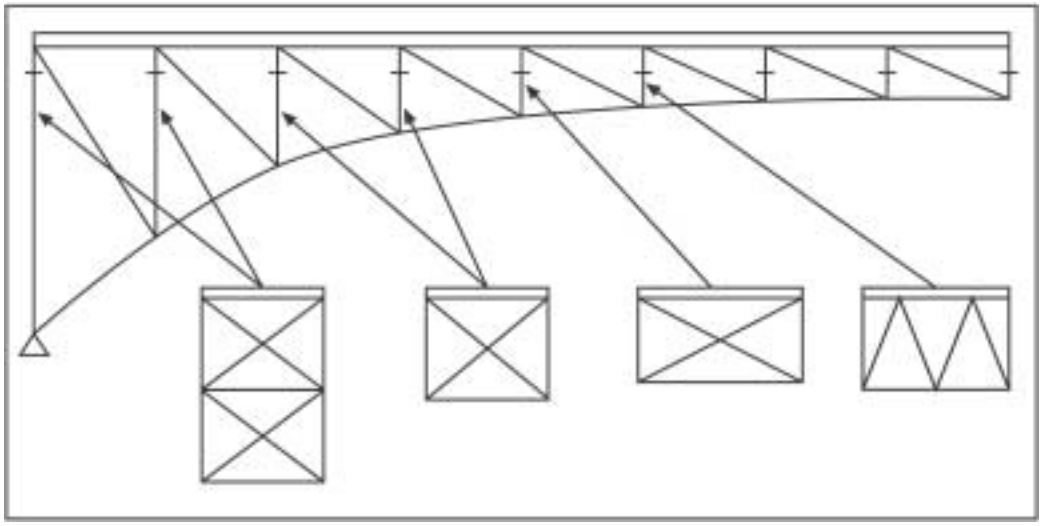

Figure 3.10 Details of cross-frames

3.4.3 Misleading Appearance

Evidence of deterioration can sometimes be misleading. Many apparently severely-deteriorated concrete bridges have been found capable of carrying normal loads, although their load-carrying capacities cannot, as yet, be explained analytically. One example is a highly deteriorated, reinforced concrete T-beam bridge, which was tested by Bakht and Mufti (1992c). From load testing, it was found, for reasons that could not be fully quantified analytically, that the bridge could be kept open to traffic with a posting limit of 19 tonnes. Notwithstanding such cases, two examples are presented below where behaviour can be readily explained.

3.4.3.1 Cantilever Sidewalk

It looked like cast iron brackets supported the sidewalk of an old arch bridge. Many of these brackets were so cracked that their capacity to sustain the sidewalk loading was suspect. A load test on the bridge, with loads about five times the design load for the sidewalk, showed that the applied loading did not induce any strain, even in the brackets that were sound (Bakht, 1981). It was subsequently found that the brackets were only ornamental, and that the cantilevered deck slab, itself, was more than capable of sustaining the sidewalk loading.

3.4.3.2 A Bridge Without Construction Drawings

The next example is an old 5.5 m span slab-on-girder bridge with steel girders and a concrete deck slab with monolithic parapet walls. Construction drawings of the bridge were not available. The bridge cross-section is shown in Figure 3.11, together with the relevant outer dimensions.

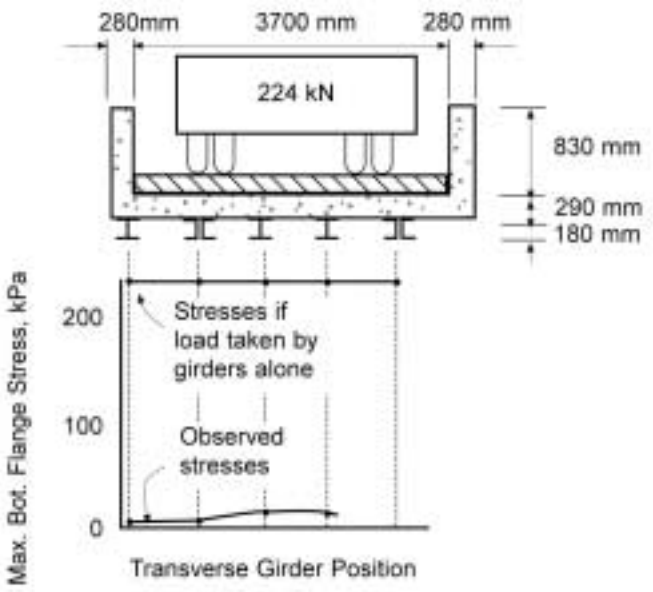

Figure 3.11 Bottom flange strains in girders

Recently, it was found that an outer girder had somehow moved away from under the bridge. An analytical evaluation of the load-carrying capacity of the bridge, concluded that the girders were not capable of carrying even their own dead load. Since the bridge was known to have carried normal traffic for a number of years, it was not closed but was reluctantly restricted to vehicles having gross weights of less than two tonnes.

A very brief test with a 22 t vehicle showed that the girders only took a very small portion of the applied loading. As shown in Figure 3.11, the stresses in the bottom flanges of the girders were only a fraction of the stresses that would have been induced if the girders had sustained all the loading by themselves. It was concluded that the bridge was not a slab-on-girder bridge after all. It was, in fact, a slab bridge with up-stand beams. The "girders" were only a part of the formwork, and had simply been left behind after construction.

3.4.4 Summary

Several significant "surprises" encountered during bridge testing in Ontario have been presented in this Section. They provide an introduction to static field testing, where the instruments sometimes seem to "lie". It is tempting to disregard such readings as being the result of an instrument malfunction. In most cases, however, it was found that the unexpected readings from the instruments were, in fact, caused by unexpected bridge behaviour.

The surprises presented in this Section also underline the fact that some aspects of bridge behaviour never enter into design considerations, so they can escape the attention of even the most experienced bridge designers and analysts. Some of the surprises found in bridge testing may have a significant effect on the load-carrying capacity of the bridge, while others have only a minor effect. From the various examples, it is clear that, in most cases, the load-carrying capacities of bridges are higher than those obtained from usual calculations.

However, there are some cases where the load-carrying capacity of a bridge can be lower than expected. A carefully planned and executed bridge test is invaluable in identifying the strengths and weaknesses of an existing bridge.

3.5 Proof Loads

In the context of bridge testing, the term proof load is used for the maximum load of a given configuration that the bridge has withstood without suffering any damage. An obvious question is asked with respect to proof testing of a structure: what should be the minimum magnitude of the proof load for a structure to be regarded as structurally adequate? Unfortunately, after considering all the factors, a satisfactory answer to this question is not available.

Both the Ontario Highway Bridge Design Code (OHBDC, 1992) and the Canadian Highway Bridge Design Code (CHBDC, 2000) implicitly require that, to classify a bridge as structurally-adequate and permitted to carry unrestricted traffic, the proof load should be of such magnitude as to induce at least the same maximum load effects as those induced by factored design live loads including the dynamic load allowance, *DLA*. It is recalled that the factored design live load, including impact, is α_L (1 + *DLA*) L_n, where α_L is the live load factor, and L_n the load effect due to unfactored live loads. The factored design live load is equivalent to the nominal live load causing failure. Since the proof load tests are always conducted within the linear elastic limit of the structure, the OHBDC and CHBDC criteria for proof loads can be seen to be excessively safe.

It can be demonstrated that the minimum level of the proof load required by the OHBDC and CHBDC should be reduced to account for: the dead-to-live load ratio for the structure under consideration, and the live load that a structure can take beyond its elastic limit up to failure. A more realistic proof load than the one specified by the current codes for evaluation, should also take into account these two factors. Until a more realistic basis is established, however, the OHBDC and CHBDC criterion is recommended for determining the level of proof loads.

3.5.1 Proof Loads Versus Legal Loads

A comparison of minimum required proof loads and corresponding maximum vehicle loads permitted in a jurisdiction will readily show whether the former are excessive or not. For this exercise, we considered the legal loads permitted in Ontario and compared them with the proof loads specified by the OHBDC (1992). The values of the *DLA* are as given in the code and the live load factor α_L is taken as 1.26. It is noted that while the OHBDC specifies α_L = 1.4 for new designs, it permits a smaller value, 1.26, for the evaluation of primary components of those multiple load path structures that are re-evaluated within five years.

For comparison of legal and proof loads, the convenient concept of equivalent base length, B_m, is used. This forms the basis of legal weights in Ontario and is discussed, for example, by Agarwal and Cheung (1987). For a given base length, there are specific values of total load W corresponding to the legal loads and the required proof loads, respectively. The ratio of proof load to legal load, denoted as K, is plotted in Figure 3.12 against B_m, for Ontario conditions. It can be seen from this figure that for $B_m = 0$, which corresponds to single axles, the proof load is about 3.5 times the legal load. This high ratio appears reasonable because, in practice, single axle loads are known to exceed the legal limit by a very large margin. For larger values of B_m, the value of K, plotted in Figure 3.12, is fairly close to 2.0 suggesting that the proof loads are about twice as heavy as the legal loads. This again appeals to engineering judgement because exceedance of the gross vehicle weight, be it accidental or deliberate, is rarely more than about 50 percent, in which case the remaining 50 percent can cater to the *DLA* and other possible infractions of load regulations.

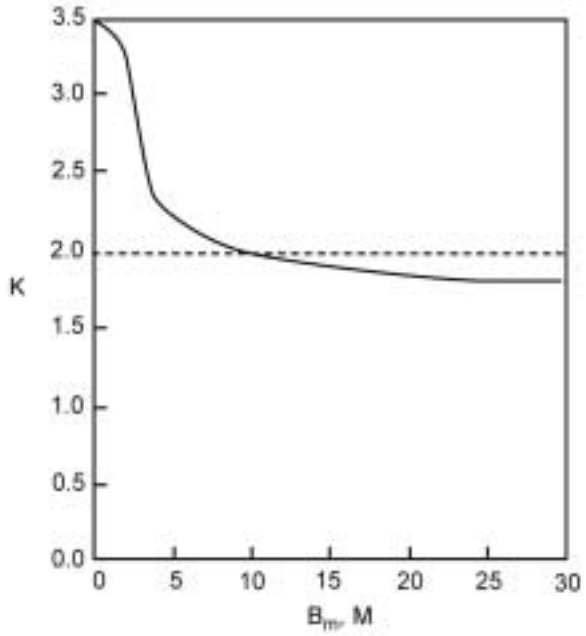

Figure 3.12 Ratio of required proof load to legal load for various values of B_m

It must be emphasized that a very large safety margin is already included in the proof load as specified by the OHBDC (1992). This is because this proof load is almost invariably below the elastic limit of the structure, above which nearly all bridges have a substantial reserve of strength.

The design of a short-span bridge is usually governed by single axle, two-axel or three-axle groups. It is instructive to study the relationship between legally permissible weights on these axle groups and proof loads for short-span bridges. A simply-supported span of 6.0 m and a two-axle group with an inter-axle group spacing of 1.85 m is chosen for this study. The maximum weight permitted on such an axle, in Ontario, is 9.55 tonnes or 93.5 kN. The maximum bending moment induced by a factored OHBDC design vehicle is 624 kN·m. Assuming that longitudinal bending moments govern the design, the proof load on the bridge should induce the maximum moment of at least this magnitude, for the bridge to be declared structurally adequate.

As explained previously, the test vehicle has a two-axle group with an inter-axle spacing of 1.85 m. If this axle group is to induce a maximum moment of 624 kN·m in a simply-supported span of 6.0 m, the weight on each axle should be 296 kN. In this case, the total proof load on the two-axle group is 592 kN, and the ratio of proof to permissible weights, *K*, is about 3.2. Such a large value of *K* can be justified only on the grounds that the exceedance of permissible weights on two-axle groups can be very high, as it is for single axles.

It is obvious that an excessively high evaluation load will lead to the unnecessary rejection of otherwise safe bridges, regardless of whether they are evaluated analytically or by testing.

3.5.2 Proof Loads for Deficient Bridges

The structural deficiency of a bridge is quantified by both the OHBDC (1992) and CHBDC (2000) by a factor *F,* called the scale-down factor. This factor is defined by the following equation for a component with factored resistance R_f.

Equation 3.1

$$F = \frac{R_f - \textit{load effects due to factored permanent loads}}{\textit{load effects due to factored live loads}}$$

Clearly, when $F \geq 1.0$, the bridge is structurally adequate and can be opened to unrestricted traffic.

The OHBDC (1992) has provided a chart to convert the scale-down factor to posting loads. A similar but non-dimensionalized chart is provided by CHBDC (2000) for the variable CL Evaluation Loads.

Both the OHBDC and CHBDC also permit extrapolation of the test results to determine the live load carrying capacity, if the maximum applied test load is limited by the capacity of the test equipment, and the stability of the bridge or its components is not a concern with any further increase in load. Such an extrapolation, including methods of analysis, projected maximum load capacity and determination of the scale-down factor is, however, subject to the approval of the authority having jurisdiction on the bridge.

4 DYNAMIC FIELD TESTING

Although not as old as static field-testing, dynamic testing of bridges is not new. Since the 1920s, all highway bridges in Switzerland with spans greater than 20 m are required to be tested dynamically. These tests were, and still are, conducted under a vehicle of fixed axle configurations running at different speeds and over a "bump" of prescribed size on a bridge.

Dynamic testing of bridges can be subdivided into four distinct categories:

- stress history tests
- *DLA* tests
- ambient vibration tests
- pull back tests

These categories of tests are discussed in the following subsections.

4.1 Stress History Tests

Stress history tests are carried out to establish the distribution of stress ranges in fatigue-prone components of a bridge. The data, continuously obtained for a short time due to the passage of vehicles on the bridge, are used to establish its fatigue life. An early instrument used for acquiring data from stress history tests comprised a number of compartments, each relating to a pre-assigned range of strain. Every time a component experiences a strain that falls within the strain range of a component, the counter in the component is increased by one. At the end of an observation period, the instrument provides a histogram of different strain ranges induced in the instrumented component. The Ministry of Transport Ontario (MTO) tried this technique but soon abandoned it because of difficulties in interpretation of the collected data. With modern facilities for storing large amounts of data, a more suitable approach is to obtain a continuous record of strains at a reasonable rate of sampling, and then process the data to obtain the frequency distribution of different stress ranges.

4.2 DLA Tests

The impact factor or dynamic load allowance *DLA* is an abstract entity which is not given to easy quantification. Dynamic testing of bridges is often undertaken as a research exercise to obtain information about representative values of the *DLA* which could be used in the formulation of code provisions. Some evaluation codes, e.g. the OHBDC, 1992 and the CHBDC, 2000, permit the determination of *DLA* by dynamic testing. As explained in this subsection, the determination of *DLA* is not without its own difficulties.

4.2.1 Definition of Dynamic Increment

Fuller et al. (1931) proposed that the impact increment of dynamic force be defined as the amount of force, expressed as a fraction of the static force, by which the dynamic force exceeds the static force. Recognizing that the "impact increment of dynamic force" is not necessarily the same as the "impact increment of stress", the latter was defined as the amount of stress, expressed as a fraction of static stress, by which the actual stress, due to moving loads, exceeds the static stress.

Researchers interpreting test data from dynamic load tests have often used the term "dynamic increment" for the same quantity that has been defined by Fuller et al. (1931) as the impact increment of stress, or that could have been defined as the impact increment of deflection. However, there is no uniformity in the manner in which this increment is calculated from test data. Different ways of calculating the dynamic increment can be explained conveniently with the help of Figure 4.1, which has been constructed from data of an actual dynamic test with a two-axle vehicle on a simply supported plate girder bridge, reported by Biggs and Suer (1956). This figure shows the variation of both the dynamic and static deflections at the mid-span of a girder with respect to time. The dynamic deflections were obtained when the test vehicle travelled on the bridge at normal speed. The static deflections were obtained when the vehicle travelled at crawling speed, so as not to induce dynamic magnification of deflections. Figure 4.1 also shows the median deflections that were obtained by averaging consecutive peaks of dynamic deflections. The median deflections are not the same as the static deflections. However, a numerical procedure for filtering out the dynamic portion of the response can give median responses that are fairly close to the static responses, especially in bridges having spans larger than about 20 m.

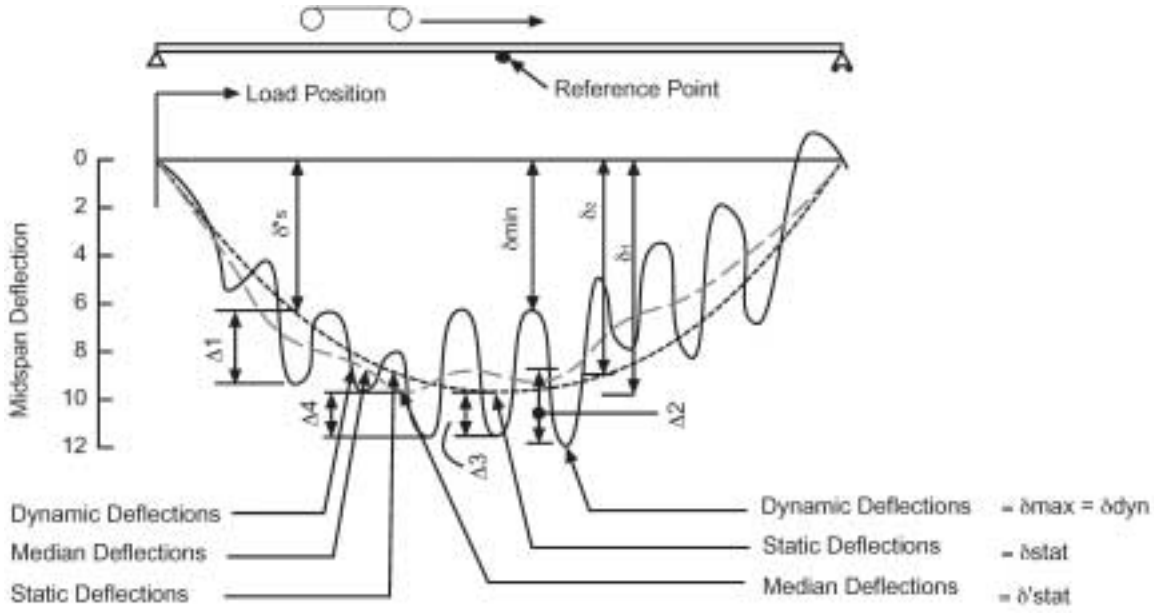

Figure 4.1 Mid-span deflections of a beam under a moving vehicle load

It is noted that a fictitious scale of deflections has been introduced in Figure 4.1 in order to facilitate the explanation regarding interpretation of the test data. Referring to this Figure, a notation is introduced that is defined in Section 6. This notation can be more general if the word deflection is replaced by response.

In Figure 4.1, a scale of deflection is used in which δ_{stat} is 10.0 units. With this definition, the various deflection quantities have the following values.

$\delta_{stat} = 10.0$; $\delta_{max} = 12.3$; $\delta'_{stat} = 9.9$; $\delta_{min} = 6.2$; $\delta_1 = 9.1$; $\delta_2 = 9.8$; $\delta^*_s = 6.4$;
$\Delta_1 = 3.2$; $\Delta_2 = 3.1$; $\Delta_3 = 2.0$; $\Delta_4 = 2.0$

Bakht and Pinjarkar (1990) have shown that various definitions have been used to obtain dynamic increments from test data, or similar parameters given other names. Some of the more important of these definitions are now described. For the sake of convenience, all these different parameters will henceforth be referred to generically as dynamic amplification factors, and will be denoted by the symbol *I*. The various definitions are noted below, together with the value of *I*, corresponding to the data given in Figure 4.1, and also noted above.

Equation 4.1 $$I = \frac{\Delta_1}{\delta_S^*} \left(=0.500\right)$$

Equation 4.2 $$I = \frac{\Delta_3}{\delta_{stat}} \left(=0.200\right)$$

Equation 4.3 $$I = \frac{\Delta_4}{\delta_{stat}} \left(=0.202\right)$$

Equation 4.4 $$I = \frac{\delta_{\max} - \delta_{\min}}{\delta_{\max} + \delta_{\min}} \left(=0.330\right)$$

Equation 4.5 $$I = \frac{\delta_{\max} - \delta_2}{\delta_2} \left(=0.255\right)$$

Equation 4.6 $$I = \frac{\delta_{\max} - \delta_1}{\delta_1} \left(=0.352\right)$$

Equation 4.7 $$I = \frac{\delta_{\max} - \breve{u}'_{\text{stat}}}{\breve{u}'_{\text{stat}}} \left(=0.242\right)$$

Equation 4.8 $$I = \frac{\delta_{\max} - \delta_{stat}}{\delta_{stat}} \left(=0.230\right)$$

It can be seen that values of *I* obtained by the above equations range between 0.2 and 0.5.

Bakht and Pinjarkar (1990) have cited 26 published references in which one or another of the definitions listed above has been used for calculating *I*. In nearly all of the references there is little or no discussion or justification for using a particular definition of the dynamic amplification factor. This suggests that each of the various definitions was regarded as being axiomatic and requiring no justification. Yet, the variety of results noted above confirms that the definition of *I* is far from being axiomatic. What can be regarded as axiomatic, however, is the definition of the amplification factor for the response at a given instant. According to this definition, $I = \Delta/\delta_s$, where Δ is the difference between the static and dynamic responses at the instant under consideration, and δ_s is the corresponding static response.

The axiomatic definition of the amplification factor given immediately above is used, justifiably, in all the analytical studies. However, it is of little use in bridge design because its value changes with time and load position. What is required for design purposes is a single value of the amplification factor in which the maximum dynamic response can be computed from the maximum static response, so that:

Equation 4.9 $$\delta_{\max} = \delta_{stat}(1+I)$$

Ideally, the amplification factor obtained from Equation 4.9 should lead to the same value of δ_{max} as was measured in the field, i.e. 12.30. None of the definitions correspond to the correct value of δ_{max}, except Equation 4.8, which is, in fact, the same as Equation 4.9. It is interesting to note that the apparently logical definition given by Equation 4.8 has not been used in any of the references cited by Bakht and Pinjarkar (1990).

4.2.2 Factors Responsible for Misleading Conclusions

Technical literature reports a fairly large scatter in the values of dynamic amplification factors of a given response, even when the bridge and the vehicle are the same. From these observations it can be readily concluded that the dynamic amplification factor is not a deterministic quantity. To obtain a single value of this factor for design purposes, it is necessary to know the statistical properties of the scatter of data; in particular, the mean and variance of the amplification factor. The various parameters that can influence the statistical properties of the amplification factors computed from the test data are discussed in the following section. If not accounted for carefully, these parameters can misleadingly influence the way in which the measured data are interpreted.

4.2.2.1 Vehicle Type

It is already known that the dynamic amplification factor for a bridge is influenced significantly by the dynamic characteristics of the vehicle with respect to those of the bridge. Despite this fact, most dynamic tests on bridges have been conducted with specific test vehicles. The data from such tests cannot, for obvious reasons, be regarded as representative of actual conditions. The amplification factors obtained from tests using specific test vehicles can only provide a qualitative insight into the problem of bridge dynamics. They should not be used to obtain the final single value of the impact factor that is used in calculations for design or evaluation. A representative value of the impact factor can be calculated realistically only when data are gathered under normal traffic, and over relatively long periods of time.

A well-planned proof test is carried out with gradually increasing loads, ensuring that the loads are not allowed to increase beyond the limit of linear elastic behaviour.

There are very few published examples of proof tests conducted outside Ontario; examples of those conducted in Ontario are reported by Bakht (1981, 1988), Bakht and Csagoly (1979), Bakht and Mufti (1992 a and c).

4.2.2.2 Vehicle Weight

Several researchers have concluded from observed data that the dynamic amplification factor due to a vehicle decreases with the increase of vehicle weight. In light of this information, it can be appreciated that the amplification factors corresponding to lightly-loaded vehicles, which are irrelevant to the design load effects, are likely to unduly bias the data on the higher side. The data corresponding to lightly-loaded vehicles should not be used at all in the calculation of the impact factor, unless, of course, the impact factor is sought specifically for lighter vehicles, as may be the case for evaluating the load-carrying capacity of an existing substandard bridge.

4.2.2.3 Vehicle Position with Respect to Reference Point

Consider a three-lane slab-on-girder bridge with five girders, all instrumented for dynamic response measurement, carrying a vehicle in the far right-hand lane so that two girders under the vehicle carry its load directly. In this case, the two left girders, being remote from the applied load, will carry a very small portion of the static load. Yet, the dynamic amplification of the small portion of the static load carried by these two girders is likely to be fairly large. It has been observed by several researchers that the dynamic amplification factor at a reference point well away from the load can be larger than that for a reference point directly under the load. Clearly, the former amplification factor has no relevance as far as the maximum static load effects are concerned at the cross-section of a bridge.

The statistical properties of the dynamic amplification factor, as computed from the test data, can be regarded as realistic only if the extraneous data from outside the zone of influence are excluded from consideration. It is surprising that the attempt to exclude such extraneous data has been explicitly mentioned in only a few of the references cited by Bakht and Pinjarkar (1990).

Chan and O'Connor (1990) have tried to calculate the dynamic amplification of load effects by recording the sum of the strains of all girders. From dynamic test data on a short span girder bridge, they have calculated alarmingly high values of the dynamic increment. Bakht et al. (1992) have contended that the high values of dynamic increment reported by these researchers are the result of including extraneous data corresponding to those girders that are transversely remote from applied loads.

4.2.3 Recommendations

In light of the above discussion, it is concluded that it is not a practical proposition to determine a representative value of the *DLA* for a given bridge by dynamic testing. The values of the *DLA* specified by OHBDC (1992) and CHDBC (2000) probably reflect the state-of-the-art. Dynamic testing of bridges is, nevertheless, a useful research tool in formulating more reliable specifications for *DLA* for different kinds of bridges.

4.3 Ambient Vibration Tests

Ambient vibration tests are conducted to determine the vibration characteristics of a structure that has been excited by wind, human activity, or traffic. Typically, the response of the structure is measured by strategically-placed accelerometers. An example of the record of output from an accelerometer is shown in Figure 4.2, in which the accelerations are plotted against time (Ventura et al., 1994). It can be seen in this Figure that, during the observation period, the structure experienced accelerations of up to slightly more than 0.1 *g*. The selection of the locations and number of the accelerometers requires not only expertise in dynamic testing, but also detailed knowledge of the behaviour of the structure. As noted by Ventura et al. (1996), a detailed analysis of the structure is useful in deciding upon the test set-up for ambient vibrations.

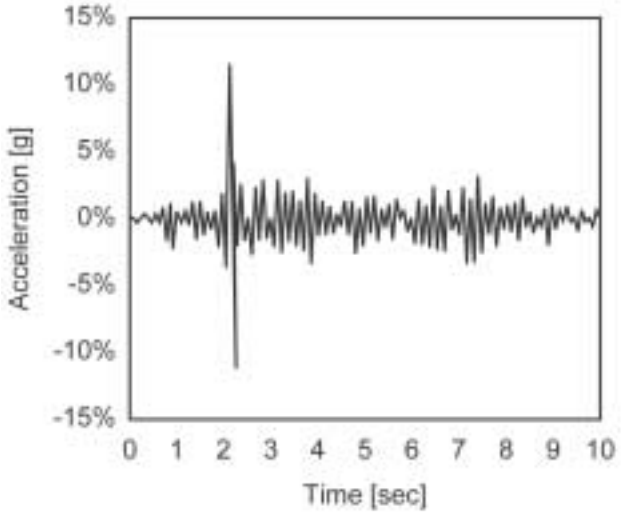

Figure 4.2 Accelerations plotted against time (Ventura et al., 1994)

The plot of accelerations against time, such as that reproduced in Figure 4.2, can be regarded as a function f (*t*), which is described by the following series.

Equation 4.10 $$f(t) = A_1 \sin 2\pi f_1 t + A_2 \sin 2\pi f_2 t + A_3 \sin 2\pi f_3 t + A_4 \sin 2\pi f_4 t + \ldots$$

where f_1, f_2, f_3, f_4, etc. are the various natural frequencies of the structure, and A_1, A_2, A_3, A_4, etc. are the modal amplitudes or modal ratios. The modal amplitude for each frequency is closely related to its spectral density or power spectral density (PSD).

Vibration records are analysed into frequencies and PSDs by special-purpose computer programs, such as EDI (1995). Records of PSDs are then normalized to give them each the same weight. Thereafter, the normalized PSDs corresponding to instruments recording the data in the direction of the vibration under consideration are averaged to obtain the average normalized power spectral density (ANPSD). An example of an ANPSD plot is shown in Figure 4.3. It is noted that the acceleration plot of Figure 4.2 represents only a part of the data that led to the density function of Figure 4.3. An ambient vibration test, leading to ANPSD plots, is also referred to as a modal test.

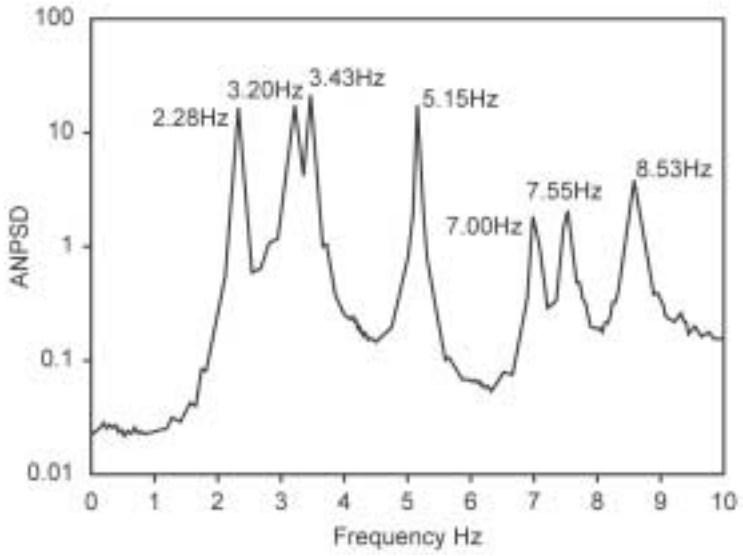

Figure 4.3 An average normalized power spectrum density plot of signals corresponding to vertical vibration (Ventura et al., 1996)

As can be seen in Figure 4.3, an ANPSD plot identifies the various peak frequencies, most of which are likely to be the natural frequencies of the structure. The plot, however, might also include the frequencies of a dominant exciting force, such as a heavy truck. In order to ensure that the ANPSD plot contains only the natural frequencies of the structure, the identified frequencies should be compared with analytically predicted frequencies. If the plot does contain extraneous frequencies, the test must be repeated and the ANPSD plot recreated until the frequencies of exciting forces are purged and a repeatable plot is obtained.

If a number of accelerometers are permanently installed on a structure, their output synthesized into a repeatable ANPSD plot can be regarded as the signature of the structure. Any change in the pattern of ANPSD should indicate a shift in the frequency pattern and, hence, a change in the stiffnesses or mass of the structure.

The various analytical methods for vibration-based damage detection are described in Appendix C.

In practice, there are a number of limitations associated with vibration-based damage assessment. They are summarized in the following Sections.

4.3.1 Low Sensitivity Damage

Vibration characteristics are global properties of the structure and, although they are affected by local damage, they may not be very sensitive to such damage. As a result, the change in the global properties may be difficult to identify unless the damage is very severe or the measurements are very accurate.

4.3.2 Complexity of the Damage Identification Algorithms

The identification of a possible damage site and severity of damage, on the basis of a change in global properties derived from measurements at a limited number of sensor locations, is a problem that can be resolved. Sophisticated and complex mathematical techniques, including nonlinear programming, need to be employed to obtain the most probable solution. In fact, this is an area of ongoing research. The methods that are currently available cannot deal with situations where the damage introduces non-linearity in the structure. Such non-linearity may, for example, result from the presence of active cracks.

4.3.3 Effect of Factors Other Than Damage

Global vibration characteristics are often affected by phenomena other than damage, including environmental effects such as a change of mass caused by water waves and snow accumulation, and thermal effects caused by temperature variation. Whenever the structural system is constrained or indeterminate, thermal effects introduce axial stresses in the structural elements. The presence of such axial stresses changes the stiffness of the structure and may alter its vibration characteristics. The boundary conditions in a structure can have a significant effect on its stiffness and, if these boundary conditions are prone to change with the age of the structure, they may lead to a change in the vibration characteristics even when there is no damage in the structure.

4.4 Pull Back Tests

Since the traffic loads do not excite a bridge in the lateral direction in any significant way, it is usually difficult to determine its lateral vibration characteristics from the results of an ambient vibration test. The lateral vibration characteristics of a bridge can be obtained accurately from a pull back test. This type of test can be conducted by pulling the structure laterally by means of cables anchored in the ground or to a fixed object, and releasing the cables suddenly. The response of the structure is monitored with the help of accelerometers, and the process of analyzing the data is the same as for ambient vibration tests. In a pull back test, the structure vibrates freely, so the test also yields information about the damping characteristics of the bridge for lateral vibrations.

A pull back test on a three-span continuous bridge is described by Ventura et al. (1996). For this test, the piers of an abandoned railway bridge were used to anchor the cables, then released by a special-purpose quick-release mechanism.

The calibration for a frame of Confederation Bridge was conducted by pull tests and measuring the resulting tilt from a known applied load, as described by Azarnejad et al. (1999).

During one of the lateral pull tests, the fracture of the slings caused a dynamic release of the full load and resulted in free vibration of the frame. The recorded data was used to determine the natural frequencies of the structure using sepectral analysis.

5 PERIODIC MONITORING

Periodic monitoring is conducted to investigate any detrimental change that might occur in a structure or to its repairs. Most of the components of this monitoring system are common to static and dynamic field testing, described in Sections 3 and 4, respectively. Customarily, continuous monitoring is only applied to those structures that are either extremely important, or if there is a doubt about their structural integrity. The latter might be the case if the structure is likely to be exposed to extreme events, such as severe earthquakes and hurricanes, or if its design includes an innovative concept that does not have a history of performance to prove its long-term worthiness. Similarly, a check on the health of a structure repaired with an innovative technique could be made by means of periodic monitoring. Although the authors of this manual are not aware of a specific case study to date, periodic monitoring complemented by field testing can also be useful in the gradual extension of the life of a rapidly-deteriorating structure.

Since the details and techniques of all possible periodic monitoring methods is too vast to be covered in this guideline, this section will illustrate the usefulness this SHM subsystem, mainly with the help of a number of case histories.

5.1 Monitoring Through Ambient Vibrations

As discussed in Section 4.3, ambient vibration records can provide a useful signature of the bridge response, provided that the records are free from the dynamic characteristics of an exciting force. For example, Abe et al. (1999) described an ambient vibration system that is being used to monitor the health of the Haukachu suspension bridge in a wind-prone and seismically-active location in Northern Japan. They used a statistical technique to sift the information pertaining to the free modes of vibration from the recorded data. It is emphasized that, for periodic monitoring, the instruments should preferably be installed permanently on the structure after identifying critical locations.

Although records of ambient vibrations have been taken for several bridges in Canada (e.g. Ventura et al. 1994, 1996; Black and Ventura, 1998), this technique is yet to be used for periodic monitoring of bridges. An accurate identification of frequencies and modal shapes for two railway bridges in Austria has also been tried (Weznel and Pichler, 1997).

5.2 Monitoring Through Testing Under Moving Traffic

Periodic records of bridge responses, such as strains, can be used to track changes in the behaviour of a bridge. The Mufti et al. (1999) report on the monitoring of the steel plate girder of the Salmon River Bridge is an example of this particular SHM subsystem. As reported by Newhook and Mufti (1996), one simply-supported span of this bridge incorporates a concrete deck slab without tensile reinforcement, known as a steel-free deck slab. The innovative slab derives its strength mainly through transverse steel straps that lie outside the slab and are welded to the top flanges of the steel girders. A cross-section of the Salmon River Bridge span with the steel-free deck slab is shown in Figure 5.1.

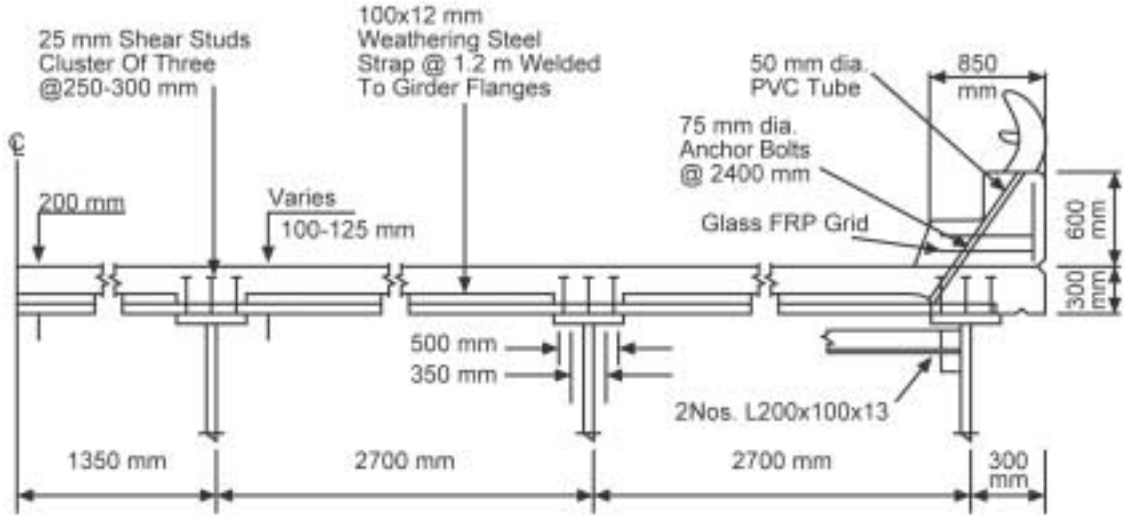

Figure 5.1 Cross-section of the Salmon River Bridge steel-free deck slab

The health of the Salmon River Bridge has been monitored periodically for the last five years, under the auspices of ISIS Canada. Since the deck slab of this bridge is the first application of the novel concept of steel-free deck slabs, it was considered desirable to track the performance of the bridge, as it might be affected by an unanticipated deterioration of the slab without tensile reinforcement.

A measure of the performance of the deck system of a bridge is the manner in which its girders share the vehicle loads. During short intervals of periodic monitoring, the strains of the bottom flanges of the girders of the Salmon River Bridge are recorded at a high sampling rate. The maximum values of girder strains corresponding to a single truck travelling in each of the two marked lanes on the bridge are isolated. The non-dimensional distribution factors for bottom flange strains are obtained by dividing the selected strains with the corresponding average girder strains. Plots of distribution factors for bottom flange strains recorded in one set of readings are reproduced in Figures 5.2 (a) and (b), corresponding to single trucks in the north and south lanes, respectively. These figures also contain corresponding distribution factors obtained from finite element analyses in which no allowance was made for a possible loss of stiffness of the concrete slab due to the absence of tensile reinforcement. Excellent correspondence between the observed and analytical plots of the distribution factors confirm that the steel-free deck slab participates fully in transverse load distribution between the girders.

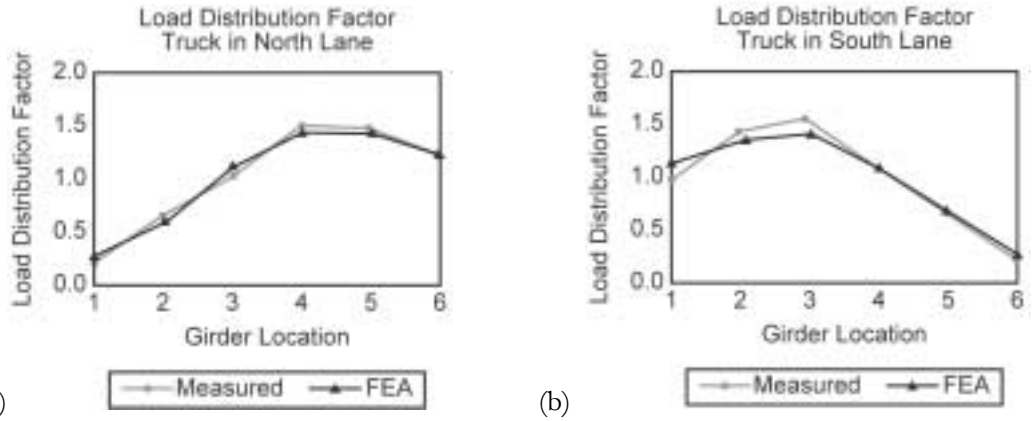

Figure 5.2 Distribution factors for bottom flange strains: (a) due to truck in north lane (b) due to truck in south lane

Transverse plots of the distribution factors, such as those in Figures 5.2 (a) and (b), provide an accurate measure of the load distribution characteristics of a girder bridge that is affected by both longitudinal and transverse flexural rigidities of the bridge. The deck slab contributes to the former through its composite action with the girders. The deck slab, straps and cross-frames collectively contribute to the transverse flexural rigidity of the deck system. If the transverse pattern of the distribution factors discussed above remains unchanged, then it can be concluded with confidence, that the deck slab has not suffered any deterioration in its stiffness. Through a number of periodic observations, it has been found that the distribution plots, of the kind presented in Figures 5. 2 (a) and (b), have remained the same for the Salmon River Bridge. Thus, periodic monitoring continues to provide confidence in the concept of the steel-free deck slab.

5.3 Monitoring Through Static Field Testing

Static field testing is a relatively expensive undertaking, so it is rarely used for periodic health monitoring of a structure. One rare example of this method is the periodic testing of the Chatham Bridge in Ontario. In the Chatham Bridge, the deteriorated reinforced concrete deck slab was replaced with a steel-free deck slab (Ali et al., 1997). Engineers from MTO have already tested the bridge twice. The first test was conducted on the bridge before rehabilitation and the second test soon after rehabilitation. These two tests confirmed that the load distribution characteristics of the bridge were somewhat improved by the steel-free deck slab. A third test is planned in the near future to confirm that the steel-free deck slab has not deteriorated. Details of the tests and their results are yet to be published.

5.4 Monitoring Crack Growth

All concrete components, except those with full prestressing, develop cracks during the early stages of being subjected to high loads. Until the formation of cracks has stabilized, the behaviour of the concrete component remains inelastic. When the cracks cease to develop under a given system of applied loads, the structure shakes down to an elastic state. On the other hand, if the cracks continue to grow indefinitely, there is cause for concern about the health of a structure. For certain components, the monitoring of crack growth can be used as a subsystem of SHM. An example of these components is the steel-free deck slab, discussed in Section 5.3.

As noted by Agarwal (1990), all concrete deck slabs develop cracks. The steel-free deck slabs also develop cracks. However, unless special provision is made for controlling the crack widths, the cracks tend to be fewer and wider. It is noted that five of the earliest steel-free deck slabs, Bakht and Mufti (1998), do not have special provisions for controlling cracks, so these cracks are relatively wide and easily noticed. There is a steel-free deck slab with special provisions for controlling cracks that is free of cracks visible to the naked eye (Newhook et al., 2000).

Crack growth is being monitored periodically in the deck slab of the Salmon River Bridge. This is being done to confirm that crack growth ceases in steel-free deck slabs at a fairly early stage. Mufti et al. (1999) have noted that the cracks in the deck slab of the Salmon River Bridge, shown in Figure 5.3, have remained unchanged over the years.

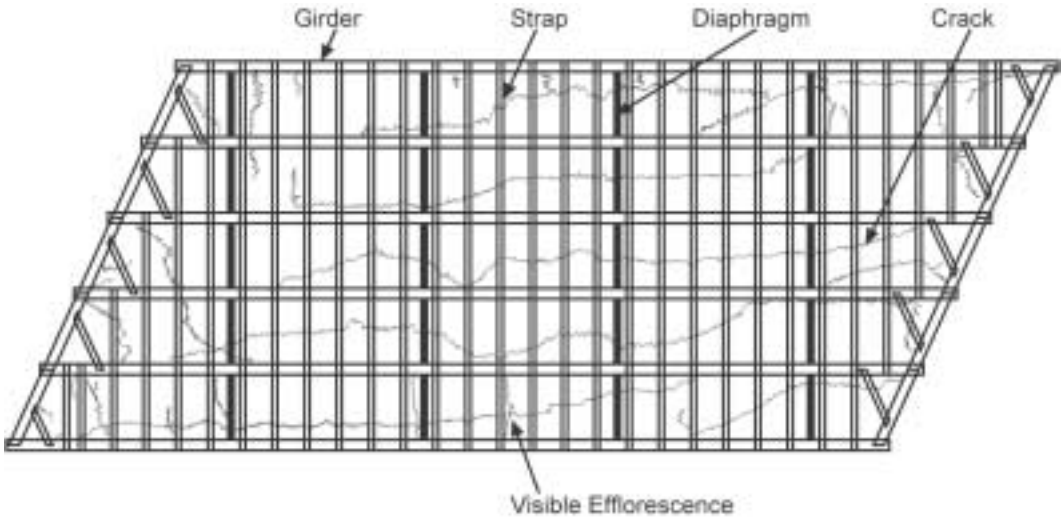

Figure 5.3 Crack pattern on the underside of the deck slab of the Salmon River Bridge

Although growth of cracks in steel-free deck slabs is currently being monitored manually, plans are underway to develop an acoustic emission system that could detect the end of crack growth.

A dynamic test was conducted over a transverse crack on the underside of the steel-free deck slab of the Chatham Bridge, which is discussed in Section 5.3. For this test, a 30 mm high temporary bump was placed close to the crack location, and a fully loaded five-axle test truck travelled over the bump. The opening of the crack was measured by means of a sensitive strain transducer. As can be seen in Figure 5.4, the crack did open under each axle. However,

even the maximum crack opening was less than 0.002 mm. It is expected that in the future, similar tests on the slab will yield similar results.

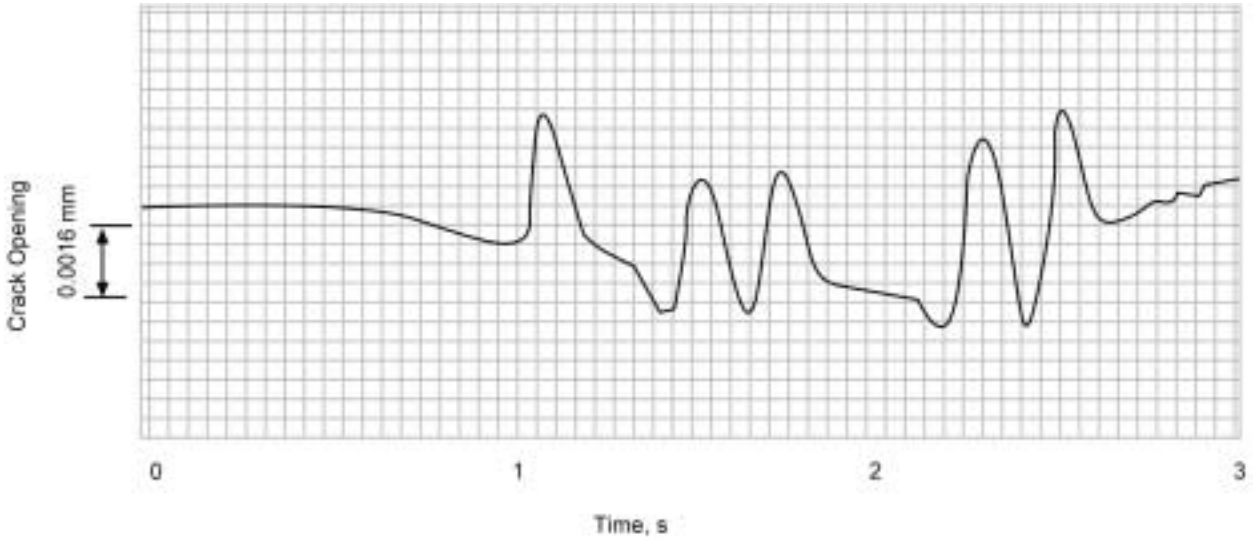

Figure 5.4 Crack opening in a steel-free deck slab under a five-axle truck

5.5 Periodic Monitoring of Repairs

Static field tests done before and after repairs can be useful in quantifying the effectiveness of repairs for enhancing various stiffnesses of the structure. For example, Stallings et al. (2000) have described such tests on a short-span concrete T-beam bridge that was strengthened by gluing carbon fibre reinforced polymer (CFRP) plates to the bottom and sides of the beams. Load tests on the bridge before and after repairs confirmed that the FRP repairs marginally reduced the live load deflections. It should be noted, however, that these tests can not provide realistic information about the enhancement of the load-carrying capacity of the structure, as affected by the repairs.

A novel technique incorporating a casing of glass fibre reinforced polymer (GFRP) with fibres oriented in the circumferential direction was used to repair a deteriorated concrete column on a bridge in Ontario. The gap between the casing and the column was filled with expansive grout. It was expected that, after expansion, the grout would induce radial pressure on the deteriorated concrete, thus enhancing its compressive strength. This technique was described by Erki and Agarwal (1995). Since the radial compressive force on the old concrete due to the expansive mortar is directly related to the hoop tension in the FRP casing, circumferential strains on the latter can be used to quantify the effectiveness of repairs. Soon after the layer of expansive concrete set, the FRP casing was instrumented with two electrical resistance strain gauges at each of three sections, at the top, middle and bottom of the column. The tensile strains remained at a constant level soon after peaking, and dropped slightly during the first ten days. These kinds of records, while being extremely useful in a limited sense, lose credibility on a longer-term basis because the electrical resistance gauges, which are glued using standard procedures, eventually tend to drift. A more useful tool for this kind of monitoring is the fibre optics Long Gauge described by Tennyson and Mufti (2000).

6.1 Beddington Trail Bridge

Location: Calgary, Alberta
Opened to Traffic: November 1993

References:
1. Rizkalla and Tadros (1994).
2. Tennyson and Mufti (2000).
3. Web site: www.isiscanada.com

Figure 6.1 Beddington Trail Bridge – Calgary, Alberta

6.1.1 Bridge Description

The Beddington Trail Bridge, as shown in Figure 6.1, is the first bridge in Canada to be outfitted with FRP tendons and a system of structurally integrated optical sensors for monitoring. The bridge opened to traffic in November 1993. The Beddington Trail Bridge is a two-span, continuous 25° skew bridge of 22.83 and 19.23 m spans, each consisting of 13 bulb-Tee sections, pre-cast, pre-stressed concrete girders.

Two different types of carbon fibre reinforced polymer (CFRP) tendons were used to pretension six pre-cast concrete girders. Carbon fibre composite cables (0.625″ diameter) produced by Tokyo Rope of Japan were used to pretension four girders, while the other two girders were pre-tensioned using two Leadline rod tendons (0.375″ diameter) produced by Mitsubishi Kasei. Continuity of the two spans was achieved using post-tensioned steel tendons extended along the entire length of the bridge.

6.1.2 Instrumentation for Monitoring

Fibre Bragg Grating (FBG) sensors were installed to monitor the bridge's behaviour during construction and under serviceability conditions. ElectroPhotonics Corporation Canada installed a total of 20 FBG sensors. A four-channel Bragg Grating fibre laser sensor system was used as a data acquisition system at different locations along the bridge girders that were pre-tensioned by the CFRP. The system involved four independent Bragg Grating tuned fibre lasers that were multiplexed in order to be pumped by one semiconductor laser. Each fibre laser was attached to the surface of the tendon to serve as a sensor. The sensors were connected, through a modular system, to a laptop computer used at the construction site to record the measurements at different stages of construction, and after completion of the bridge. The optic sensor system measured the absolute strain rather than a strain relative to an initial calibration value (the latter being characteristic of electric resistance strain gauges and mechanical gauges). The network of FBG sensors was connected to a junction box that was provided for on-site monitoring.

6.1.3 Diagnostic Results

To check the integrity of the carbon fibre cables and the FBGs, measurements were made in November 1999. Readings under traffic loads were consistent with those taken in 1993 with no observed change in structural behaviour. This project is the first civil engineering application in Canada to use fibre optic sensors (FOS), so it is an important project for assessing the durability and functional life of FOSs. During the 1999 assessment, 18 of the original 20 FOSs were still functional after 6 years of service life. The dynamic response of the structure, as recorded by a FBG sensor on a tendon for a one truck pass, was assessed and the shape of the curve was found to be consistent with that predicted for a three axle truck.

6.2 Salmon River Bridge

Location: On the Salmon River near Kemptown, Nova Scotia
Opened to Traffic: December 1995

References:

1. Newhook and Mufti (1996).
2. Newhook and Mufti (1996).
3. Bakht and Mufti (1998).
4. Doncaster et al. (1998) ACMBS II
5. Mufti et al. (1999).
6. Web site: www.isiscanada.com

6.2.1 Bridge Description

The first fibre reinforced concrete bridge deck slab without steel reinforcement was constructed over the Salmon River on Trans Canada Highway 104, as shown in Figure 6.2. The highway is divided into an eastbound section and a westbound section. Each section carries two traffic lanes. The bridge has two simply supported spans of 31.20 m each and includes a composite concrete slab on steel girders with a skew angle of 22°-15'-0". The eastbound section has one span constructed with a deck slab with conventional steel reinforcement and the other span has a steel-free deck. The deck slab with conventional steel reinforcement is 225 mm thick and the steel-free deck is 200 mm thick, with chopped

polypropylene fibres randomly mixed at a volume fraction of 0.55 percent. The bridge deck is supported on six steel plate girders, at a spacing of 1.2 m.

Figure 6.2 Salmon River Bridge – Nova Scotia

The curb/parapet that supports the aluminum barrier wall is also constructed with an innovative design. The concrete barrier wall contains inclined steel rods encased in PVC tubes. These rods are bolted at the top of the wall and to the steel cross-frames below the deck. FRP was used in the curbs to provide durability similar to the steel-free deck. Two horizontal layers and one vertical layer of a 150×150 mm NEFMAC glass fibre reinforced polymer (GFRP) grid were also used. Although the steel-free side has an initial cost of 6 percent more than the steel-reinforced side, the overall design tends to have a less expensive life-cycle cost because of expected lower maintenance costs.

6.2.2 Instrumentation for Monitoring

Out of a total of 23 foil strain gauges, 15 were installed on the girders below the steel-free deck welded at mid-span, as shown in Figure 6.3. The strain gauges were placed near the top and bottom flanges. Two outer girders had additional gauges installed on their webs midway between the flanges, and eight foil gauges were installed at several straps at mid-span and at the end of the span. In addition to the conventional strain gauges, three FBG sensors were installed in the GFRP grid embedded in the curb section. These sensors were embedded in the NEFMAC grid during manufacture. This was the first reported attempt in the world to use integrated FOSs to monitor the performance of the FRP reinforcement inside the concrete of a bridge structure.

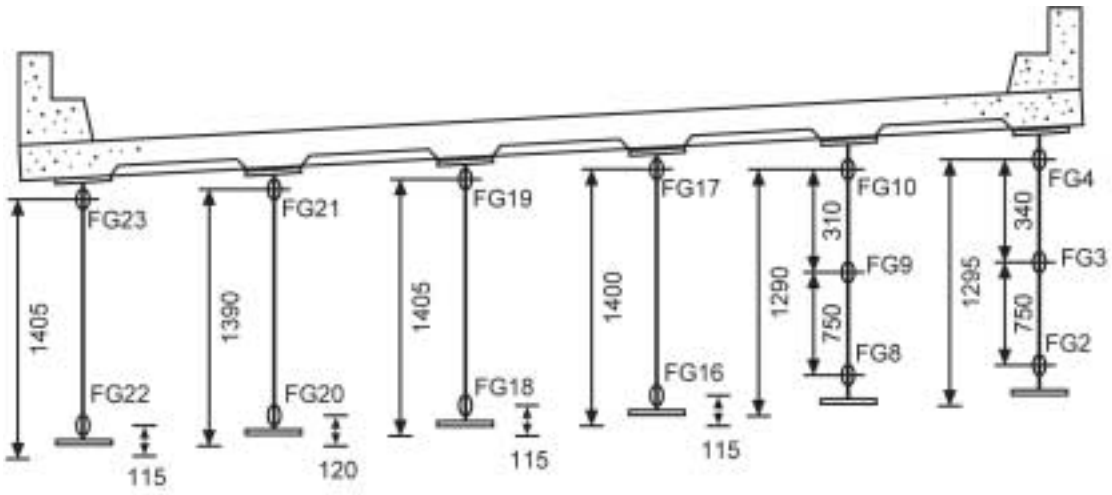

Figure 6.3 Sensor locations in the Salmon River Bridge

Field assessment of the steel-free deck has focused on: mapping of crack patterns and growth; load sharing among the bridge girders; fatigue performance of the welded strap connections; and participation of the curbs in carrying live loads.

6.2.3 Diagnostic Results

The field assessment results of the Salmon River Bridge show that the steel-free deck is performing adequately under field conditions. In the initial seven days of moist curing, no plastic shrinkage cracking occurred. Detailed visual inspections in May of 1996 revealed that two types of cracks had occurred, one type being small transverse cracks that appeared in the outside edge of the deck, and the second being a single longitudinal crack that occurred in each panel of the deck for almost the entire length of the bridge. However, after six months of construction, these cracks appeared to stabilize and are not affecting the remaining life of the deck. The crack pattern map is shown in Figure 5.3.

Three sensors were installed in the curbs and parapet, but only two survived the construction work. The relative difference in strain levels is less than 10 microstrain, indicating that the curb has been isolated from participating in the bending behavior of the deck. A discussion on the load-sharing effects in the girder, under normal traffic, is provided in Section 5.2.

6.3 Chatham Bridge

Location: Kent Country Road No. 10 in Chatham, Ontario
Opened to Traffic: November 1996

References:

1. Aly et al. (1998).
2. Bakht and Mufti (1998).
3. Doncaster (1998).
4. Web site: www.isiscanada.com

6.3.1 Bridge Description

The Chatham Bridge, as shown in Figure 6.4, is an old steel girder bridge with two traffic lanes and four simply supported spans over the busy expressway, No. 401, in western Ontario. The bridge has a 13.1 m exterior and 20.1 m interior spans. The bridge has five girders at a spacing of 2.1 m. Due to severe deterioration of its original 178 mm thick reinforced concrete slab, the two interior spans were replaced with a 225 mm thick rectangular deck slab with steel reinforcement, designed by the conventional OHBDC empirical method. The two exterior spans were replaced by the innovative, 175 mm thick, steel-free deck slab containing chopped polypropylene fibres at a volume fraction of 0.55 percent.

(a) (b)

Figure 6.4 Chatham Bridge – Ontario (a) view of bridge (b) view of deck replacement

A half cross-section of the Chatham Bridge steel-free deck is shown in Figure 6.5. The cantilever overhangs and the outer panels of this slab have a grid of CFRP placed near the top surface. The CFRP NEFMAC grid, which is resistant to the deleterious effects of de-icing salts in concrete, was used so that the durability of the entire slab in the outer spans would remain as high as that of the segments that are truly free of any reinforcements. To achieve full arching action, the steel-free slab is confined by galvanized steel straps (20 x50 mm) welded to the top flange of the girders at a spacing of 1.0 m.

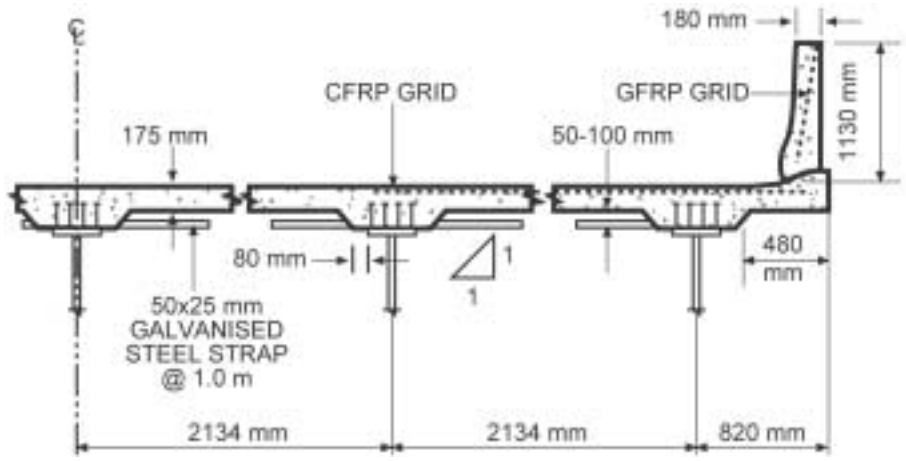

Figure 6.5 Half cross-section of steel-free deck slab of the Chatham Bridge

A durable bridge barrier wall, reinforced with a planar grid of GFRP, is connected to the deck slab with double-headed tension bars made of stainless steel. The new barrier wall is known as the Ontario Bridge Barrier (OBB). The OBB conforms to the highest performance level in the new CHBDC and is incorporated in the steel-free deck slabs of the Chatham Bridge.

6.3.2 Instrumentation for Monitoring

The north side exterior span of the bridge has been instrumented by the MTO with permanently installed resistance strain gauges. Among these, 24 are still in service, with eight located on the NEFMAC inside the deck slab. Two types of FOSs were cast in the slab in conjunction with conventional embedded strain gauge transducers. The new steel-free deck was also instrumented with a FBG sensor on a 2.0 m GFRP bar, a RocTest embeddable fibre optic gauge, and an EGP-Series embedment strain gauge. Figure 6.6 shows the gauges installed in the deck under a layer of NEFMAC grid, before the concrete was poured.

Figure 6.6 Installed sensors in steel-free deck with carbon fibre NEFMAC

For field testing, additional instruments, such as accelerometers and displacement transducers, were temporarily placed on the structure. Dynamic and static tests were conducted at each of the three phases of the rehabilitation process: first, with the old deck in place; second, with half of the new steel-free fibre reinforced concrete deck in place; and third, with the old deck completely replaced. The last test was performed in the first week of June 1997. It has been confirmed that the steel-free deck slab acts compositely with the girders, and is able to withstand a static wheel load of about 500kN (50 tonne), without any distress.

6.4 Confederation Bridge

Location: Northumberland Strait, separating Prince Edward Island from the mainland. The bridge connects Borden, Prince Edward Island, to Cape Tormentine, New Brunswick.
Opened to Traffic: June 1997

References:
1. Tadros (1997)
2. Mufti et al. (1997).
3. Cheung et al. (1997).
4. Web site: www.isiscanada.com

6.4.1 Bridge Description

The 13.1 km long Confederation Bridge is the world's longest pre-stressed concrete box girder bridge built over salt water. It replaced the ferry service that linked Prince Edward Island to New Brunswick since 1832. The bridge, shown in Figure 6.7, has 44 main spans of 250 m each, and each span is made up of four massive pre-cast elements. The bridge width is 11 m from barrier to barrier wall, including one lane and one emergency shoulder in each direction. Each main span consists of main girders of pre-cast concrete boxes ranging in depth from 4.5 m to 14 m, and 190 m in length, complete with drop-in-spans of pre-cast concrete box girders 60 m in length. The navigation span elevation of the bridge is 60 m. It is one of the largest infrastructure projects in Canada, and used the most modern concrete manufacturing process for construction, with a 100 year design life.

Figure 6.7 Confederation Bridge

6.4.2 Instrumentation for Monitoring

A comprehensive program is in place to monitor both the short-term and long-term behaviour of the bridge. To minimize the cost and to obtain correlated data, monitoring devices were installed in the same two consecutive spans, one rigid frame and one drop-in-span, located in the deep-sea part of the strait. In this section of the manual, only the fibre optic monitoring system installed by ISIS Canada will be discussed.

A total of 22 sensors were installed on several sections of the reinforcing steel and eventually embedded within a large pre-stressed concrete main girder component. In May and July of 1996, members of the ISIS Dalhousie University group in Halifax installed ten FBG strain sensors in segments of Confederation Bridge. Six FBG sensors were installed in main girder number 31, and four were installed in the adjacent drop-in span. ElectroPhotonics Corporation installed another twelve FBG sensors in the drop-in span, four as temperature sensors and eight as strain sensors. Ordinary FBG sensors were bonded to 2.0 m long sections of 15M rebar, and the rebar was embedded in concrete, as shown in Figure 6.8. At the construction site the instrumented rebar sections were tied into the structural rebar that was being built in jigs on the ground.

Figure 6.8 Photograph showing sensors installed on a rebar cage

Three fibre optic gauges were installed in each of the two webs which made up Section C1 of girder No. 31. Eight fibre optic gauges, two temperature sensors and six strain sensors were installed in each web of Section 3 of drop-in span No. 31. Vibrating wire strain gauges, installed by Public Works Canada, were placed within 50 cm of each of the fibre optic sensors. Two types of gauges were located close together to allow for a comparison of results. The sensors were monitored with FLS3100 modules supplied by ElectroPhotonics Corporation.

6.4.3 Diagnostic Results

An important aspect of this project was to test the robustness of FOS under actual construction conditions, on a large scale project. The sensors in the two bridge sections were checked once in August 1996, while the sections were still in the yard, and a second time in March 1997, after being placed over the Northumberland Strait, before the bridge was open to traffic. All six sensors in the main girder section were functioning properly. Three of the 12 strain sensors installed in the drop-in span were damaged during construction; one of the leads was broken off at the concrete, and two of the connectors were jammed with concrete and are currently giving low signal values. All four temperature sensors were functioning properly. No report is currently available on the observed data.

6.5 Crowchild Trail Bridge

Location: Northwest Calgary, Alberta
Opened to Traffic: September 1997

References:

1. Bakht and Mufti (1998).
2. Tadros et al. (1998)
3. Afhami and Cheng (1999).
4. Web site: www.isiscanada.com

6.5.1 Bridge Description

The Crowchild Trail/University Drive Bridge in Calgary is a two-lane, one-way traffic overpass that has three continuous spans of 29.83, 32.82, and 30.23 m. The original superstructure of the bridge, comprising pre-stressed concrete box girders, was demolished in May 1997. A new superstructure was constructed in June 1997, using steel-free concrete bridge deck technology. Refer to Figure 6.9. The new superstructure is the first continuous span steel-free bridge deck in the world.

Figure 6.9 Crowchild Trail Bridge – Calgary, Alberta

Steel-free construction eliminates the problem of bridge deck deterioration due to corrosion of the reinforcing steel. The new superstructure is composed of five 900 mm deep steel girders with a steel-free polypropylene fibre reinforced concrete deck. Four evenly spaced cross frames brace the girders in each span. Transverse steel diaphragms join the girders at the supports. The superstructure is supported by five bearings at each abutment and two bearings at each pier.

The steel-free deck slab is 9030 mm wide and 185 mm thick, and the straps and girders were made composite with the concrete slab by stainless steel studs. GFRP bars were used in overhanging cantilevers and at the regions of interior supports. Prefabricated GFRP reinforcing grid, NEFMAC, was utilized in the barrier walls. GFRP C-Bars were used to minimize the width of transverse cracks in the steel-free deck over the intermediate bridge piers. By way of comparison, the capital cost of the GFRP and the steel free deck slab was $20,000 less than a conventional deck slab. This reinforcement is 2% of the total superstructure cost.

6.5.2 Instrumentation for Monitoring

The performance of the rehabilitated structure was investigated by using intelligent sensing and monitoring technologies. The objective of the project was to develop intelligent sensing in real time in order to monitor the structure's performance. The instrumentation and monitoring program was developed at the University of Alberta in collaboration with ISIS Canada, the City of Calgary, and SPECO Engineering Ltd. The program includes the study of static and dynamic behaviour of the bridge under vehicle loads, its thermal effects, load transfer in transverse direction, and the performance of glass fibre reinforcement.

A total of 103 strain gauges (86 electrical strain gauges and 17 electrical embedded strain gauges), 2 fibre optic strain sensors, and 5 thermisters were used in the monitoring program. All of these sensors were installed in the north span of the bridge, during construction in 1997. To control their alignment, thermisters and concrete strain gauges were embedded in pre-cast concrete blocks. Four thermisters monitored the temperature profile in the deck. A fifth thermister measured air temperature.

Seventeen embedded strain gauges were placed in a total of five pre-cast blocks: three in the positive moment region; and two in the negative moment region. Thirty of the remaining 86 electrical resistance strain gauges were installed on GFRP reinforcements, shear studs of the steel straps, NEFMAC grids, and stainless steel studs. After removal of the concrete forms, the other 56 gauges were installed on girders, straps, and cross-frames. Eighteen gauges were mounted on two straps to monitor the lateral distribution of strap strains at two sections, one in the positive and one in the negative moment regions. Due to space constraint, the gauges were installed on the bottom face of the straps.

Thirty-four strain gauges were used to monitor the steel girders. The webs of all five girders were instrumented with three gauges at both positive and negative moment regions. Four gauges were also installed on the flanges of girder No.1, to measure any warping of the girders and to better examine strain distribution at a cross section. Twenty strain gauges and two FOSs were mounted on the glass fibre reinforcement. The girders and straps were monitored by 34 and 18 strain gauges respectively. Another 14 strain gauges were used to monitor the shear studs, NEFMAC, and cross bracing of the bridge. In addition to these, ten cable transducers and four accelerometers were temporarily used in the second year tests in 1998.

All electrical strain gauges were 120 Ω, 5 mm foil gauges, compensated for steel at room temperature up to 80°C, and had a thermal output of ±2 με/°C. A two-component epoxy was selected for resistance to moisture and most chemicals.

6.5.3 Field Testing

The first year of testing (1997) included static truckload tests, ambient vibration tests, effect of temperature, and dynamic measurements under passing trucks. The second year of testing (1998) included static and dynamic truckload tests and ambient vibration tests. A single truck loaded to 395 kN was used for all the tests. Before the truck came onto the bridge, initial readings were taken and the wheels were moved onto the loading points at which time the readings were taken. In addition, crack patterns were mapped in August 1997, August 1998 and June 1999. Ten cable transducers and four accelerometers were temporarily used in 1998 to measure deflections and vibrations, respectively. Accelerometers were temporarily placed directly on the bottom flange.

6.5.4 Diagnostic Results

The two FOSs, all thermisters, and 100 of the 103 electrical strain gauges were functional after the construction of the bridge was completed. The three non-functional gauges were located in the side barriers, two on the stainless steel studs and one on the NEFMAC.

Strain measurements revealed that the location of the neutral axis in the negative moment region, where concrete is mostly in tension, was lower in 1998 compared to 1997. This observation indicated that, as expected, the concrete cracks in the negative moment region led to a reduction in the composite action between the steel girders and the concrete deck. The location of the neutral axis in the positive moment region did not change noticeably with time.

Measured girder deflections corresponding to the tests in 1997 and 1998 showed an improvement in load distribution characteristics. The improvement in load distribution characteristics can arguably be attributed to the decrease in effective flexural rigidity of the composite girders due to slab cracking in the negative moment regions. With a single truck on the right lane, the bridge was excited at a frequency of 3.5 Hz in its second vertical mode. For this frequency, the dynamic factor was always less than 1.15, and the damping ratio was 1.3 percent of critical. As of June 1999, cracks visible on the bottom surface of the bridge deck showed no serviceability concern. All the cracks were considered caused by temperature and shrinkage, and were less than 0.4 mm in width. Transverse cracks were observed immediately after construction in 1997. The longitudinal cracks at the bottom surface were seen in 1998. Observations in 1999 confirmed that crack growth has been retarded.

6.6 Taylor Bridge

Location: Headingley, Manitoba
Opened to Traffic: October 1997

References:

1. Rizkalla et al. (1998).
2. Shehata and Rizkalla (1999).
3. Wardrop Engineering Inc. (1999).
4. Korany and Rizkalla (2000).
5. Web site: www.isiscanada.com

6.6.1 Bridge Description

The Taylor Bridge is located on Provincial Road No. 334 over the Assiniboine River in the Parish of Headingley, Manitoba. It is the world's largest span bridge that uses FRP for shear reinforcement, pre-stressing of the main girder, and a FOS system for remote monitoring. The 165 m long bridge, shown in Figure 6.10 , consists of 40 pre-stressed concrete AASHTO-type girders. The bridge is divided into five equally simple spans of 33 m. Each span consists of eight, 1.8 m deep, I-shaped pre-cast, pre-stressed concrete girders. Four girders of the Taylor Bridge were pre-stressed by two different types of CFRP, using straight and draped tendons. Two girders were reinforced for shear using double-leg CFCC, and Leadline stirrups protruded from the girders to provide composite action between the deck and the girders.

Figure 6.10 Side elevation of Taylor Bridge

A 16×18 m portion of the 275 mm thick deck slab was reinforced with CFRP Leadline bars. This deck portion represents one-half of the width of the bridge. The rest of the deck slab was reinforced with conventional steel reinforcement. Two layers of GFRP bars, known commercially as C-Bar, were used to reinforce a 14.2 m portion of the Jersey-type barrier wall. The barrier wall was connected to the deck slab by double-headed stainless steel bars. Bridge girders, pre-stressed and reinforced by CFRP, were designed to behave similarly to the other girders of the bridge reinforced and pre-stressed with steel under service loading conditions. The pre-stressing force and the eccentricity of the reinforcement were kept the

same for all girders. The initial pre-stressing level was 60 percent of the guaranteed ultimate tensile strength for CFRP pre-stressing bars, compared to 75 percent for steel strands. Manitoba Highways and Transportation conservatively estimates the design service life of this bridge built with innovative materials as 75, compared to 50 years for conventional structures.

6.6.2 Instrumentation for Monitoring

Monitoring technology for the Taylor Bridge is shown schematically in Figure 6.11. Fibre Bragg Grating (FBG) sensors were used to monitor the strains in the CFRP reinforcement of the girders, the deck slab of the Taylor Bridge, and in the GFRP reinforcement of the barrier wall. The FBG sensors used in the Taylor Bridge were fabricated by ElectroPhotonics Corporation and have a full range of 10,000 microstrain.

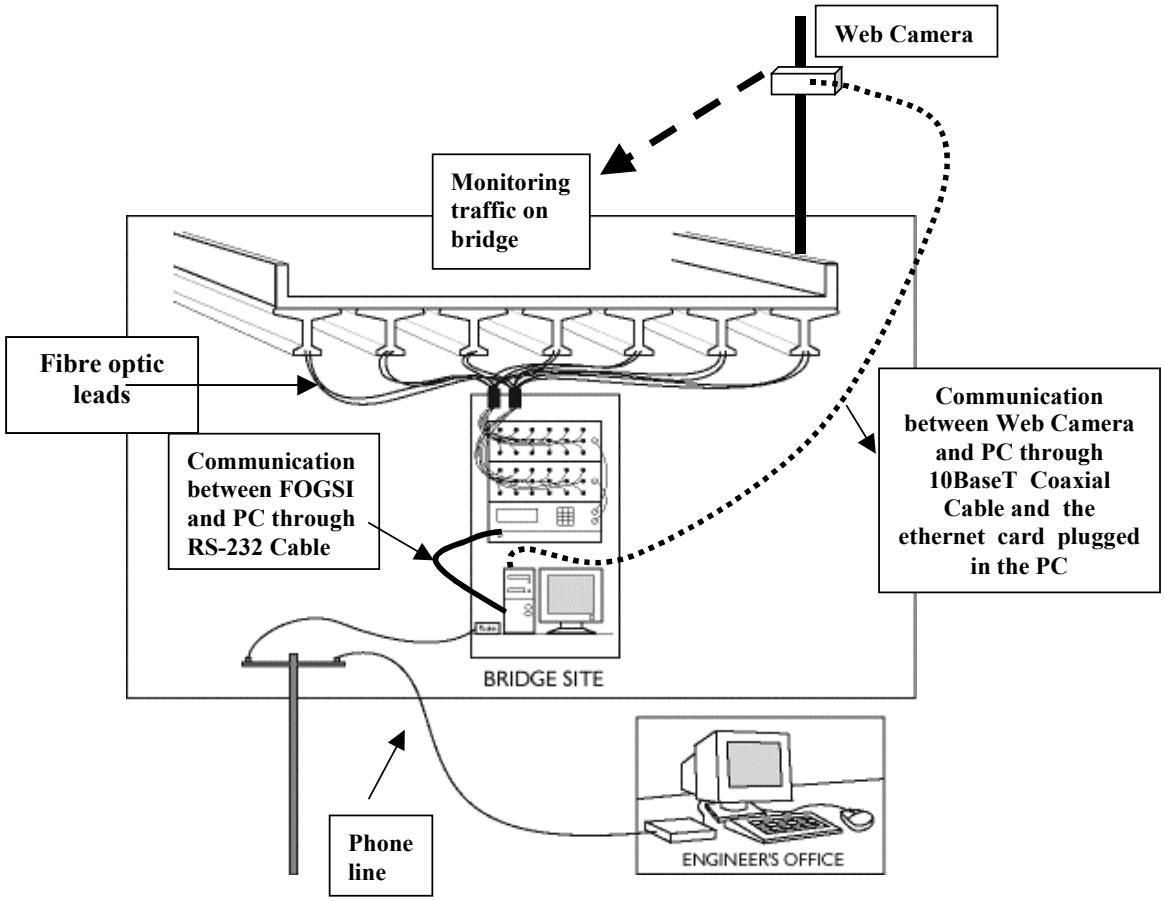

Figure 6.11 Layout of monitoring systems in Taylor Bridge

A total of 65 fibre optic sensors were installed on the reinforcements of the structural members. Out of the 65 sensors, 63 were single FBG sensors and the remaining were multiplexed FBG sensors. As shown in Figure 6.12, these 65 sensors were installed on the following bridge components: the girders reinforced by CFRP; selected girders reinforced by steel; the deck slab reinforced by CFRP; and the barrier wall reinforced by GFRP. In

addition, 20 thermocouples were used at different locations on the bridge in order to compensate for temperature effects. A 32-channel fibre optic grating indicator, the FLS3500R, was used to take strain measurements. The system as connected to a computer to download the strain readings using a telephone line. The bridge is also being monitored by 26 conventional electrical strain gauges mounted on the reinforcement to verify the FOS readings. A 32-channel data logging system (CR 10X) and two 16-channel multiplexing units were used for strain measurements. This system is also connected to an internal modem to download the strain data using an additional telephone line. Both the fibre optic multiplexing units and the data logging system were installed in a heated enclosure located in the cross diaphragm under the bridge deck slab.

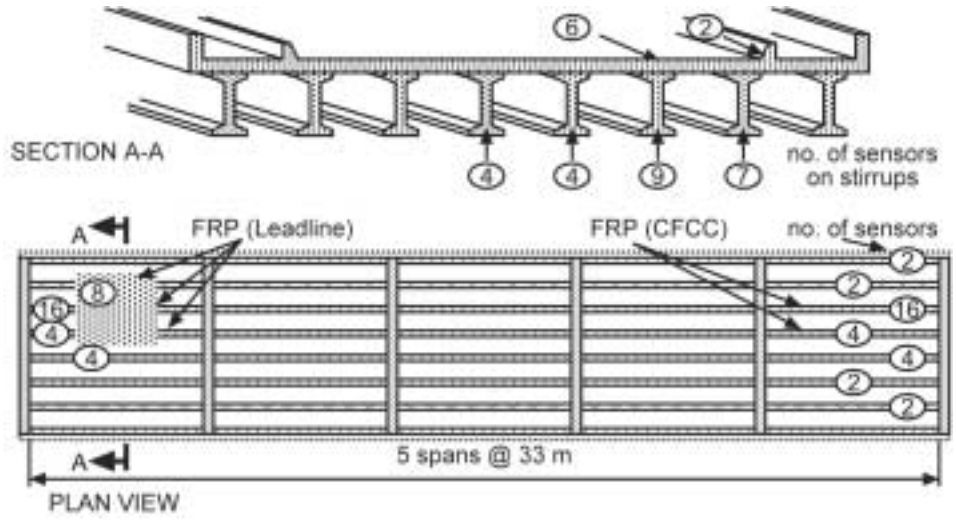

Figure 6.12 Sensor locations on the Taylor Bridge

Since January 1998, the FLS3500R has been programmed to read 32 strain sensors and 20 temperature sensors, and transmit the signals of ten selected strain sensors and 11 selected temperature sensors to the resident computer through the RS232 communication port, every 24 seconds. The modem was installed and activated in the resident computer through a telephone line. The bridge was also monitored with a camera operating in the Java Image Feed mode, continuously taking photographs that correlated with corresponding peak strain readings.

6.6.3 Diagnostic Results

FBG sensors were installed on the CFRP tendons at the end of the bridge girders in order to measure effective stress level in the tendons after release of the pre-stressing force. The strain in the CFRP pre-stressing tendons was also monitored during transportation of the girders to the bridge site. There was no significant change in the strain of the CFRP pre-stressing tendons. Diagnostic test results from monitoring can be expressed in terms of the following stages.

Load Testing of the Bridge: The output signal of a FBG sensor installed on a CFRP pre-stressing tendon at mid-span was recorded every 0.24 seconds during a test loading produced by a slow moving truck and trailer. It can be concluded from Figure 6.13, that a

36 t truck induces a strain as high as 15 microstrain in the CFRP Leadline bars. It should be mentioned that the initial pre-stressing strain was 800 microstrain (0.0080) and the ultimate strain was 13600 microstrain (0.0136). Frequent load tests will evaluate the performance of the bridge girders reinforced by CFRP.

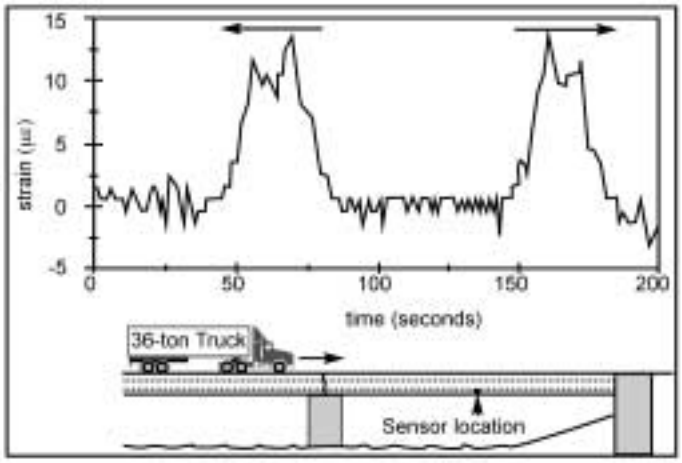

Figure 6.13 Strain responses for moving truck

Long-term Behaviour Due to Temperature Effect: Loss in the pre-stressing forces was detected by strains in the CFRP reinforcements. Figures 6.14, 6.15, and 6.16 show the variation in strain and temperature of a CFRP pre-stressing tendon over three periods of seven days in February 1998, October 1998, and June 1999, respectively. The strain and temperature were recorded every 24 seconds.

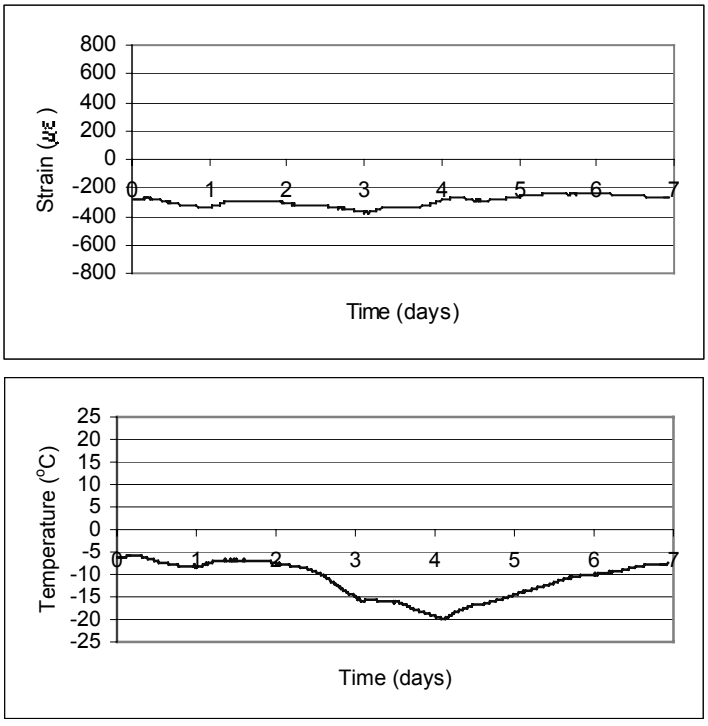

Figure 6.14 Strain and temperature data for long-term monitoring (February, 1998)

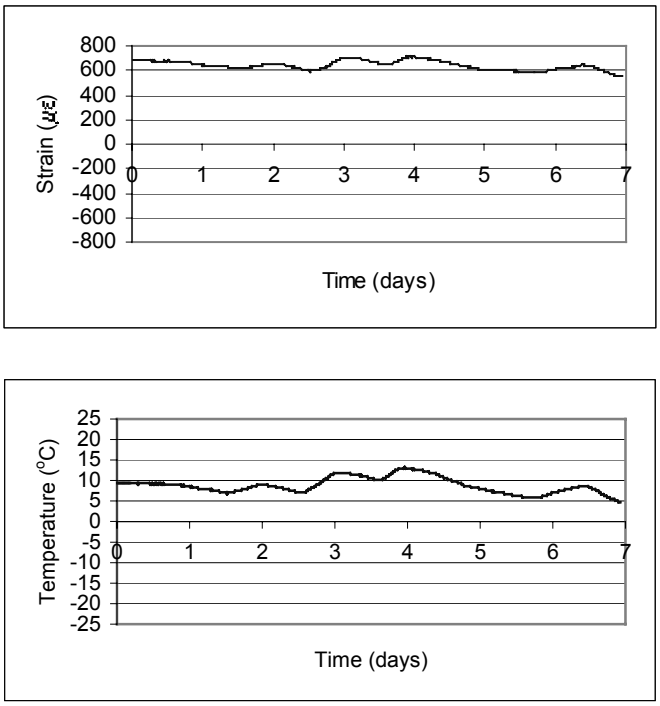

Figure 6.15 Strain and temperature data for long-term monitoring (October, 1998)

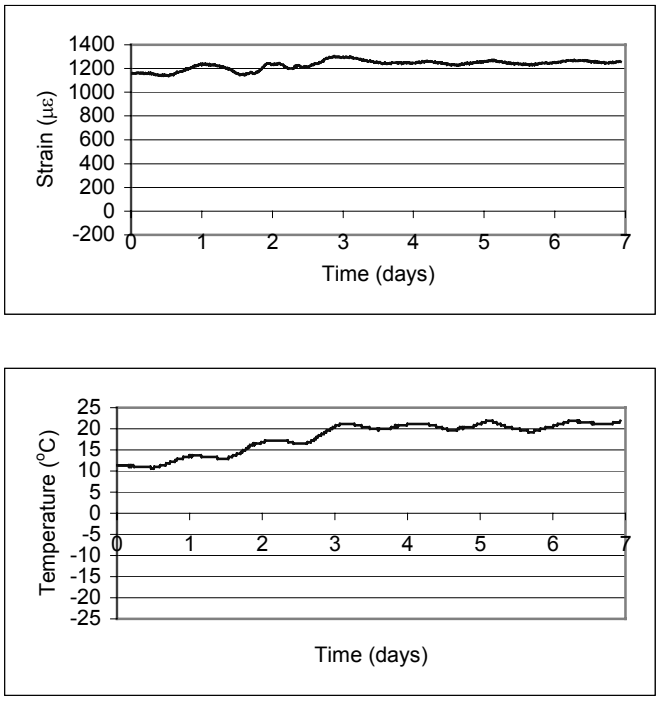

Figure 6.16 Strain and temperature data for long-term monitoring (June, 1999)

6.7 Joffre Bridge

Location: Spanning over the Saint François River in Sherbrooke, Québec
Opened to Traffic: December 1997

References:
1. Benmokrane et al. (2000).
2. Web site: www.isiscanada.com

6.7.1 Bridge Description

The Joffre Bridge, crossing over the Saint-François River in Sherbrooke, Québec, was originally built in 1950. The bridge was reconstructed in 1997 following severe deterioration of the concrete deck slab and girders, arising from reinforcement corrosion. The bridge is a two-lane, steel-concrete composite structure, consisting of five spans of different lengths between 26 m to 37 m, and five girders at a spacing of 3.7 m. The thickness of the concrete deck slab is 260 mm. The structural design was carried out according to guidelines available in the Canadian Standard (CSA A23.3 1994) for conventional steel-reinforced concrete structures for carrying CS-615 Canadian truck loading. The selected part of the deck slab (7.3×11.5 m) was reinforced with CFRP reinforcement. Refer to Figure 6.17.

Figure 6.17 Joffre Bridge - Sherbrooke, Québec

The reinforcement near the top surface of the slab comprises CFRP grids, with steel rebars placed at the bottom. The main CFRP reinforcement consists of ten CFRP grids, each 3.6 m long and 2.3 m wide.In addition, a total of 12 CFRP grids, 2.3×1.15 m, were used in laps on the joints of the main CFRP reinforcement grids, in both the longitudinal and transverse directions. The grids were placed in such a way that the longitudinal spacing was 200 mm and the transverse spacing was 100 mm, with reference to the deck slab. The cross-section of the CFRP grid is about 2000 mm^2/m in the transverse direction of the slab (reinforcement ratio 1.0 percent). The steel reinforcements consist of 15 mm diameter deformed rebars at a spacing of 150 mm, centre to centre (i.e. reinforcement ratio 0.66 percent). Concrete covers of 60 mm and 35 mm at the top and bottom of the slab, respectively, were initially recommended for this project.

6.7.2 Instrumentation for Monitoring

The bridge is extensively instrumented with three types of gauges (FOSs, vibrating wire strain gauges, and resistance strain gauges) for a total of 180 critical locations in the concrete deck slab and on the steel girders. A total of 44 FOSs were installed for strain and temperature monitoring, including 26 Fabry-Perot strain fibre optic sensors (SFO) bonded on the CFRP NEFMAC grid, six Fabry-Perot (SFO) sensors integrated into the CFRP NEFMAC grid, two Fabry-Perot temperature fibre optic sensors (TFO) and two Fabry-Perot (EFO) embedded in the concrete, three Fabry-Perot strain fibre optic weldable senors (SFO-W) welded on the steel girder, three FBG sensors bonded on the CFRP NEFMAC grid, and one Fabry-Perot (SFO) and one FBG sensor bonded on the CFRP NEFMAC bar for thermal strain monitoring. Table 6.1 summarizes sensor placement in the Joffre Bridge.

Table 6.1 - List of Fibre Optic Sensors in the Joffre Bridge

Sensor Types	Method of Instrumentation and Location	Quantity	Comments
Fibre Optic (SFO)	Integrated in CFRP NEFMAC grid of bridge deck slab	6	Strain
Fibre Optic (SFO)	Bonded to CFRP NEFMAC rod	1	Thermal Strain
Fibre Optic (SFO)	Bonded on CFRP NEFMAC grid of bridge deck slab	26	Strain
Fibre Optic (EFO)	Embedded in concrete bridge deck	2	Strain
Fibre Optic (SFOW)	Welded on web of middle steel girder	3	Strain
Fibre Optic (TFO)	Embedded in concrete deck slab	2	Temperature
Bragg Grating	Bonded on CFRP NEFMAC grid of bridge deck slab	3	Strain
Bragg Grating	Bonded to CFRP NEFMAC rod	1	Thermal Strain

6.7.3 Diagnostic Results

After the successful execution of construction and instrumentation of the sensors, the bridge was opened to traffic. Since then, static and dynamic responses of different components of the bridge are recorded regularly using computer-aided data logging systems. It was found that the temperature obtained from the Fabry-Perot TFO FOS embedded in the concrete of the bridge deck varies with time, being lower in the winter and higher in the summer. The recorded thermal strain of the NEFMAC bar from the bonded Fabry-Perot SFO FOS is small, representing a small increase with temperature. The strain values of the CFRP NEFMAC grid reinforcement obtained from the bonded and integrated Fabry-Perot SFO FOSs are almost the same, correspondingly varying with temperature and exhibiting almost the same variation with time as with temperature. Both the bonded and integrated Fabry-Perot SFO FOSs recorded a maximum strain variation of about 200×10^{-6} mm/mm in the CFRP NEFMAC grid. The variation of recorded strain with time and temperature clearly indicates that it is possible to obtain meaningful and consistent results from FOS, and that temperature is the dominant factor influencing the strain variation in the bridge deck.

6.8 Waterloo Creek Bridge

Location: Fanny Bay area in Vancouver Island, British Columbia
Opened to Traffic: March 1998

References:
1. Bakht and Mufti (1998).
2. Tsai and Ventura (1999).
3. Web site: www.isiscanada.com

6.8.1 Bridge Description

The Waterloo Creek Bridge is located in the southeast portion of the City of Courtenay at the intersection of the new Inland Island highway alignment and Waterloo Creek. It is designed to carry four lanes of traffic. A side view of the bridge and its half cross-section is shown in Figures 6.18 and 6.19. The bridge consists of two independent, parallel, single-span cast-in-place concrete deck structures supported by pre-stressed concrete I-girders. Each deck carries two lanes of traffic in a single direction. The northbound structure is constructed with a steel-free slab deck, while the southbound structure is built with a traditional steel reinforced concrete deck slab. Both bridge decks are approximately 25 m long, and 12.2 m wide with a 10° skew angle.

Figure 6.18 Waterloo Creek Bridge

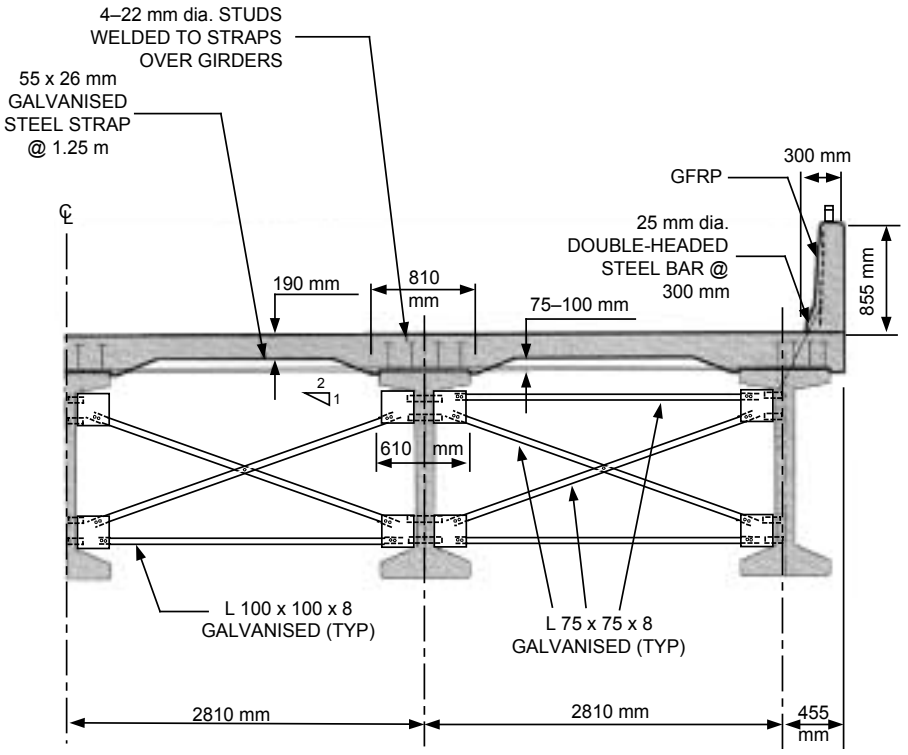

Figure 6.19 Waterloo Creek Bridge half cross-section

The northbound structure of the Waterloo Creek Bridge is the first steel-free deck slab constructed with pre-stressed I-girders. This bridge is the first integral abutment bridge to have a steel-free deck slab. The deck is 190 mm thick with a polypropylene fibre reinforced concrete slab with no internal steel reinforcement. Each deck is supported by five 1473 mm pre-stressed concrete I-girders that are built monolithically with 1000 mm thick common abutments. The spacing of the girders is 2810 mm. At the ends of the steel-free deck slab, longitudinal steel reinforcement is placed to ensure a monolithic connection between the deck and the abutment. The foundation of each abutment consists of twelve 460 mm diameter open-ended steel pipe piles.

The steel-free deck slab eliminates the problem of steel corrosion within the deck, thereby reducing maintenance costs during the service life of the bridge. The straps are equally spaced, 1.25 m apart, across the top of the adjacent girders to provide transverse restraint, and the fibre reinforced concrete functions as a compressive arching membrane.

6.8.2 Bridge Instrumentation for Monitoring

The northbound structure is instrumented with a total of 53 sensors at various components and locations on the bridge. This includes 32 foil strain gauges, ten TML embedment strain transducers, five Micro-Measurement embedment strain gauges, two Smart Rod sensors and four FOSs. The 53 sensors were installed during construction of the bridge. In addition, a total of 11 sensors, including six TML embedment strain transducers and five Micro-Measurement embedment strain gauges, were installed in the southbound structure at the same time. The details of sensor types and locations are listed in Table 6.2.

Table 6.2 - Sensor Types and Locations in Waterloo Creek Bridge		
Sensor Types	**Location**	**Quantity**
For Northbound Structure		
Foil Strain Gauge	Abutment	6
	Steel Straps	6
	Bracing	8
	Deck/Abutment	8
	Parapet/Deck	4
Fibre Optic Sensor	Steel Straps	2
	Steel-free Deck	2
TML Embedment Strain Transducer	Girder	4
	Steel-free Deck	6
Smart Rod Sensor	Steel-free Deck	2
Micro-measurement Embedment Gauges	Steel-free Deck	5
Total		**53**
For Southbound Structure		
TML Embedment Strain Transducer		6
Micro-measurement Embedment Gauges	Bridge Deck	5
Total		**11**

The data acquisition system used for the Waterloo Creek Bridge consists of a sensor connector array panel, 16 amplifier modules for signal conditioning, a 16-channel LS4 Data Logger by Lakewood Systems Ltd., an eight-channel StressNet System from Arbutus Cove Systems Inc., a Pentium 166 MMX portable computer and strain indicator model P-350 from Vishay Instruments.

In order to monitor the performance of the bridge, 24 sensors at various locations were selected to measure strains at regular time intervals. The data has been collected with two data acquisition systems. Both were installed at the site in October 1998. The Lakewood Data Logger and the StressNet system can both provide gauge excitation, signal conditioning and analog to digital conversion. Sampling rate setting, data retrieving and sensor calibration can be done on both systems by installing the corresponding data application software on a portable personal computer.

6.8.3 Diagnostic Results

Since the installation of the two data acquisition systems, the Lakewood Data Logger has been working properly in the field, collecting measured data from selected groups of 16 sensors. The StressNet System was installed to take measurements at a high sampling rate over a short period of time. A total of 12 site visits to download the measured data were undertaken between October 1998 and June 1999. The data were measured manually by using a model P-350A strain indicator. During site visits, the data collected by the data logger were downloaded. After construction, a single longitudinal crack developed in each panel of the deck. In the mid panel, the cracks were along the entire length of the bridge.

6.9 Sainte Emelie-de-l'Energie Bridge

Location: Near Saint-Emelie-de-l'Energie in the Laurentides-Lanaudiere Region, Québec.
Opened to Traffic: October 1998

References:

1. Labossiere et al. (2000).
2. Web site: www.isiscanada.com

6.9.1 Bridge Description

The Sainte Emelie-de-l'Energie Bridge, over the Noire River on Route 131, was originally built in 1951. Refer to Figure 6.20. This is a one-span bridge, 21.3 m in length, with four parallel reinforced concrete beams and a participating slab forming T-sections with spacing of 2.74 m. The total width of the bridge is 11.1 m, and the traffic lanes occupy 9.1 m. According to the Ministry of Transportation of Québec (MTQ) the Live Load Reduction Factor (LLRF) of the bridge is 0.94. Using the S6-88 standard and truckload QS-660, it was found that the flexural strength would have to be raised by 35 percent, and the shear strength by 20 percent. No significant spalling of concrete or degradation of steel rebar through corrosion, combined with the required level of reinforcement and the general condition of the bridge, made this bridge appropriate for full-scale experimentation.

Figure 6.20 Sainte Emelie-de-l'Energie Bridge - Québec

Repair work was performed in the fall of 1998. The bridge remained open to traffic during the repair period, but the lanes where FRP was being installed were closed in alternation. Carbodur strips (CFRP) were used for flexural reinforcement and Sikawrap Hex 100G (GFRP) was used for shear reinforcement. The U-shaped stirrups were wrapped around the sections, with fibres in the vertical direction, locally covering the longitudinal CFRP reinforcement in the process. The total quantity of composites installed in the bridge amounts to 490 linear meters of Carbodur strips and 210 m^2 of Sikawrap Hex 100G.

6.9.2 Instrumentation for Monitoring

In order to evaluate the structural efficiency of the FRP strengthening, the Sainte Emelie-de-l'Energie Bridge was instrumented with conventional resistance strain gauges, Fabry-Perot gauges, FBG sensors and thermocouples. A total of 66 sensors were installed in exterior and interior beams of the bridge deck. Among those 28 strain gauges, eight Fabry-Perot sensors and 20 FBG sensors were instrumented on the steel rebars, FRP reinforcements, and the top of the beam. Ten thermocouples were installed permanently to help correct potential errors due to temperature effects. Sensor locations are summarized in Table 6.3. The positions of the sensors were selected to validate the data obtained from the experimental FOSs and to provide complementary readings from various types of instruments. Other instruments used during the tests included two load cells per beam to measure strains at mid-span, and one displacement sensor under each beam. Accelerometers were also used for a number of dynamic tests.

Table 6.3 - Sensor Details in Sainte Emile-de-l'Energie Bridge

Sensor Types	Sensor Instrumented With	Number of Sensors			Total
		West End	Mid Span	East End	
Strain Gauges	Steel Rebars		4+4		8
	FRP	4+4	2+2	2+2	16
	Top of the Beam		2+2		4
Fabry-Perot	Steel Rebars		1+1		2
	FRP	0+4	1+1		6
Bragg Grating	Steel Rebars		2+2		4
	FRP	4+0	2+2	2+2	12
Thermocouple	Top of the Beam		2 + 2		4
	Steel Rebar		2 + 2		4
	FRP	1 + 1	2 + 0	1 + 1	6
Total					**66**

6.9.3 Field Testing

Static load tests were performed on the bridge using three, 33 t, four-axle trucks to apply simulated traffic loading to the structure. Four different loading paths were identified as axis A to D on the bridge plan view. For dynamic load tests, three trucks were successively driven across the bridge at moderate speed, braking at the middle of the bridge. The bridge was loaded with a single truck in each of the four paths, then with combinations of two and three trucks.

6.10 Hall's Harbour Wharf

Location: Hall's Harbour, Nova Scotia
Opened to: December 1999

References:
1. Newhook (1999).
2. Newhook et al. (2000).
3. Web site: www.isiscanada.com

6.10.1 Structure Description

Hall's Harbour is a small craft fishing harbour on the Bay of Fundy Shore, in Nova Scotia. The original wharf structure was constructed in 1904 and retrofitted several times over the years. During an Atlantic storm on February 15, 1998, a 40 m section of timber piles failed, as shown in Figure 6.21.

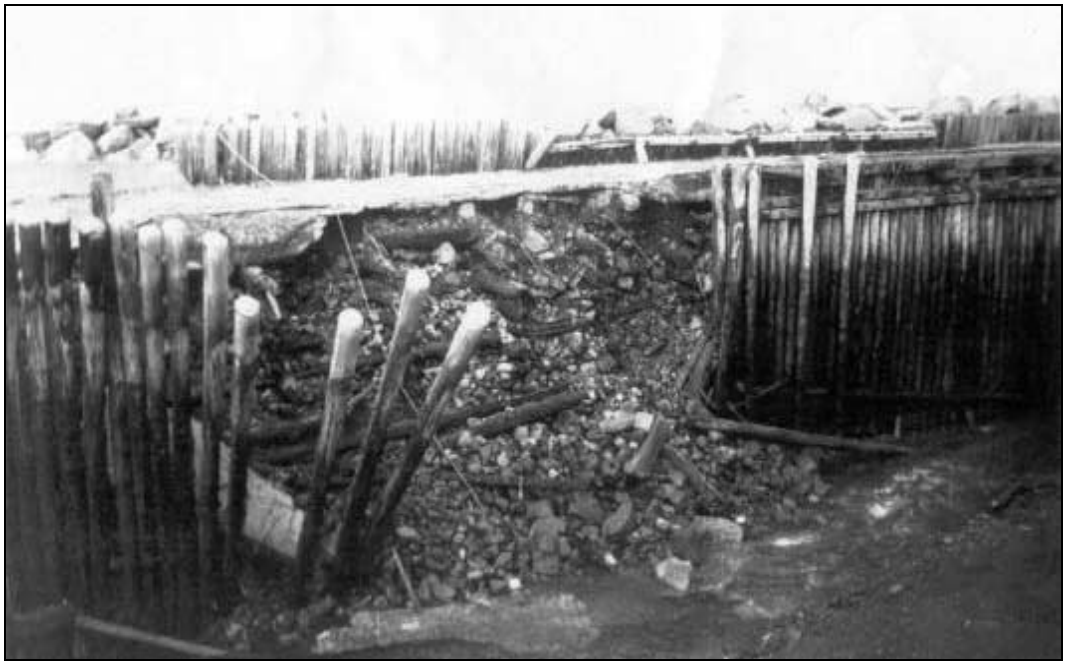

Figure 6.21 Failure of timber piles in Hall's Harbour

The damaged segment was replaced by an innovative structure using new materials and technologies, as shown in Figure 6.22. Research showed that by using innovative materials and technologies, initial capital costs were higher than those associated with using conventional methods, but the life-cycle maintenance costs should actually be reduced. The initial capital cost of the GFRP reinforcements and steel-free deck was about $20,000 more than conventional steel reinforced concrete, increasing the overall cost of the Hall's Harbour project by about 4.5 percent.

Figure 6.22 Hall's Harbour Wharf – Nova Scotia

The new structure is built with concrete deck panels on deep concrete beams (pile caps) spaced at 4 m intervals. The transverse section of the deck panel and structure is shown in Figure 6.23. The transverse beams are supported on piles at the front face, and a retaining structure at the back. The construction depth of the deck, including pile cap, is 1 m. It is built over the top of the existing wharf in order to achieve the desired increase of wharf elevation. The pile cap beams are designed to be composite with the deck slab (square 700×700 mm) and carry the entire dead load and construction live loads. The pile caps and bents have some steel reinforcement; however, reinforcement under serviceability loads is by GFRP rods. The deck panels contain synthetic fibre reinforced concrete and utilize the arching action of the slab.

The panels also contain GFRP rods to reinforce against the uplift force that is created by wave action during extreme storms. The steel straps are encased in grout-filled polyvinyl chloride (PVC) tubes to provide an economical means of achieving durability in the marine environment. Due to the absence of steel reinforcements (and the elimination of corrosion), the projected life of the wharf is increased from approximately 30 years to between 60 and 80 years, with minimum maintenance. The inclusion of fibre optic monitoring technology embedded in the GFRP rods will provide useful data to support the application of the FRPs in other marine environment structures.

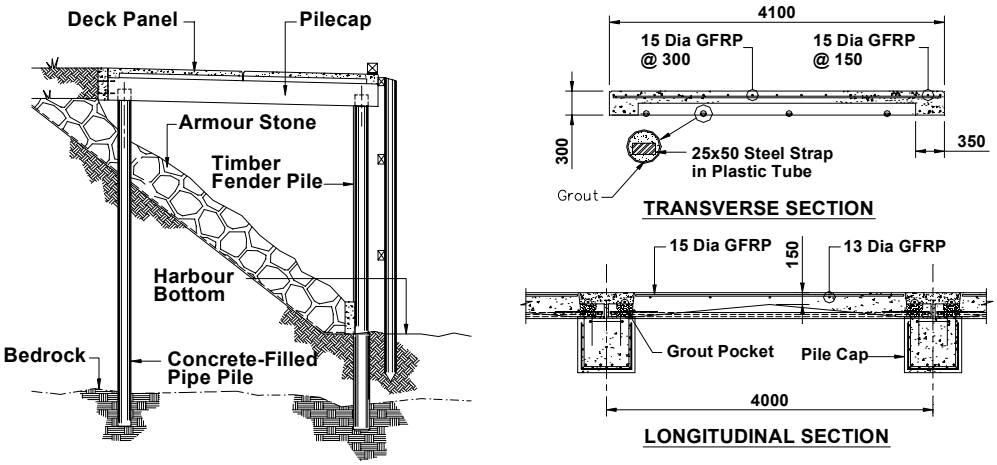

Figure 6.23 Transverse section and deck panel section of the new structure

6.10.2 Instrumentation for Monitoring

The structure was instrumented with FOSs to monitor its durability and performance. A total of 35 sensors were installed in different parts of the structures. Sensor locations distributed in panels and beams of the structure are shown in Figure 6.24. Eighteen Fabry-Perot sensors were attached in two pile cap beams in one panel. Seven FBG sensors were installed in two pile cap beams, one panel and two straps. Foil gauges were installed as checks on the FOSs. Currently, the Fabry-Perot fibre optic sensor datalogger, and a RocTest DMI unit is being remotely monitored via phonelines, from various research locations across Canada.

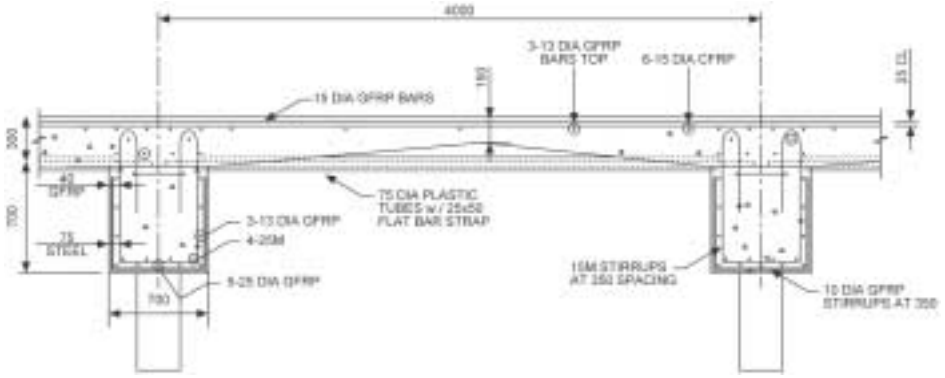

Figure 6.24 Sensor locations shown in cross-sectional view

7 NOTATION AND DEFINITIONS

7.1 Notation and Definitions

A_i	Modal amplitude or modal ratio
AASHTO	American Association of State Highway and Transportation Officials
ANPSD	Average normalized power spectral density
B_m	Equivalent base length
CFRP	Carbon fibre reinforced polymer
CHBDC	Canadian Highway Bridge Design Code
CR-10x	Campbell recorder – 10x
CS-615	Canadian standard – 615, for truck loading
DLA	Dynamic load allowance
FBG	Fibre Bragg Grating
FLS3500	Fibre light sensor 3500 read out unit (Fibre optic grating strain indicator, ElectroPhotonics Corporation)
FOS	Fibre optic sensor (s)
FRP	Fibre reinforced polymers
f_i	Natural frequency
g	Acceleration of gravity
GFRP	Glass fibre reinforced polymer
I	Dynamic amplification factor
K	Ratio of required proof load to legal load
L	Span length
L_n	Load effect due to unfactored live loads
LLRF	Live load reduction factor
LS4	Lakewood Systems 16 channel datalogger
LVDT	Linear variable differential transformer
MTO	Ministry of Transportation of Ontario
MTQ	Ministry of Transportation of Quebec
NFEMAC	Grid type fibre composite material for reinforcing concrete
OHBDC	Ontario Highway Bridge Design Code
PVC	Polyvinyl chloride
P-350	Strain indicator model of Vishay Instruments
RS-232	Recommended standard-232 (Electronic Industries Association)
QS-660	Quebec standard – 660, for truck loading
SFO	Strain fibre optic sensor
SFO-W	Strain fibre optic weldable sensor
SHM	Structural health monitoring
TFO	Temperature fibre optic sensor
TML	Tokyo Measuring Instruments Laboratory
W	Total vehicle load
α_L	Live load factor
δ_{max}	Maximum deflection under the vehicle travelling at normal speed
δ_{min}	Minimum dynamic deflection in the cycle of vibration containing δ_{max}
δ_{stat}	Maximum deflection under the vehicle travelling at crawling speed
δ'_{stat}	Maximum deflection obtained from the curve of median deflections
δ_1	Static deflection corresponding to δ_{max}
δ_2	Median deflection corresponding to δ_{max}
δ^*_s	Static deflection at the same location where Δ_1 is recorded
Δ_1	Maximum difference between dynamic and static deflections

Δ_2	Maximum difference between dynamic and median deflections
Δ_3	Difference between dynamic and static deflections at the same load location that causes δ_{stat}
Δ_4	Difference between dynamic and median deflection at the same load location that causes δ'_{stat}

8 REFERENCES AND BIBLIOGRAPHY

8.1 References and Bibliography

Abe, M., Fujino, Y., Kajikura, T., Yanagihara, M., and Sato, M., (1999). *"Monitoring of a Long Span Suspension Bridge by Ambient Vibration Method,"* Structural Health Monitoring, Technomic Publication, Lancaster, PA., USA, pp.400-407.

Afhami, S., and Cheng, J.J.R., (1999). *"Field Instrumentation and Monitoring of Crowchild Trail Bridge in Calgary, Alberta"*, Project Report, University of Alberta.

Agarwal, A.C., (1990). *"Load Testing of New Concrete Bridge Deck Slabs,"* Developments in Short and Medium Span Bridges '90, Canadian Society for Civil Engineering, Montreal, Québec, Canada, pp. 277-289.

Agarwal, A. C., (1991). *"Burlington Skyway Expansion Joint Testing,"* Structures Research Report SRR-91-02, Ministry of Transportation of Ontario, Downsview, Ontario, Canada.

Aktan, A.E., Tsikos, C.J., Catbas, F.N., Grimmelsman, K., and Barrish, R. *"Challenges and Opportunities in Bridge Health Monitoring",* Proceeding of the 2nd International Workshop on Structural Health Monitoring, Stanford University, Stanford, CA, pp.461-473.

Agarwal, A.C., and Cheung, M.S.,(1987). *"Development of Loading Truck Model and Live Load Factor for the Canadian Standards Association CSA-S6 Code,"* Canadian Journal of Civil Engineering, Vol. 14(1).

Ali, A., Bakht, B., and Schaefer, J., (1997). *"Design and Construction of a Steel-free Deck Slab in Ontario,"* Proceedings, CSCE Annual Conference, Vol. 6, pp. 81-90.

ASTM E251, (1992). *"Standard Test Method for Performance Characteristics of Bonded Resistance Strain Gauges".*

ASTM E1237, (1993). *"Standard Guide for Installing Bonded Resistance Strain Gauges".*

Azarnejad, A., Mayne, D., and Brown, T.G., (1999). *"Ice Dynamics and Load Measurements".* Proceedings of OMAE99, 18th International Conference on Offshore Mechanics and Arctic Engineering, St. John's, Newfoundland, Canada.

Bakht, B., (1981). *"Testing of the Manitou Bridge to Determine its Load Carrying Capacity,"* Canadian Journal of Civil Engineering, Vol. 8(2).

Bakht, B., (1988). *"Testing of an Old Short Span Slab-on-girder Bridge,"* Structures Research Report SRR-88-01, Ministry of Transportation of Ontario, Canada.

Bakht, B., Billing, J.R., and Agarwal, A.C., (1992). Discussion of *"Wheel Loads from Highway Bridge Strains: Field Studies."* ASCE Journal of Structural Engineering, Vol. 116 (9).

Bakht, B., and Csagoly, P.F.,(1979). Bridge Testing. *"Structures Research Report 79-SRR-10,"* Ministry of Transportation of Ontario, Canada.

Bakht, B., and Csagoly, P.F., (1980). *"Diagnostic Testing of a Bridge,"* ASCE Journal of the Structural Division, Vol. 106 (7).

Bakht, B., and Jaeger, L.G., (1987). *"Behaviour and Evaluation of Pin-connected Steel Truss Bridges,"* Canadian Journal of Civil Engineering, Vol. 14(3).

Bakht, B., and Jaeger, L.G., (1990a). *"Observed Behaviour of a New Medium Span Slab-on-girder Bridge,"* Journal of the Institution of Engineers (India).

Bakht, B., and Jaeger, L.G., (1990b). *"Bridge Testing - a Surprise Every Time,"* ASCE Journal of Structural Engineering, Vol. 116(5).

Bakht, B., and Mufti, A.A., (1998). *"Five Steel-free Deck Slabs in Canada,"* Structural Engineering International, Vol. 8(3), pp. 196-200.

Bakht, B., and Mufti, A.A., (1999). *"Testing of Two Shear-connected Concrete Plank Bridges,"* Technical Report of JMB Structures Research Inc., submitted to BC Ministry of Forests.

Bakht, B., and Mufti, A.A., (1992a). *"Behaviour of a Steel Girder Bridge with Timber Decking,"* Structures Research Report SRR-92-02. Ministry of Transportation of Ontario, Canada.

Bakht, B., and Mufti, A.A., (1992b). *"Evaluation by Testing of a Bridge with Girders, Floor Beams and Stringers,"* Structures Research Report SRR-91-05, Ministry of Transportation of Ontario, Canada.

Bakht, B., and Mufti, A.A., (1992c). *"Evaluation of a Deteriorated Concrete Bridge by Testing,"* Proceedings, 4th International Colloquium on Concrete in Developing Countries, held in Kingston, Jamaica, Canadian Society for Civil Engineering.

Bakht, B., Mufti, A.A., and Francis, J., (1999). *"Transverse Load Distribution in Sawn Timber Bridges,"* CSCE Annual Conference, Vol. I, pp. 61-71.

Bakht, B., and Pinjarkar, S.J., (1990). *"Review of Dynamic Testing of Bridges,"* Transportation Research Record 1223, Transportation Research Board, Washington, D.C., USA.

Bemokrane, B., Zhang, B., Lord, I., Nicole, J.F., and Masmoudi, R., (2000). *"Application of Fibre Optic Sensors for Structural Health Monitoring of Bridges and Other Structures"*, Research Report, University of Sherbrooke, Québec.

Biggs, J.M., and Suer, H.S., (1956). *"Vibration Measurements on Simple-span Bridges,"* Highway Research Board Bulletin 124, Highway Research Board, Washington, D.C., USA.

Black, C., and Ventura, C.E., (1998). *"Ambient Vibration Measurements of the Lindquist Bridge,"* UBC Earthquake Engineering Research Lab, University of British Columbia.

Cawley, P., and Adams, R.D. (1979). "*The Location of Defects in Structures from Measurements of Natural Frequencies*," Journal of Strain Analysis, Vol. 14, 49-57.

Chan, H.C., and O'Connor, C., (1990). *"Wheel Loads from Highway Bridge Strains: Field Studies,"* ASCE Journal of Structural Engineering, Vol. 116 (7).

Chang, F.-K., (1999) (Editor). *"Structural Health Monitoring 2000 Workshop,"* Proceedings of the 2nd International Workshop, Stanford University, CA, USA.

Chase, S.B, (1999). *"Dynamic and Field Testing of Bridges in the New Millennium: A Look Forward, a Discussion of the Most Important Aspects, Issues, Policies, and Proceedings Relating to Testing and Evaluation of Bridges,"* a White Paper Prepared for the Transportation Research Board Committee A2C05 Dynamics and Field Testing of Bridges.
CHBDC, (2000). *Canadian Highway Bridge Design Code*, Canadian Standards Association, Rexdale, Ontario, Canada.

Cheung, M.S., Tadros, G.S., Brown, T., Dilger, W.H., Ghali, A., and Lau, D.T. (1997). *"Field Monitoring and Research on Performance of the Confederation Bridge"*, Canadian Journal of Civil Engineering, 24(b), pp. 951-962.

Daniel, I. M., and Ishai, O., (1994). *"Engineering Mechanics of Composite Materials,"* Oxford University Press, New York, NY, USA.

Doebling, S.W., Farrar, C.R., Prime, M.B., and Shevitz, D.W. (1996). "*Damage Identification and Health Monitoring of Structural and Mechanical Systems from Changes in Their Vibration Characteristics: A Literature Review*," Los Alamos National Laboratory, Los Alamos, New Mexico, Report No. LA 13070-MS.

Doncaster, A.M., (1998). *"An Evaluation of Fibre Optic Sensors for Monitoring of Civil Engineering Structures"*, M.A.Sc. Thesis, Dalhousie University.

EDI., (1995). *U2, V2 and P2 Manuals*, Experimental Dynamic Investigations Ltd.

Erki, M.A., and Agarwal, A.C., (1995). *"Strengthening of Reinforced Concrete Axial Members Using Fibre Composite Materials - a Survey,"* Proceedings, CSCE Annual Conference, Vol. II, pp. 565-574.

Farrar, C.R, Baker, W.E., Bell, T.M., Cone, K.M., Darling, T.W., Duffey, T.A., Eklund, A., and Migliori, A. (1994). "*Dynamic Characterization and Damage Detection in the I-40 Bridge Over the Rio Grande*," Los Alamos National Laboratory, Los Alamos, New Mexico, Report No. LA 12767-MS.

Farrar, C.R., Duffey, T.A., Goldman, P.A., Jauregui, D.V., and Vigil, J.S. (1996a). "*Finite Element Analysis of the I-40 Bridge Over the Rio Grande*," Los Alamos National Laboratory, Los Alamos, New Mexico, Report No. LA 12979-MS.

Farrar, C.R., and Jauregui, D. (1996b). "*Damage Detection Algorithms Applied to Experimental and Numerical Modal Data from the I-40 Bridge*," Los Alamos National Laboratory, Los Alamos, New Mexico, Report No. LA 13074-MS

Fuller, A.H., Eitzen, A.R., and Kelly, E.F., (1931). *"Impact on Highway Bridges,"* Transactions ASCE, Vol. 95, Paper 1786.

Gu, W. M., (1982). *"A Simplified Method for Eliminating Error of Transverse Sensitivity of Strain Gauge,"* Experimental Mechanics, Vol. 22, No. 1, pp. 16-18.

Housner, G.W., Bergman, L.A., Caughey, T.K., Chassiakos, A.G., Claus, R.O., Masri, S.F., Skelton, R.E., Soong, T.T., Spencer, B.F., and Yao, J.T.P., (1997). *"Structural Control: Past, Present and Future"* Journal of Engineering Mechanics, ASCE, Vol. 123, No.9.

Jaeger, L.G., and Bakht, B., (1989). "Bridge Analysis by Microcomputer," McGraw Hill, New York, NY, USA.

Klipec, B.E., (1977). *"How to Avoid Noise Pickup on Wire and Cable,"* Instruments & Control Systems, Vol. 50, No. 12, pp. 27-30.

Korany, Y., and Rizkalla, S.H., (2000). *"Taylor Bridge...The New Generation"*, ISIS Technical Report.

Labossière, P., Neale, K.W., Rochette, P., Demers, M., Lamothe, P. Lapierre, and Desgagné, G., (2000). *"Fibre reinforced Polymer Strengthening of the Ste-Emelie-de-L'Energie Bridge: Design Instrumentation and Field Testing"*, Canadian Journal of Civil Engineering, Vol. 27, No. 5, pp.916-927.

Lee, C., (1998). *"Accelerated Corrosion and Repair of Reinforced Concrete Columns Using CFRP Wraps,"* Department of Civil Engineering, University of Toronto, M.A.Sc. Thesis.

Mallick, P. K., (1993). *"Fiber-reinforced Composites, Materials, Manufacturing, and Design,"* Second Edition, Marcel Dekker, Inc. New York, NY, USA.

Measurement Group Tech Note TN-501-2, (1992). *"Noise Control in Strain Gauge Measurements,"* Raleigh, NC, USA.

Measurement Group Tech Note TN-509, (1993). *"Errors Due to Transverse Sensitivity in Strain Gauges,"* Raleigh, NC, USA.

Meyer, M. L., (1967). *"A Simple Estimate for the Effect of Cross Sensitivity on Evaluated Strain Gauge Measurement,"* Experimental Mechanics, Vol. 7. pp. 476-480.

Morrison, R., (1986). *"Grounding and Shielding Techniques in Instrumentation,"* 3rd Edition, John Wiley & Sons, Inc., New York, NY, USA.

Mufti, A.A., Newhook, J.P., and Mahoney, M.A., (1999). *"Salmon River Bridge Field Monitoring,"* Proceedings, CSCE Annual Conference, Vol. I, pp. 51-60.

Mufti, A.A., Tadros, G., and Jones, P.R., (1997). *"Field Assessment of Fibre-Optic Bragg Grating Strain Sensors in the Confederation Bridge,"* Canadian Journal of Civil Engineering, Vol. 24, pp. 963-966.

Newhook, J.P, Bakht, B., Tadros, G., and Mufti, A.A., (2000). *"Design and Construction of a Concrete Marine Structure Using Innovative Technologies,"* ACMBS-III Conference Proceedings, Ottawa, pp. 777-784.

Newhook, J.P., (1999). *"Advanced Composite Materials in Small Craft Harbours"*, ACM News, Vol. 7, No. 1.

Newhook, J.P., and Mufti, A.A., (1996). *"A Reinforcing Steel-free Concrete Bridge Deck for the Salmon River Bridge,"* Concrete International, Vol. 18(6), pp. 30-34.

OHBDC, (1992). *Ontario Highway Bridge Design Code*, Ministry of Transportation of Ontario, Downsview, Ontario, Canada.

Rizkalla, S.H., Shehata, E., Abdelrahman, A., and Tadros, G., (1998). *"Design and Construction of a Highway Bridge with CFRP"*, ACI Concrete International.

Rizkalla, S.H., and Tadros, G., (1994). *"A Smart Highway Bridge in Canada"*, Concrete International, 1994, pp. 42-44.

RocTest, Telemac, (2001). *"Sensoptic –Fibre Optic Sensors, Transducers and Data Loggers,* Catalogue.

Sargent, D.D., Ventura, C.E., Mufti, A.A., and Bakht, B., (1999). *"Testing of Steel-free Bridge Decks,"* Concrete International, Vol. 21(8), pp. 55-61.

Shehata, E., and Rizkalla, S.H., (1999). *"Intelligent Sensing for Innovative Bridges"*, Journal of Inteligent Materials and Structures, Vol. 10, pp. 304-313.

Sikorsky, C., (1999). *"Development of a Health Monitoring System for Civil Structures Using a Level IV Non-Destructive Damage Evaluation Method,"* Proceedings of the 2nd International Workshop on Structural Health Monitoring 2000, Stanford University, CA, USA, pp. 68-81.

Stallings, J.M., Tedesco, J.W., El-Mihilmy, M., and McCauley, M., (2000). *"Field Performance of FRP Bridge Repairs,"* ASCE Journal of Bridge Engineering, Vol. 5(2), pp. 99-106.

Tadros, G., (1997). *"Design and Construction of the Northumberland Strait Crossing Fixed Link Project,"* Canadian Civil Engineer, Vol. 12(7), pp. 18-21.

Tadros, G., Tromposh, E., and Mufti, A.A., (1998). *"Superstructure Replacement of the Crowchild Trail Bridge"* Proceedings of the 5th International Conference on Short and Medium Span Bridges, Calgary.

Tennyson, R.C., and Mufti, A.A., (2000). *"Monitoring Bridge Structures Using Fibre Optic Sensors,"* Proceedings of European COST F3 Conference on System Identification of Structural Health Monitoring, June 6-9, 2000, Universidad Politéenica de Madrid, Madrid, Spain.

Tsai, P., and Ventura, C.E., (1999). *"Waterloo Creek Bridge Project"*, Field Assessment Report No. 2, University of British Columbia.

Ventura, C.E., Felbar, A.J., and Stiemer, S.F., (1996). *"Determination of the Dynamic Characteristics of the Colquitz River Bridge by Full-scale Testing,"* Canadian Journal of Civil Engineering, Vol. 23(2), pp. 536-548.

Ventura, C.E., Felbar, A.J., and Prion, G.L., (1994). *"Dynamic Evaluation of a Medium Span Bridge by Modal Testing,"* Developments in Short and Medium Span Bridge Engineering '94, Canadian Society for Civil Engineering, Montreal, Québec, Canada.

Wardrop Engineering Inc., (1999). *"Remote Monitoring of Taylor Bridge"*, Progress Report.

Weznel, H., and Pichler, D., (1997). ***"****Structural Assessment of Railway Bridges by Ambient Vibration Testing,"* Recent Advances in Bridge Engineering, Proceedings of US-Canada-Europe Workshop on Bridge Engineering, held in EMPA, Zurich, Switzerland, pp. 275-282.

Appendix

A SENSORS

Various types of sensors commonly used in civil engineering applications are discussed in Section 2. This appendix focuses on how the sensors are used in practice. Guidelines are provided for the selection of sensors, protection against mechanical and chemical damage, reduction of noise, and the collection of more representative data.

A.1 Strain Measurement

Foil gauges, fibre optic gauges or vibrating wire gauges, are commonly used to measure strain in civil engineering applications. Among these three types, foil strain gauges are the least expensive and the most widely used. However, they become less attractive when the distance between the gauge and the readout unit increases. This is due to the fact that the low-level voltage signal produced by the foil strain gauge is susceptible to electromagnetic and electrostatic interference from external sources. When unconditioned signals from foil gauges are transmitted a relatively long distance, the electrical noise superimposed by the electromagnetic and electrostatic fields becomes significant and can lead to inaccurate results and incorrect interpretation of the strain signals. The problem is more severe for dynamic measurements, since filtering the noise can change the characteristic of the original signal. As will be discussed later, electrical noise can be significantly reduced in the measurement signals by using special wiring considerations and conditioning the signal close to the gauge. The additional cost of these measures is a controlling factor when the application of foil strain gauges is compared with other alternatives.

Sensitivity of strain gauges to moisture and humidity is another concern, especially when long-term measurement is planned, particularly in a harsh environment, and when it is important to maintain a stable reference (zero-stability) for the gauges. Special provisions are often needed to protect the gauges in order to obtain acceptable measurements.

Vibrating wire strain gauges produce AC signals in which the frequency of the signals is important for determining the strain. Since frequency can be transmitted over relatively long cable lengths (over 1.5 km) without appreciable degradation, this type of gauge becomes more suitable when the readout unit is located some distance from the gauge. The installation of these gauges is relatively simple and there are no special considerations for use in concrete or in exposed environments. However, the gauges are fairly bulky and therefore are not suitable where space is limited.

The signals produced by fibre optic gauges are in the form of light and are, therefore, completely immune to electromagnetic and electrostatic interference. They can be used for a variety of applications and, specifically because of their small diameter, they are very suitable for embedment in composite reinforcing bars and sheets. The major drawback of these gauges is the high cost of both the sensors and their readout units.

A.1.1 Foil Strain Gauge

Foil strain gauges are generally attached to the surface of structural components and wired to readout units. As the component experiences strain, the change in length at the surface of the component is transmitted to the strain gauge through the connecting substances. From there, the corresponding signal is transmitted to the readout unit through the lead wires. To ensure the output of the readout unit represents the true strain change in the material, it is important to understand the various factors that affect the quality of the measurements, as discussed in the following subsections.

A.1.1.1 Strain Gauge Selection

Foil strain gauges are produced with various characteristics for use in different applications and situations. The first step in using a foil strain gauge is making an appropriate selection from the wide range available in the market. Before using a strain gauge, it is necessary to ensure that the selected gauge is compatible with environmental and other operating conditions, and at the same time best satisfies the installation and operating constraints. In general, the constraints for the selection of strain gauges are: required accuracy and stability of the measurement; required elongation; type and duration of the measurement; the environment; and ease of installation.

Cost of the strain gauge is usually not a prime consideration in selection, because the cost of the gauge is usually a small fraction of the total installation cost. In many cases, selecting a more expensive gauge that provides additional features saves on installation time, and consquently decreases the total installation cost.

Strain sensing alloys: The principal component determining operating characteristics of a strain gauge is the strain sensitive alloy used in the foil grid. Common alloys used in production of strain gauges are constantan, nickel-chromium and isoelastic alloys. Strain gauge thermal output, zero-stability, fatigue life, and sensitivity to strain are the criteria used to determine the suitability of one alloy over other alloys.

The thermal output of a strain gauge is the strain erroneously detected by the strain gauge as a result of temperature change. This subject and the methods for compensating for the thermal output are discussed in A.1.1.6. Zero-stability is an important property when measurement is carried out over a long period of time. Gauges with poor stability exhibit continuous drift under constant strain, which makes the measurement inaccurate. When maintaining a stable reference (zero-stability) is not critical, strain gauge drift is not detrimental.

Among strain gauge alloys, constantan alloy is the oldest and still the most widely used. This is because constantan has the best overall combination of properties needed for many strain gauge applications. For example, it has an adequately high strain sensitivity, or gauge factor, that is relatively insensitive to strain level and temperature. Moreover, constantan is characterized by good fatigue life and relatively high elongation capacity.

When strains are measured over long periods of time (months or years) a nickel-chromium alloy is the preferred choice because it offers significantly better zero stability. Nickel-chromium is also characterized by good fatigue life. The thermal output of nickel-chromium alloy strain gauges is comparable to that of constantan strain gauges.

For dynamic strain measurements, isoelastic alloy can provide certain advantages. This alloy has superior fatigue life in comparison to other alloys, and has a high gauge factor (approximately 3.2 compared to 2.0 for constantan and nickel-chromium). The latter characteristic improves the signal-to-noise ratio in dynamic testing. However, the isoelastic alloy has poor thermal output and zero stability characteristics. Therefore, it is not a good choice when these characteristics are important.

Carrier materials: A conventional foil strain gauge is constructed on a plastic backing, or carrier. This makes the gauge easier to handle and provides electrical insulation between the metal foil and the instrumented component. In general, a foil strain gauge is attached directly by bonding the backing material to the test object. The most common backing material is polyimide. Polyimide is a tough and extremely flexible carrier, and can be contoured readily

to fit small radii. Glass fibre reinforced epoxy-phenolic is also used as a backing material. This is the preferred backing material when the gauge is subjected to extreme temperatures (beyond $\pm 100^{\circ}C$). However it does not have the flexibility of polyimide backing.

Weldable strain gauges are also available in the market. This kind of gauge consists of a specially manufactured foil strain gauge pre-bonded to a metal carrier for spot welding to steel components. Adhesively bonded strain gauges are preferred over weldable strain gauges when the highest accuracy is desired. However, where bonding conditions are not ideal, the weldable type is the preferred choice. Weldable gauges are more costly than bondable gauges, but the overall installation cost is reduced significantly because of the shorter installation time, and elimination of the strict requirements for surface preparation and adhesive curing required for bondable strain gauges. It should be noted that the bonding component should be free from drift.

Another type of foil strain gauge on the market is the embedment strain gauge. This type of strain gauge is used for measuring strains inside concrete structures. An embedment gauge consists of a long foil gauge (about 100 mm) embedded in a polymer concrete block. The long length of the embedded strain gauge is necessary to ensure that the measured strain is the average strain in aggregate materials, and not the localized strain due to discontinuities in concrete. The concrete cover protects the embedment strain gauge against mechanical damage during construction, as well as moisture and corrosive attacks afterwards. It also provides a means for the proper transfer of strain from the structure to the strain gauge.

Gauge length: The gauge length of a strain gauge is the active or strain-sensitive length of the strain gauge. This length is illustrated in Figure A.1. The end loops and solder tabs are insensitive to strain because of their relatively large cross-sectional area and low electrical resistance. Therefore, the end loops and solder tabs are not considered as part of the gauge length. Strain gauges are available in a wide range of gauge lengths. Where there are no special considerations, gauge lengths between 3 mm to 6 mm are preferable because of lower cost, availability, and ease in installation. Strain gauges of less than 3 mm in gauge length tend to exhibit degraded endurance when subjected to cyclic strains, and degraded performance in terms of the maximum allowable elongation, the stability under static strain.

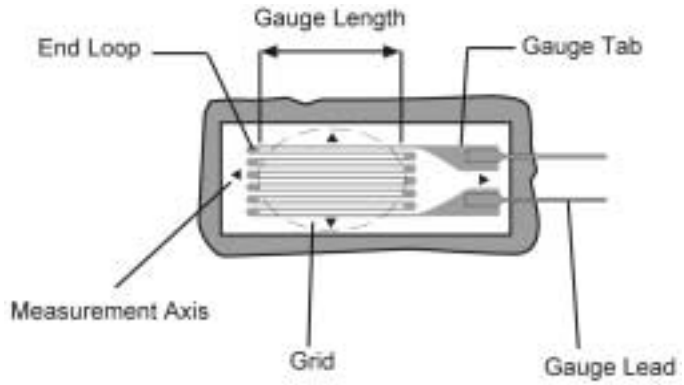

Figure A.1 Gauge length of a strain gauge

Generally, small gauge lengths are required when the objective is to measure the value of strain at a certain point. In such cases, the suitable gauge length depends on the intensity of the strain variation in the vicinity of the point. A smaller gauge length is required for highly localized strain, due to the fact that a strain gauge tends to average the strain over the area covered by its grid. Figure A.2 demonstrates how the strain indicated by a strain gauge could be lower than the strain of the point that it represents.

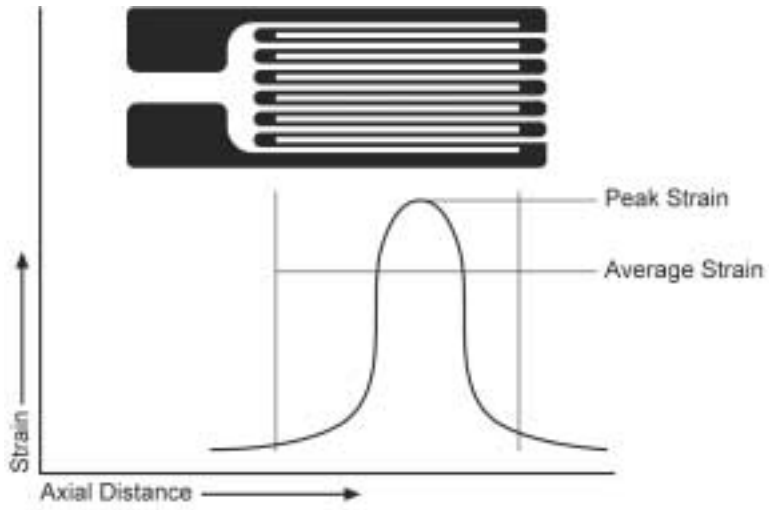

Figure A.2 Strain gauge averaging effect

When the average strain is sought over a specific length, the gauge must be long enough to ensure that an average strain can be determined over the specific length under consideration. An example of this, in civil engineering applications, is the measurement of strains in a concrete structure. In such instances, the desired strain is usually the average strain, not the severe strain fluctuation at the interfaces of the aggregate particles and cement. In this instance, the strain gauge should be long enough to span several pieces of aggregate. As a general rule, when measuring strains on components made of composite materials of any kind, the gauge length should be large, in comparison to the dimensions of the inhomogeneities in the material. For example, the gauge length of strain gauges used on concrete should be at least 5 times the size of the largest aggregate in the concrete.

The other advantage of larger length strain gauges is that they provide improved heat dissipation. This consideration is important when the gauge is installed on a polymer or other substrate with poor heat transfer properities, such as fibre reinforced polymers. When adequate heat dissipation does not exist, the electrical current in the strain gauge causes high temperatures in the gauge, backing, adhesive, and test specimen surface. This can noticeably affect gauge performance and accuracy.

Gauge resistance: Strain gauges are commonly produced to have a resistance of 350 ohms or 120 ohms. In general, the higher resistance gauge is preferable because it generates low volumes of heat, for the same applied voltage. This characteristic is very important for materials with low heat conductivity, such as composite materials. As discussed earlier, low heat conductivity causes a temperature increase in the gauge and material during strain measurement, and therefore can alter the magnitude of the recorded strain from its real value.

Higher gauge resistance also has the advantage of decreasing lead wire resistance effects and unwanted signal variation caused by a change in lead wire resistance that comes from temperature fluctuations. The other advantage of using a higher-resistance strain gauge is that it improves the signal-to-noise ratio of the measurement. These subjects will be discussed in more detail later.

In situations where small strain gauges are used to record varying strains for a long period of time, the 120 ohm gauges have an advantage over the 350 ohm strain gauges because of their longer fatigue life.

Thermal expansion coefficient: To minimize the thermal output of strain gauges, the thermal expansion coefficient is matched to a specified value during the production process. These strain gauges are referred to as self-temperature compensated and are available for materials with a certain value of thermal expansion coefficient. It is always good practice to select a strain gauge with a thermal expansion coefficient that matches or is close to the material of the instrumented component. In anisotropic materials, such as composite materials, the thermal expansion coefficient is direction-dependent. The strain gauges used for this type of material must be selected based on the thermal expansion coefficient in the direction of the measured strains.

Grid width: Narrow grid strain gauges are preferable when severe strain gradients exist perpendicular to the gauge, and the strain is measured over a short length. Otherwise, wider grids are the preferred choice because they improve the heat dissipation and enhance gauge stability, particularly when the gauge is attached to a material with poor heat conductivity. For non-homogeneous materials, such as concrete, wider gauges produce more representative results, because the strain is averaged over the width covered by the gauge.

Other considerations: Manufacturers of strain gauges provide some optional features. These options are usually accompanied by a price increase, but this can be offset by the benefits offered. Some of the optional features are discussed below.

Some strain gauges have a thin protective layer, called encapsulation, over their grids. Encapsulation protects the grid from finger smudges and other contamination during installation and, therefore, contributes significantly to longer term gauge stability. It also provides some protection against humidity and other environmental effects for indoor applications.

Figure A.3 shows strain gauges with integral terminals and solder dots. These features ease the soldering process of the lead wires to the strain gauge. This is particularly important for the nickel-chromium strain alloy, where soldering directly to the alloy is difficult.

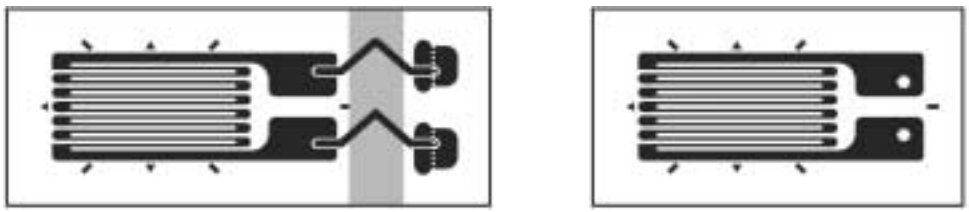

Figure A.3 Left: Strain gauge with integral terminals, Right: Strain gauge with solder dots

Strain gauges with pre-installed lead wires are also available. These gauges are useful for materials with low thermal conductivity, because the risk of damaging the test material and the gauge during soldering operations is avoided.

Another useful feature that helps improve the performance of strain gauges is the bondable terminal. Refer to Figure A.4. When using bondable terminals, lead wires are not attached directly to the solder tabs of the gauge. Instead, they are installed on the bondable terminals that are attached to the base material adjacent to the gauge. Small, flexible jumper wires, curved to form strain relief loops, are then connected from the terminals to the gauge solder tabs. This configuration prevents damaging the strain gauge or degrading its performance due to the forces transmitted along the main lead wires.

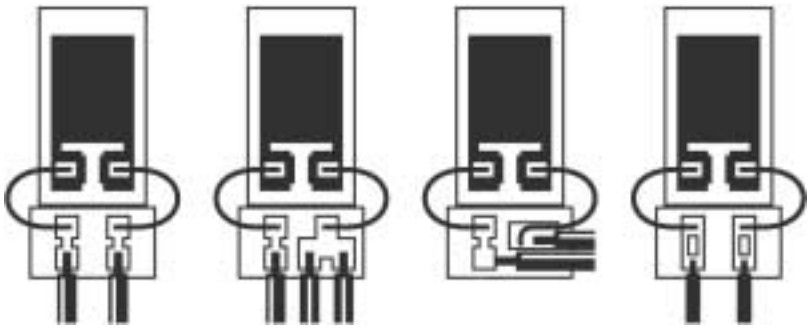

Figure A.4 Various configurations of lead wire connection to bondable terminals

A.1.1.2 Attachment Techniques

To detect strains, foil strain gauges must be properly connected to the components that the strain is measuring. For embedment strain gauges, this connection is simply achieved by tying them to a reinforcing bar in concrete. However, for bondable and weldable strain gauges, special preparation and installation techniques are required. These gauges are usually attached to the surface of the component.

Bondable strain gauges are bonded to the surface of the component by using an adhesive specially produced for this purpose. Strain gauge producers provide various types of adhesives for different applications. Among these adhesives, the cyanoacrylate adhesives (also referred to as general purpose adhesives) are very popular because of their ease of application and quick curing rate at room temperature. Under normal conditions, cyanoacrylate adhesives begin curing within a minute, but require 24 hours to set. The bond produced by this type of adhesive is weakened by exposure to high humidity, and will gradually become harder and more brittle. Therefore, this type of adhesive is not recommended for monitoring projects that exceed one or two years. Moreover, adequate protective coatings must be provided when the adhesive is subjected to high humidity.

Epoxy adhesive is another kind of adhesive used for bonding strain gauges. The bonds produced by epoxy adhesives have good resistance to moisture and most chemicals, and the adhesive properties do not degrade with time when properly protected. The epoxy adhesives are available in single-component and two-component packages. The two-component package contains a bottle of epoxy resin and a bottle of hardener, which must be mixed just before application. Epoxy adhesives generally require a few hours to cure, and then post-cure at elevated temperature. The cure time increases for lower temperatures. For example,

M-Bond AE-15 adhesive from Micro-Measurements requires a cure time of 1 hour at 80°C. This increases to 6 hours at 50°C. A two-hour post-cure is also recommended at 15°C above the maximum operating temperature for this adhesive.

Special-purpose adhesives are also available for certain conditions. For example, curing at a temperature as low as +5°C, polyester adhesive is useful when it is not feasible to maintain an elevated temperature for curing. However, in general, there are some shortfalls. Special-purpose adhesives do not have the same quality of bond as epoxy adhesives. Therefore, when using this kind of adhesive, consult the adhesive specifications provided by the supplier, and be aware of the corresponding shortfalls so that the required specifications for the strain measurement are not compromised.

The first step for strain gauge bonding is surface preparation. The surface for the strain gauge attachment must be relatively flat, fully clean and chemically neutralized, and slightly abraded. The procedure, equipment and materials used for achieving this may vary from one substrate material to another. For example, for surface abrasion of metallic materials, it is acceptable to use abrasive paper or grit blasting. Composite material surfaces should be smoothed more cautiously in order not to damage the near-surface fibres. Concrete surfaces must be coated with an epoxy adhesive to fill the pores and voids.

During the curing stage of the adhesive, it is necessary to maintain a uniform pressure on the strain gauge. This is called clamping pressure. In the case of a fast-curing (cyanoacrylate) adhesive, the required pressure is easily applied with the thumb or finger, and needs to be maintained for a minimum of one minute. However as mentioned earlier, a fast-curing adhesive is not recommended for long-term strain measurements.

For long-term applications, the curing time for the adhesive is relatively long, and it is always necessary to maintain a specified uniform clamping pressure for this time period. The suppliers specify the required clamping pressure and curing time for the adhesive. Since the curing process usually takes several hours, and may involve elevated temperature, it is important that the clamping device be physically stable and capable of holding the specified force for the required time. Figures A.5 and A.6 illustrate some clamping techniques.

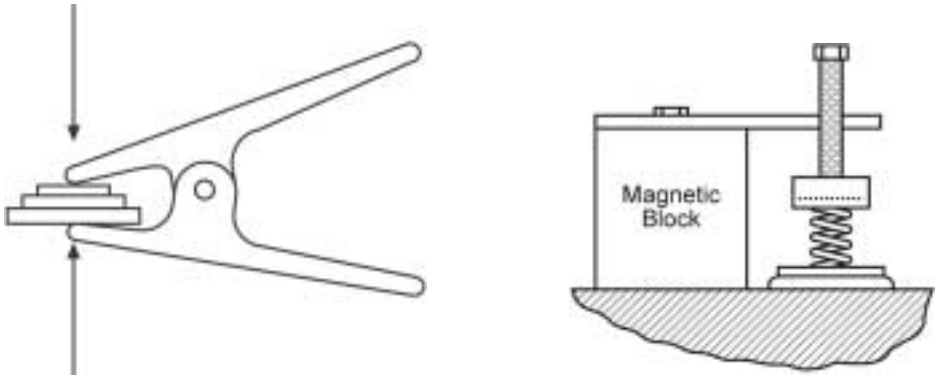

Figure A.5 Two clamping techniques. Left: common spring clamp Right: clamp with magnetic block

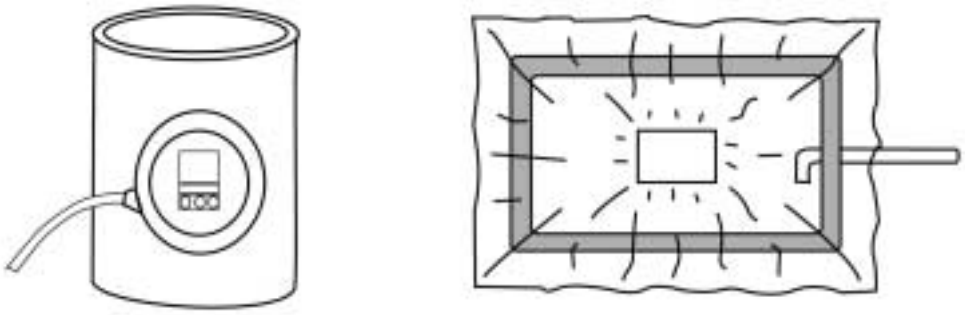

Figure A.6 Two vacuum clamping techniques. Left: commercially-available vacuum pads Right: homemade vacuum clamping fixture

Components required for strain gauge clamping are shown in Figure A.7. These components include a release film, a pressure pad, a metal clamping plate and a clamping device for applying a constant force. The release film is used between the gauge/adhesive and the pressure pad. It prevents the pressure pad from adhering to the adhesive and the gauge. For low-temperature curing epoxies (< 65°C), it is common to use cellophane tape. However, for higher curing temperatures, Teflon film, or a similar material, is used as the release film. The pressure pad is made from a relatively flexible material in order to distribute the clamping force uniformly over the gauge area. The pressure pad should not be so soft as to extrude from under the clamping plate. The metal clamping plate is used to distribute the clamping force over the entire area of the pressure pad. It should have sufficient thickness so that it does not deform under the clamping force. Moreover, it should be formed to match the contour of the surface to which the strain gauge is attached.

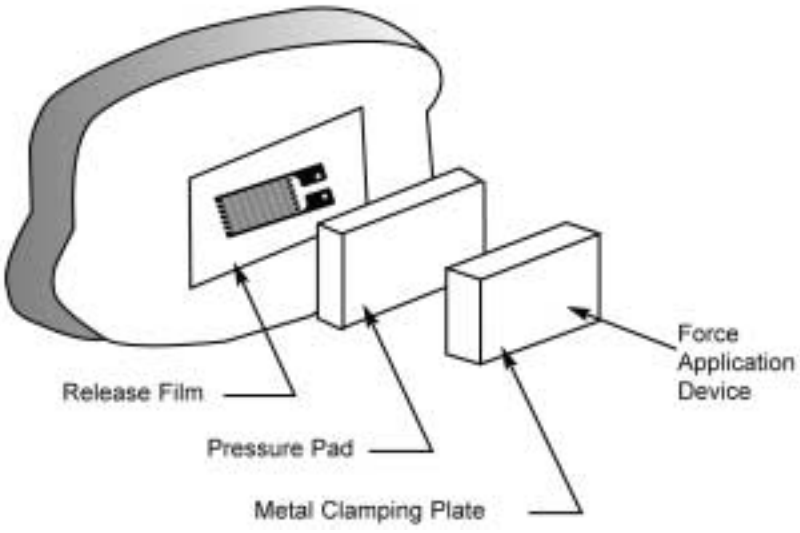

Figure A.7 Components for strain gauge clamping

In comparison to bondable strain gauges, the attachment of weldable strain gauges is simple and fast. The surface preparation requirement is minimal and the gauge is useable immediately after spot welding and lead wire attachment. For efficient welding, the surface that the weldable strain gauge will be attached to must be free of grease, rust, scale, oxides and irregularities. This can be easily achieved by using an appropriate solvent for degreasing, and grinding the surface with silicon-carbide paper, or a wheel grinder, to create a smooth surface. Spot welding is accomplished with a portable, rechargeable hand-probe spot welder. Figure A.8 shows a weldable strain gauge attached to a reinforcing bar.

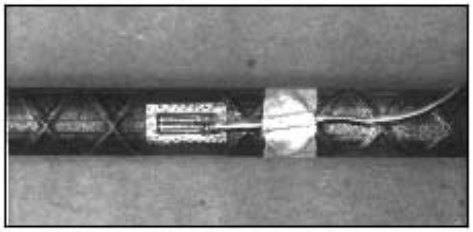

Figure A.8 A weldable strain gauge attached to a reinforcing bar

A.1.1.3 Environmental and Mechanical Protection

The effects of moisture, chemical attacks or mechanical damage can all easily degrade strain gauge performance. As a result, strain gauges need varying degrees of protection according to the severity of the environment in which they must operate, and the length of time that they must be operational. For a short-term laboratory application, an encapsulated gauge may operate properly without additional protection. However, for field applications, or when open-face gauges are used, strain gauges should always be covered with a suitable coating as soon as possible after installation.

Experience has shown that moisture is the most common cause of field installation failure. The presence of moisture usually results in low electrical resistance to the ground, causing circulating currents between the gauge and the ground, and electrical noise in the measurement. This causes grid corrosion and creates an intragrid conductive path that results in inaccurate measurement and zero-drift. Due to these facts, providing effective protection against humidity should always be employed with any long-term strain measurement. Checking the zero-drift of the gauge can easily monitor the effectiveness of a protective coating. Resistance-to-ground measurement can also indicate strain gauge deterioration. When it is not practical to produce a zero-strain condition for the operating gauge, installing an additional strain gauge on a strain-free surface in the same environment is recommended. Monitoring the zero-drift and resistance-to-ground of this gauge will then provide useful information regarding the effectiveness of the protection system used.

Strain gauge suppliers provide various materials for protecting strain gauge installations under different conditions. Depending on the environmental conditions, a single material or a combination of materials may be used. For example a single layer of Nitrile rubber coating may provide adequate protection for field installation, where the gauge is not subjected to rain and snow. However, for more severe cases, one should use two layers of Nitrile rubber coating separated with aluminum foil. For coatings that are electrically conductive, a Teflon sheet, or similar material, should cover the open-face grid and the lead wire connections before the coating is applied. Epoxy coatings provide good protection against chemicals, but they absorb moisture and, therefore, are not suitable for long-term measurement in a high humidity environment.

Generally, protection against humidity and chemical attacks also provides adequate protection against normal mechanical damage. However, extra protection may be required for more severe conditions, such as when strain gauges are used in reinforced concrete or when they are pre-installed on structural components. For example, adding a neoprene rubber patch over the coating or using a thicker layer of rubber-like materials can provide extra protection.

Common materials generally used for protection of strain gauges come in liquid or paste form and are applied to the surface of the strain gauge with a brush or spatula, to provide a coating of sufficient thickness. It is necessary to extend the coating at least 10 mm beyond the gauge and terminals. When several layers of coating are applied, the overlying coating should extend beyond the previous layer. The surface that the coating is applied to must be clean and chemically neutralized. Therefore, if there is a possibility that the surface has been re-contaminated after the strain gauge installation, it must be cleaned and neutralized before the coating is applied.

It is important to note that a good protective coating not only seals moisture out of the gauge installation, but will also seal in any moisture in the area at the time of the coating application. For maximum stability in high moisture environments, it is therefore important to warm the gauge installation prior to applying the protective coating in order to remove any excessive moisture. In normal environments, the protective coating should be applied immediately after installation to prevent moisture from collecting in the gauge area.

Special attention must be paid to the place where the lead wires exit the protective coating, to ensure that an adequate bond exists between the lead wire insulation and the protective coating. Without a proper seal, moisture can be drawn into the gauge area along the lead wires by the capillary action. To produce a proper seal, the lead wires should be separated in the area where the coating is applied and the coating material should adequately cover both under and around each lead wire. Vinyl- and Teflon-insulated lead wires must be chemically treated before applying the epoxy coating to produce a bondable surface. Normally, the treatment is performed before attaching the lead wires to the strain gauges. ASTM E1237-93 requires that the lead wires be coated for a minimum distance of 25 mm from the installation.

Moisture absorption through the lead wires connected to a strain gauge can result in inaccurate measurement and zero drift. Therefore, it is important that the lead wire insulation be waterproof and protected against damage. When lengths of lead wires are spliced together, the spliced joints must be protected and waterproofed with heat shrinkable tubing. Good electrical and mechanical connection at the spliced joints is also essential for avoiding noise generation.

A.1.1.4 Lead Wire Effects

The lead wires used for connecting a strain gauge to the readout unit can cause two types of errors in the strain measurement. One error is due to resistance changes in the lead wires as a result of temperature changes that are indistinguishable from resistance changes in the strain gauge. The other error is known as lead wire desensitization and becomes a concern when the magnitude of the lead wire resistance is not negligible in comparison to that of the gauge.

In general, a three-wire connection is the preferred method of wiring strain gauges to a bridge circuit when a quarter configuration is used. For half and full bridge configurations, when strain gauges form two adjacent arms of the bridge, temperature changes do not affect

the measurement. However, for half bridge configurations, the lead wire desensitization must be corrected according to procedures given in standard textbooks.

A.1.1.5 Sensitivity to Transverse Strain

Foil strain gauges are sensitive not only to the strains that are along their primary sensing axis, but also to the strains in the transverse direction. This characteristic introduces some degree of error in the detected strain.

Transverse sensitivity of strain gauges is small, and as a result, the corresponding error is generally insignificant. However, for situations in which the transverse strain is large compared to the longitudinal strain, the amount of error can be significant if it is not accounted for.

It is common to define the strain sensitivity of a gauge by its gauge factor (GF). The gauge factor is the ratio of the rate of resistance variation caused by uniaxial stress applied along the gauge axis of the strain gauge. This definition, although adequate for most practical applications, masks the presence of transverse sensitivity. In fact, a foil strain gauge has two gauge factors, GF_a and GF_t, relevant to the gauge axis that it is aligned to and perpendicular to a uniaxial strain field, respectively.

The gauge factor (GF) reported by strain gauge manufacturers is theoretically correct only when the gauge is attached to a material with a Poisson ratio equal to that of the material used for gauge calibration. Moreover, the gauge must be in a uniaxial stress field that is parallel to its axis. For other conditions, the detected strain carries a certain amount of error.

A.1.1.6 Temperature Effect

Sensitivity of foil strain gauges to temperature change is the most serious error source in static strain measurement. This is in addition to the error produced due to temperature effect on lead wires. This error is the result of two concurrent effects. One is the variation of electrical resistance of the gauge caused by temperature, and the other is the result of the difference between the thermal expansion coefficient of the gauge and the substrate material to which the gauge is attached. The error produced by these two effects is generally referred to as thermal output of the gauge and is algebraically added to stress-induced strains.

The thermal output of a strain gauge is superimposed on the gauge output due to mechanical strain. Therefore, to obtain the correct value of the strain, it is necessary to determine the magnitude of the thermal output of the gauge and deduct it from the strain indicated by the readout unit. It may appear that the thermal output is proportional to the temperature change. However, this is not correct.

Theoretically, the error due to thermal output can be completely eliminated by using an additional gauge, often known as a "dummy" gauge. This gauge, which is identical to the active gauge, is attached to an unstrained piece of the same material that the instrumented component is attached to. The dummy gauge and the active gauge are used to form two adjacent arms of the Wheatstone bridge circuit. With this set-up, as long as the two gauges undergo identical temperature changes, the thermal output of the two gauges will eliminate each other. Therefore, the detected strain by the readout unit will only be due to stress-induced strain in the active strain gauge. For this method to work correctly, it also requires that the lead wires are connected to the active and dummy gauges in the same way in terms

of material, size and length, and they are routed together so that the resistance change due to temperature change is equal.

Although the use of a dummy gauge for temperature compensation is quite effective, it has its own difficulties. This is generally because, in practice, it may not be feasible to create an unstrained condition for the dummy gauge while it is under an identical environment to that of the active gauge.

Use of strain gauges with thermal properties that match the thermal properties of the substrate material is an effective method for minimizing thermal output. Referred to as temperature-compensated gauges, these strain gauges are available for certain types of materials. With these gauges, the error due to thermal output of the gauge for a certain range of temperature change is small. However, a correction is still required to obtain reliable measurement when the variation of temperature is beyond the range.

The thermal output graphs provided by the manufacturer gives the thermal output of the gauge as well as the variation of the gauge factor with temperature. There are also two other important items of information: the lot number of the gauges; and the test material used to measure the thermal output characteristics. It is important to note that the thermal output data of these graphs are specifically applicable only to the gauges that are applied to the same material and from the same designated lot number. With these graphs, correcting the strain measurement for thermal output can be accomplished using the following equation:

Equation A.1

$$\epsilon = \overline{\epsilon} - \frac{GF_{GR}}{GF_0}\left[(\epsilon_{TO})_T - (\epsilon_{TO})_O\right]$$

where

ϵ	Corrected strain
$\overline{\epsilon}$	Indicated strain
$(\epsilon_{TO})_T$	Thermal output of the gauge at the temperature that the measurement is carried out
$(\epsilon_{TO})_O$	Thermal output for the temperature under which the readout unit is balanced
GF_0	Gauge factor used for setting the readout unit
GF_{GR}	Gauge factor used for producing the thermal output graph (usually =2)

The above equation is based on the fact that the variation of the gauge factor with temperature is insignificant. In order to include this effect in the correction, divide the strain obtained from Equation (A.2) by GF, given by the following equation:

Equation A.2

$$GF = \frac{1 + \Delta GF(\%)}{100}$$

where ΔGF(%) is the variation of the gauge factor in percent as a result of temperature change. This value can be obtained from the thermal output graph of the gauge.

Strain gauge manufacturers usually do not provide the thermal output graph of strain gauges for use on FRPs. This is due to the fact that the thermal (and other) properties of polymers vary from lot to lot and, because of different formulations, vary greatly from one manufacturer to another for, nominally, the same FRP. Moreover, the thermal properties of FRPs change with time and humidity. This creates a situation in which there are no suitable FRPs for use in directly measuring thermal output characteristics. As a result, for the gauges

that are temperature-compensated for FRPs, the thermal output data is provided on steel specimens. For these conditions, when the thermal output graph of the gauge is for material that is different from the material that is used, the strain due to thermal output can be obtained from the following relationship:

Equation A.3

$$\varepsilon_{T2} = \varepsilon_{T_1} + \frac{GF}{GF_o} \bullet \frac{1+K_1}{1-\nu OK_t}(\alpha_{s2} - \alpha_{s1})\Delta T$$

where α_{S1} denotes the thermal expansion coefficient of the material for which the thermal output data is available, and α_{S2} denotes the thermal expansion coefficient of the material whose strain is being measured. ϵ_{T1} is the thermal output from the graph for a given temperature.

Equation A.4

$$\varepsilon_{T2} = \varepsilon_{T1} + (\alpha_{s2} - \alpha_{s1})\Delta T$$

It is important to note that the determination of thermal output for strain measurement of composite materials involves a similar problem, because strain gauge manufacturers do not provide any thermal output data. Moreover, the thermal expansion coefficient for composite material is different in different directions, and it depends on the ratio of fibre to matrix volume. In multi-layer composite panels, the number of layers and their orientations also affects the thermal properties. Therefore, it is preferable to directly obtain the thermal output characteristic of this kind of material by conducting an experiment on a piece of the material under consideration. For such a test, the following conditions must exist:

- The lot number of the test strain gauge is identical to that used for the real structure.
- The test piece on which the thermal output is recorded is identical to the real structure.
- The axis of the test strain gauge, with respect to the direction of fibres, is identical to that of the gauges that are attached to the structure.
- The same attachment technique is used for both the test gauge and the gauges on the structure.

Equations (A.3) and (A.4) can also be used to obtain approximate thermal outputs of the strain gauges that are attached to the composite materials. However, care must be exercised that the thermal expansion of the material used in these equations is for the direction that the gauge is attached. Calculation of this thermal expansion involves some complexity. Readers may wish to refer to textbooks that deal with fibre reinforced composites, such as Mallick (1993), and Daniel and Ishai (1994).

A.1.1.7 Noise Control

The signal produced by foil strain gauges is a low-level one and therefore is susceptible to interference from other sources. The interference generates unwanted signals that add to the signals produced by the foil strain gauge. The unwanted signals are referred to as noise. Capacitive and magnetic coupling to long lead wire runs, electrical leakage from the gauge to the substrate material through the gauge backing, and cross-talk between adjacent pairs of lead wires are the common sources of noise in strain measurements. If special measures are not taken, the noise can lead to inaccurate results and incorrect interpretation of the strain signals. This problem becomes more critical for bridge applications, as the lead wires connecting the strain gauges to readout units are relatively long. In such situations, the lead wires are generally the principal source of noise induction in strain signals.

Two different methods are commonly used for minimizing the noise effect that is induced through the lead wires, converting the signal to a high level signal at its source, and applying special attention to the wiring and shielding it against environmental noise. It is also common to consider a combination of the two techniques when the lead wires are relatively long and the noise level is high. This section provides some general information for noise reduction based on the second method. To produce a high level signal at its source, consult with the supplier of the sensor to determine the availability and suitability of the instruments in terms of specific needs. For a more detailed discussion on this subject, refer to Measurement Group Tech Note TN-501-2 (1992), Klipec (1977) and Morrison (1986).

In general, the noise induced in strain signals through the lead wires is categorized into two basic types: electrostatic and magnetic. The two types of noise are fundamentally different, and therefore require different noise reduction measures. Any electrical device that generates, consumes or transmits power can cause these two types of noise. For example:

- AC power lines
- transformers
- motors and generators
- arc welders
- fluorescent lamps
- radio transmitters

The magnitude of the noise from these sources increases with the voltage of the current and the length of the lead wires connected to the sensors. The noise effect drops as the distance from the noise source increases.

Electrostatic noise is generated in a conductor subjected to an alternating electrostatic field. Any source of voltage with or without current flow generates an electrostatic field. When the intensity of the field changes, electrical charges with identical alternating natures are produced in the conductor through the phenomenon of capacitive coupling. Fluorescent lighting and AC power lines are the most common source of electrostatic noise.

To protect a lead wire from electrostatic noise, it is common to shield the lead wire with a conductive foil or braided wire. With this method, the electrical charges are captured by the shield and can be drained off by grounding the shield. If the shield is not properly grounded, the charges can be transmitted into the lead wire through the shield-to-cable capacitance. Between the two common types of cable shields, the conductive foil shields provide 100 percent cable coverage and gives better shielding ability.

Magnetic noise is generated in a conductor when it cuts the flux lines of a magnetic field. Magnetic fields are created either by the flow of electric current or by the presence of permanent magnetism. In the presence of an electrical current with an alternating nature, such as 50/60 Hz power lines, an alternating magnetic field is generated around the current line. When a stationary conductor is subjected to this field, it automatically cuts the magnetic flux lines as the field expands and collapses due to the alternating nature of the current. Therefore, a noise voltage is generated in the conductor. Similarly, a conductor moving through the earth's magnetic field captures a noise voltage as it cuts the earth's magnetic flux lines. The former situation occurs in bridge applications when an AC power line passes in the proximity of the bridge. The latter situation occurs when the lead wires connected to the sensors move through the earth's magnetic field as a result of the bridge vibration under the dynamic loads.

Minimizing the magnetically induced noise by shielding is neither efficient nor cost effective. The common method for elimination of this kind of noise is to produce identical noise voltage in the lead wires connected to the sensors. The readout unit used for the sensors must then have the characteristic to reject the common-mode signals. In this condition, the read-out unit cancels out identically induced noise voltage in the lead wires. To assure that the noise signal produced in the lead wires is identical, it is necessary for the lead wires to be the same length and located close together. In practice, this requirement is achieved by using twisted-conductor cables. In theory, the more twists per unit of conductor length, the better the results.

When a number of lead wires from different sensors are run adjacent to each other for a long distance, noise can be generated as a result of both magnetic and electrostatic coupling between the signals of the different sensors. More serious problems can occur when the lead wires for excitation are drawn adjacent to the signal lead wires for a long distance (>15m), carrying high-level voltage. This effect is known as cross-talk noise, and can be minimized by employing an instrumentation cable composed of individually shielded pairs. When using such cables, it is important that all the shields be grounded at the end of the cable connecting to the readout unit.

A number of diagnostic measures need to be performed to assess the presence and the magnitude of noise in the output of a readout unit, as well as to find the sources of the noise. These measure are briefly discussed as follows:

- The first consideration should be to evaluate the effect of noise sources on the readout unit itself. For this, all the strain gauge leads must be disconnected from the readout unit. Then operate the readout unit by connecting it to a circuit that is close to the unit and similar to the strain gauge. With this configuration, the noise affecting the lead wires is eliminated and therefore the noise effect on the readout unit, itself, can be evaluated.

- The effect of lead wires can be evaluated by measuring the output of the strain gauge circuit at the readout unit end of the wires, while no excitation voltage is applied. When the structure undergoes vibration, any additional noise at this stage can be an indication of the effect of the earth's magnetic field on the lead wires.

A.1.2 Fibre Optic Strain Gauges

Fibre optic strain gauges are commercially available in different forms. In the simplest form, a fibre optic strain gauge consists of an optical fibre lead with a bare fibre optic sensor at one end, and a special connector to the readout unit at the other end. In this form, the fibre optic sensor is small in diameter and can be used for embedment in fibre-composite sheets and bars. It can also be used for bonding directly to the surface of a component. In such a case, it might be necessary to put a layer of insulation over the fibre optic gauge to protect it against environmental and mechanical damage.

Other forms of fibre optic strain gauges include weldable and embeddable types (Refer to Figure A.9). These gauges are for attachment to steel and embedment in concrete, respectively, and require minimal effort for installation and protection. These gauges contain an ordinary (bare) optical sensor bonded and encapsulated inside a stainless steel container. Although these gauges are more expensive than the ordinary bare gauges, the higher cost is compensated by the fact that in practice they are easier and faster to install.

Figure A.9 Fibre optic strain gauges. Left: embeddable strain gauge Right: weldable strain gauge

As discussed earlier, one of the advantages of fibre optic strain gauges over conventional foil strain gauges is that the optical gauges measure the absolute strain. However, be aware of the fact that when the fibre optic gauge is attached to a component, a residual strain is induced in the gauge. The amount of the residual strain increases when the adhesive used for bonding is cured at elevated temperatures. Therefore, to obtain the actual strain of the material, the residual strain in the gauge after attachment must be recorded and deducted from the subsequent recordings.

A.1.2.1 Installation and Protection Techniques

Depending on the type of fibre optic strain gauge, installation and protection techniques vary. A bare fibre optic gauge is usually bonded to the surface of the component. It is also embedded in materials such as fibre-composite bars, grids and sheets. When embedded, no additional protective measures are considered. However, a bonded optical gauge needs protective layer(s) against physical and environmental attacks.

In general, adhesives used to attach conventional foil strain gauges can also be used for bonding optical gauges. The surface that the gauge is being attached to must be cleaned and chemically neutralized before the adhesive is applied. The bare sensor is made of glass, and surface abrasion can easily impair its optical characteristic and life. Therefore, during gauge installation, care must be taken that the bare sensor is not touched by hands or placed on any surface which has not been previously wetted with adhesive. Similar to procedures used for foil strain gauges, the protective coating is applied after the adhesive is cured.

Weldable gauges are installed by welding them in place. For efficient welds, the surface that the gauge is being welded to must be free of grease, rust, scale oxides and surface irregularities. The weldable gauges consist of an optical sensor encapsulated in a steel tube. Therefore, the gauges do not require protection against humidity. However, if the installation is in a harsh environment, the sensors may require a coating for protection against mechanical damage.

Embeddable gauges can be placed directly in concrete without any extra precautions against humidity or the chemical environment of the concrete. However, care should be taken to avoid damage to the gauge and its cable when placing and vibrating the concrete. It is also essential that large pebbles or aggregate do not rest against the gauge, as this will cause localized strain discontinuities that may influence the gauge readings. This might require picking out the coarse aggregate around the gauge by hand. Alternatively, an embeddable strain gauge can be cast into a concrete briquette before being placed in the structure.

A.1.2.2 Temperature Effect

As with conventional strain gauges, fibre optic strain gauges indicate strain change with temperature. The strain produced due to the temperature is superimposed on the mechanical strain detected by the optical gauge. The mechanical strain, therefore, is obtained by deducting the temperature-induced strain from the total strain detected by the gauge.

In a Bragg Grating gauge, the temperature-induced strain is the result of two phenomena: the thermo-optic response of the grating, and the difference between the thermal coefficients of the gauge and the substrate material. This strain, $\grave{o}_T$, can be calculated from the following equation:

Equation A.5

$$\varepsilon_T = (\beta_O + \alpha_S - \alpha_G)\Delta T$$

where β_O represents the response of the gauge itself with temperature, and α_S and α_G are the thermal expansion coefficients of the substrate material and the gauge, respectively. ΔT is the temperature change with respect to the temperature at the installation time.

Due to its special structure, a Fabry-Perot gauge responds to temperature change only if there is a mismatch between the thermal expansion coefficient of the gauge and the substrate material, i.e.

Equation A.6

$$\varepsilon_T = (\alpha_S - \alpha_G)\Delta T$$

The thermal expansion coefficient of the non-compensated Fabry-Perot gauges is as low as $0.5\mu\varepsilon/°C$. Therefore, the strain detected by these gauges is practically the total strain produced in the material (summation of mechanical and thermal strain). The mechanical strain, $\in_T$, therefore is given by:

Equation A.7

$$\varepsilon_T = \varepsilon - \alpha_S \Delta T$$

where $\in$ is the total strain. For the self-compensated Fabry-Perot gauge, the thermal expansion coefficient of the gauge is close to that of steel. Therefore, when these gauges are used with material with a similar thermal expansion coefficient, the detected strain does not carry the temperature effect.

A.1.3 Vibrating Wire Strain Gauges

Vibrating wire (VW) strain gauges are relatively bulky (usually larger then 100 mm in length) and are produced for embedment in concrete or attaching to the surface of components. Surface strain gauges can be welded, bolted or bonded to the material. Embeddable strain gauges can be directly placed in concrete or cast into a concrete briquette before being placed in their final position. In either case, the placement of large diameter aggregates in the proximity of the gauge must be avoided. This is essential for preventing stress discontinuity in the gauge area. Theoretically, the maximum aggregate size, within an envelope of 1.5 gauge lengths around the gauge, should not exceed 1/5 of the gauge length.

Vibrating wire strain gauges are encased in sealed steel tubes. The gauges are equipped with a magnet/coil assembly for exciting the wire inside the tube, and sensing its frequency. In some of the models available on the market, the magnet/coil assembly is attached to the outside of the tube, and in others it is built inside the tube. In general, VW gauges are not susceptible to humidity, however the surface gauges should be protected against direct contact with weather.

A temperature sensor is a standard feature on every VW strain gauge. The same readout unit used to read the strain, reads the temperature sensor. The temperature reading lets the user apply the necessary correction for the temperature effect. To do this, calculate the temperature-induced strain from Equation A.6 and deduct it from the strain reading. Since the temperature-induced strain is the result of the difference in thermal expansion coefficients of the gauge and the instrumented component, no temperature correction is considered when the gauge is attached to a steel component.

A.2 Linear Variable Differential Transducers

The linear variable differential transducers (LVDT) are used for displacement measurements, and consist of a hollow metallic casing in which a shaft, called the core, moves freely back and forth along the axis of measurement. The core is made of a magnetically conductive material, and a coil assembly surrounds the metallic shaft. As shown schematically in Figure A.10, the coil assembly consists of three transformer windings. A central primary winding is flanked by two secondary windings, one on either side. The outputs of the secondary windings are wired together to form a series opposing circuit. When an AC excitation is applied to the primary winding, it generates an inductance current in the secondary windings, due to the mediation of the magnetically conductive core. When the core is equidistant between both secondary windings, no voltage appears at the secondary outputs. However, when the core moves, a differential voltage is induced at the secondary output. The magnitude of the output voltage changes linearly with the magnitude of the core's excursion from the centre.

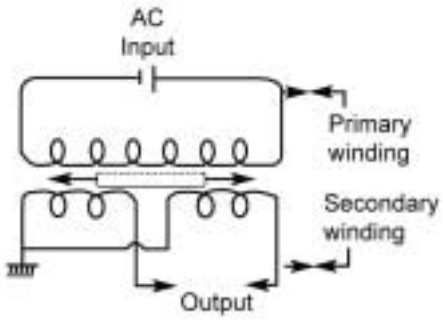

Figure A.10 Schematic diagram of a typical LVDT sensor

A.3 Accelerometers

Accelerometers used for civil engineering applications are either piezoelectric accelerometers or spring-mass accelerometers. Piezoelectric accelerometers are light and small, and operate over wide acceleration and frequency ranges. On the other hand, spring-mass accelerometers are relatively bulky and operate over a limited range of accelerations and frequencies. However, they are very sensitive to small accelerations and provide better resolution than the piezoelectric accelerometers.

The piezoelectric accelerometer is made of a piezoelectric crystal element and an attached mass that is coupled to a supporting base. When the supporting base undergoes movement, the mass exerts an inertia force on the piezoelectric crystal element. The exerted force produces a proportional electric charge on the crystal (Figure A.11). Since the force is equal to mass times acceleration, the charge is proportional to acceleration.

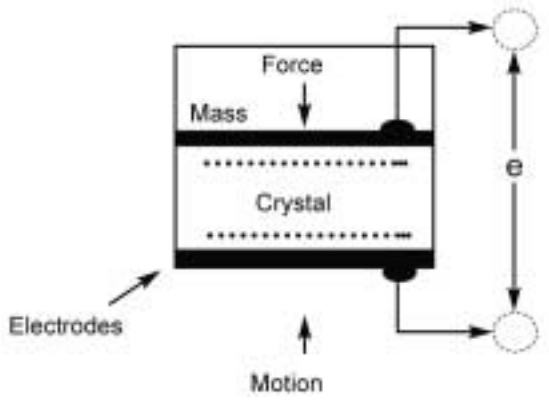

Figure A.11 Schematic diagram of a piezoelectric accelerometer

A.3.1 Spring-mass Accelerometers

The spring-mass accelerometer is essentially a damped oscillator.

A.4 Temperature Sensors

Temperature can be measured by a diverse array of sensors. Three types commonly used for civil engineering applications are: resistive; vibrating wire; and fibre optic temperature sensors.

A.4.1 Resistive Temperature Sensors

Resistive temperature sensors are based on the fact that the electrical resistance of a material changes as its temperature changes. There are two types of resistive temperature sensors: metallic sensors and thermistors. A typical metallic sensor comprises a fine platinum wire wrapped around a mandrel and covered with a protective coating, or encased in a protective housing. The variation of the platinum resistance with temperature is linear. This variation can easily and accurately be measured by installing the sensor in one arm of the Wheatstone bridge circuit.

Thermistors are based on resistance change in a ceramic semiconductor. The resistance-temperature relationship of a thermistor is negative and highly nonlinear. However, this difficulty is resolved by using thermistors in matched pairs in such a way that the nonlinearities of the two semiconductors offset each other. The operation range of thermistors is smaller than that of metallic temperature sensors, but thermistors usually provide higher accuracy.

Resistive sensors all have a very important limitation. The current for the operation of these sensors, even though very small, creates a certain amount of heat, leading to an erroneous temperature reading.

A.4.2 Vibrating Wire Temperature Sensors

Vibrating wire temperature sensors operate similarly to VW strain gauges. A change in temperature causes a change in the frequency signal output from the VW temperature sensor. The readout device processes the signal and converts it to a voltage proportional to the temperature, or displays a reading in temperature units. The VW temperature sensor is encased in a cylinder to prevent physical contact between the sensor and the material. Therefore, no special precaution is needed for the effect of the strains on the reading of the sensor.

Appendix

B DATA ACQUISITION SYSTEM

A data acquisition system collects data from various sensors. A general understanding of this system and its components is essential in order to design an efficient and useful monitoring program. This appendix introduces two common data acquisition systems, the manual and the computer-based system.

In a manual system, the operator visually reads the data from the readout units, and records it manually. Since this system does not need bulky equipment, it is an economical and convenient way to collect data from a small number of sensors for a short period of time. However, for more general applications, a computer-based data acquisition system must be used. The components of this data acquisition system, as shown in Figure B.1, are signal conditioners, one or more data acquisition boards, and a computer.

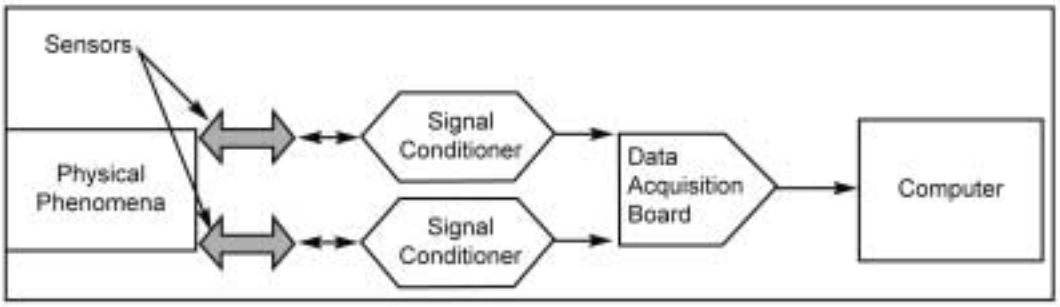

Figure B.1 Components of a computer-based data acquisition system

Sensors are the components that are in physical contact with the structure and register the required attributes of the structure. Electronic and optical sensors are two common types of sensors. An electronic sensor transmits electrical signals in terms of electrical charges or a change in voltage. By comparison, the optical sensors transmit light signals.

In a conventional data acquisition system, the readout unit receives the data directly from the sensors and converts it into engineering values. In a computer-based system, the signals from the sensors cannot usually be read directly by the computer. The signals need to pass through a signal conditioner unit and a data acquisition board before being read by the computer.

Different sensors usually require specific signal conditioners, while a single data acquisition board can receive data from a variety of signal conditioners. Signal conditioners have multiple functions. They amplify low-level signals, isolate, filter, linearize, excite, and bridge complete transducers to produce high-level signals. The output of signal conditioners, which carries the characteristic of the physical phenomenon, is analog. The function of a data acquisition board is to convert the analog signal into a digital signal for the computer. Combined units that have the functionality of both a signal conditioner and a data acquisition board, are also available.

In addition to equipment, a computer-based data acquisition system requires a data acquisition program. This program scans the data from the data acquisition board, analyzes and processes the data, makes certain decisions, and stores the processed data on the hard disk of the computer.

B.1 Sensor Readout Units and Signal Conditioners

Readout units and signal conditioners are the components that analyze and process the sensors. "Readout units" usually refers to devices used with a conventional data acquisition system that have readout displays showing values of the measured quantities. "Signal conditioners," on the other hand, are devices that are used with a computer-based system, and produce analog voltages. Otherwise, there is no significant difference between the two devices. Moreover there are some devices that combine features of the two, so the terms "readout unit" and "signal conditioner" are generally used interchangeably.

Electrical sensors usually need inputs in the form of voltage and current, and optical sensors need input in the form of light signals. These signals are also generated in the readout units and signal conditioners. In general, these devices perform the following functions:

Generating input signals for the sensor: Sensors, such as strain gauges and resistive temperature sensors, require external DC voltage or current excitation. Linear variable differential transducers (LVDT) and vibrating wire gauges require AC currents for their operation, and optical sensors require high intensity modulated light. These requirements are generated in the readout units and the signal conditioners.

Amplification: Signal conditioners amplify low-level signals received from the sensors. This increases the resolution and reduces noise. For the highest possible accuracy, the signal should be amplified so that the maximum voltage range of the conditioned signal equals the maximum input range of the data acquisition board.

Filtering: Filtering removes unwanted signals from the signal received by the sensor. The unwanted signals, called noise, are generated from external sources such as AC power lines, motors, generators, transformers, fluorescent lights, soldering irons, CRT displays, computers, electrical storms, welders, and radio transmitters, and from internal sources such as semiconductors, resistors, and capacitors.

Isolation: When the data acquisition board input and the signal being acquired by the signal conditioner are each referenced to the "ground", problems occur if there is a potential difference between the two grounds. This difference can lead to what is known as a ground loop. This may cause inaccurate representation of the acquired signal. If the potential difference between the two grounds is too large, it may damage the measurement system. The use of isolated signal conditioning modules eliminates the ground loop and ensures that the signals are accurately acquired.

Another reason for isolation is that the system being monitored may contain high-voltage transients. Isolating the sensor signals from the computer is a safety measure that protects the computer against possible damage.

Bridge completion: Sensors such as strain gauges and resistive temperature sensors operate as part of the Wheatstone bridge circuit. Signal conditioners and readout units for this kind of sensor provide the required resistors for completion of the Wheatstone bridge circuit.

B.2 Data Acquisition Boards

Signals produced by signal conditioners are analog and therefore cannot be directly connected to a computer. The data acquisition (DAQ) board converts the analog signals into digital signals, that are then recognizable by a computer. A DAQ board is called a plug-in board if it is installed inside a computer and uses the computer's power supply. Otherwise, it is called a stand-alone unit and has its own power supply. The digital signals from a stand-alone unit are then transmitted to the computer through a special cable. Some manufacturers produce units that contain both the features of the DAQ board and the signal conditioner. 'These units may be in the form of a plug-in board or a stand-alone unit.

Basic specifications available on most data acquisition products include: the number of channels, sampling rates, resolution, input range, and gain. These specifications are briefly discussed below.

Number of channels: The number of analog signals that can be connected simultaneously to a DAQ board is called the "number of channels". The number of channels for single-ended analog inputs is usually twice as many as when the analog inputs are used in differential mode.

Single-ended inputs are all referenced to a common ground point. These inputs are typically used when the input signals are at a high level (≤1 Volt), the leads from the source to the data acquisition board are short (< 4.5 m), and all input signals can share a common ground reference. If the signals do not meet these criteria, the inputs must be connected to the DAQ board in a differential mode. In differential mode, noise errors are reduced because the common-mode noise picked up by both leads is canceled out.

In a single-ended mode, one of the two leads of the analog signal is connected to the input channel of the DAQ board, and the other lead is connected to the common ground. In differential mode, both leads are connected to the DAQ board input channels.

Sampling rate: This parameter specifies how often the analog-to-digital conversions can take place. A DAQ board must be fast enough to acquire a sufficient number of points in a given time to provide an accurate representation of the original signal. Obviously, if the signal is changing faster than the DAQ board is digitizing, errors are introduced into the measured data. In fact, data that is sampled too slowly can appear to be at a completely different frequency. The distortion of the signal is referred to as aliasing. Refer to Figure B.2.

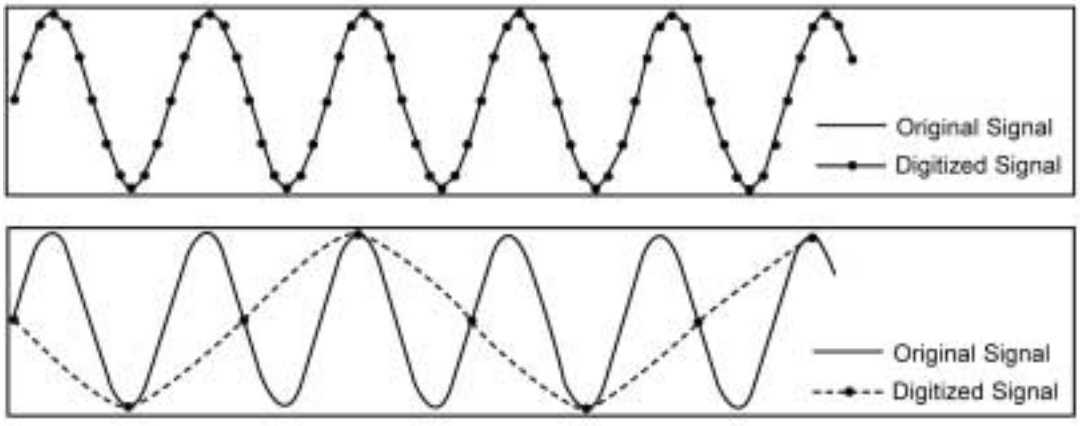

Figure B.2 Effect of low sampling rate on the reproduced signal
Top: adequately sampled Bottom: under sampled

Generally, in a multi-channel DAQ board, a single analog-to-digital converter (ADC) performs the conversion of the analog signal to a digital signal by switching between channels. This method, which is called multiplexing, is significantly less expensive than having a separate ADC for each input channel. However, because the multiplexer switches between channels, a time lag is generated between each channel sample. DAQ products capable of simultaneous sampling use sample-and-hold circuitry for each input channel. Nevertheless, for most practical cases the costly feature of sample-and-hold circuitry is not necessary for simultaneous sampling.

Sampling all the channels in a row by multiplexing is called "scanning". When using a DAQ board with a high sampling rate, all the input channels are scanned within microseconds. The time lag produced between the sampling times of different channels is insignificant for most applications; therefore the collected data creates the effect of simultaneous sampling. However, it is important to note that since the same ADC samples all the channels, the effective sampling rate of each individual channel is reduced in proportion to the number of channels being sampled. For example a DAQ board with 10 channels and a sampling rate of 1.25 MS/s (million samples per second) will effectively sample each individual channel at 125 kS/s (thousand samples per second), when all the channels are active.

Resolution: Resolution of a DAQ board is reported as a value called a "bit". A board with "α bit" resolution divides the signal voltage range into 2^{α}equal divisions. Theoretically, one half of the division is the smallest voltage change that the DAQ board can detect. To demonstrate how a DAQ works, consider a hypothetical 3-bit converter. A 3-bit converter divides the analog range into 8 equal divisions. Figure B.3 shows a sine wave and its corresponding digital image as obtained by the 3-bit ADC. Each division is represented by a binary code between 000 and 111. Clearly, the digital representation obtained from a 3-bit ADC is not a good representation of the original analog signal. However, by increasing the resolution, the number of divisions increases and therefore better representation is obtained. For example, a 16-bit ADC divides the analog range into 65536 divisions, which provides extremely accurate digital representation of the analog signal.

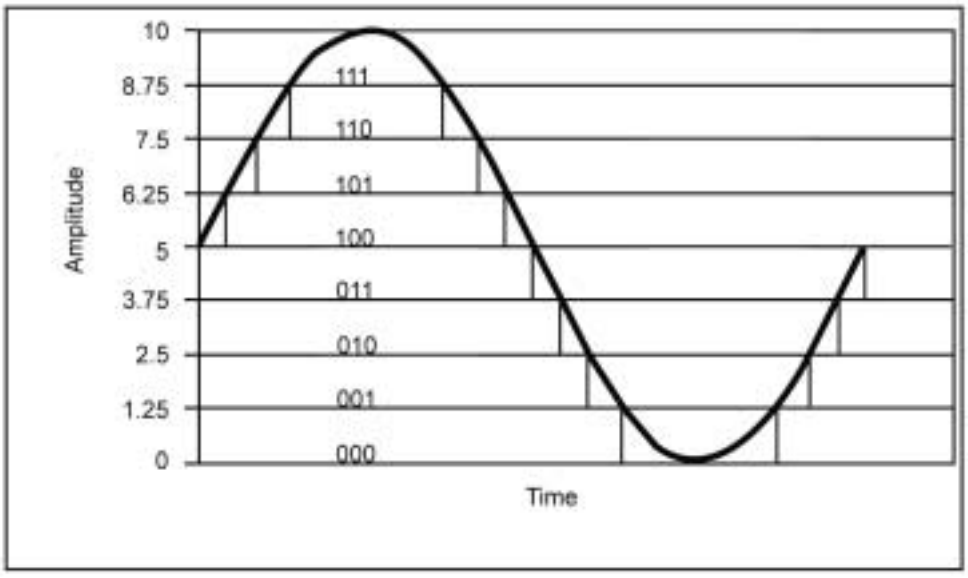

Figure B.3 Digitized sine wave with 3-bit resolution

Range: "Range" refers to the minimum and maximum voltage levels that a DAQ board can span. Some DAQ boards offer selectable ranges; for example –10V to +10V and 0 to 10V. Since the DAQ divides the whole range into equal divisions, a smaller range provides higher accuracy. Therefore, it is advisable to use the 0 to 10V range for a positive voltage signal.

Gain: Gain is a factor by which a signal is amplified. Some DAQ boards offer selectable gain; for example, 1, 5, 10, and 50. Gain is used to amplify the low voltage signal before it is converted to a digital signal, thereby increasing the accuracy of the conversion. For example, consider a board with 12-bit resolution and a selectable range of 0 to 10V. The theoretical smallest detectable voltage change is $10/(2 \times 2^{12}) = -.0012V$.

If this board is used for a signal that varies between 0 and 0.05V, the accuracy of the measurement will not be satisfactory, since any variation less than 0.0012/0.05 (=2.4%) of the largest signal is not detectable. However, if the board has a selectable gain of 50, then the accuracy of the measurement will be increased by 50 times. It is important to note that the gain selected should not be so large that the amplified signal falls outside the DAQ board range.

B.3 Data Acquisition Program

The data acquisition (DAQ) program is an essential component of a computer-based data acquisition system. It instructs the computer how often and when to scan the DAQ board, how to process the collected data, and what to save. Some suppliers provide DAQ programs with their DAQ boards. These programs are usually general and may not fit the requirements of a specific project. Therefore, you may need to develop your own DAQ program.

Some suppliers of DAQ boards provide driver software with the board. Driver software is the layer of software that directly programs the registers of the DAQ hardware, managing the operation and integration with the computer resources, such as processor interrupts, direct memory access (DMA), and memory. Driver software hides the low-level, complicated details of hardware programming and provides the user with an easy-to-understand interface. In summary, driver software is an interface program between the DAQ program developed by the user and the DAQ board. It must be installed on the computer before the DAQ program operates.

It is important to note that all driver software supports a limited number of programming languages. Therefore, before developing your own DAQ program, ensure the compatibility of the driver software with the programming language that you intend to use.

Most suppliers of DAQ boards offer their own data acquisition software that enables the development of data acquisition programs in an easy and usually graphical way. Some of the software is quite powerful, but many may have significant limitations and may not fit the requirements of a given project. Although the use of the software is usually beneficial, the user should be aware of how software limitations may affect the requirements of a particular project. Figure B.4 shows the interface window of the data acquisition program developed for the Confederation Bridge monitoring project. The program was developed by the Nova Scotia CAD/CAM centre using LabVIEW; a programming language developed by National Instruments for data acquisition applications.

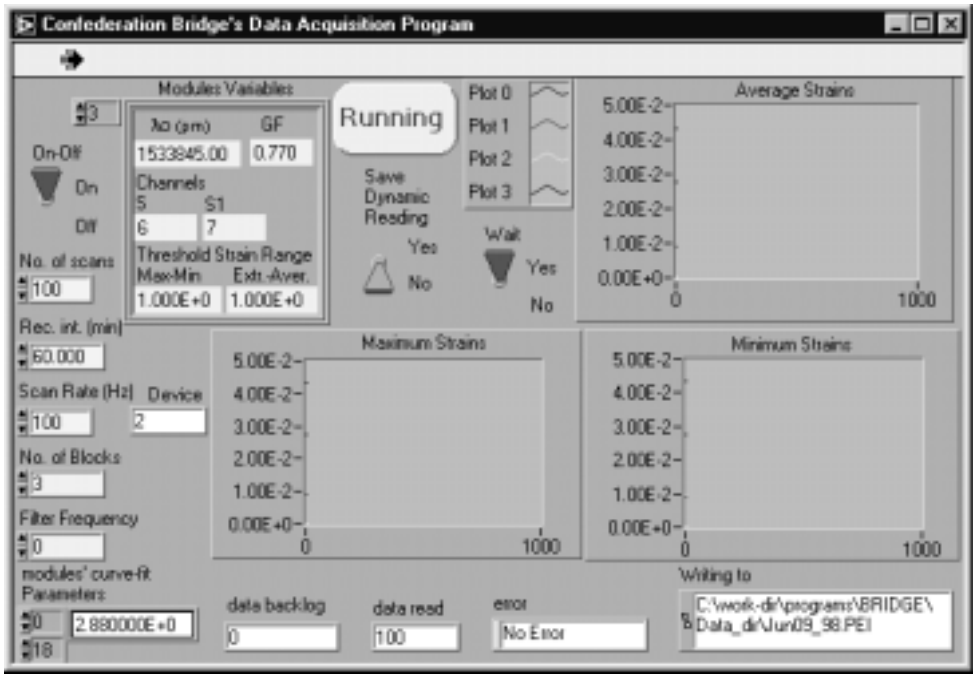

Figure B.4 The data acquisition program interface window for Confederation Bridge

The extent of a DAQ program depends on the requirement for each particular project. For example, a DAQ program may just simply scan the board at a constant rate and save the data on the hard disk of the computer. A more sophisticated program may scan the board at a fast rate, process the data, screen for unwanted data, and save only a small amount of data on the hard disk. A few examples of unlimited capability that can be achieved from a DAQ program are described below.

The simplest form of monitoring is to scan the DAQ board at a constant rate and save all the data. This method is good when the monitoring period is short, or when the variation of data is not fast. When the monitoring period is short, a rapidly varying signal can easily be recorded by selecting a fast scan rate. However, maintaining a fast scan rate for a long period of time is not always feasible. This is due to limitations in computer disk space and also to limitations in the handling and processing of bulky data. For continuous monitoring, it is advisable to create a new data file each day. The scan rate must be reasonably slow so that the files are manageable, and do not require a large space on the hard disc. Therefore, when bridge vibration and signals due to the traffic are a prime concern, this method may not be suitable for continuous monitoring of the bridge.

The method described above can be significantly improved by scanning the board with a fast scan rate and saving only the maximum, minimum, and average values of each channel, over a relatively long period of time. Therefore, when using this method for continuous monitoring, the important characteristics of the signal are not lost, and the amount of the saved data is smaller and manageable.

Appendix

C ALGORITHMS FOR VIBRATION-BASED DAMAGE DETECTION

In the past decade or so, a great deal of research has been carried out on the development of analytical techniques for vibration-based damage detection. Since vibration-based SHM found its early application in aerospace and mechanical engineering, much of the research has been carried out in these fields. Research studies on the application of vibration-based assessments for health monitoring of civil engineering structures are more recent. Doebling et al. (1996) provide an extensive bibliography related to this subject. Farrar et al. (1994) have reviewed the literature on vibration testing and damage detection in bridges.

A number of different analytical techniques have been developed for the identification of damage from detected changes in vibration properties. The more commonly used techniques are:

- methods based on mode shape curvature changes
- matrix update methods

The above list is by no means exhaustive. For example, methods have been developed that are based on the determination of a damage index, measured flexibility changes, and changes in the derived stiffness. Work has also been done on methods based on neural networks. However, additional studies will have to be carried out before these methods become suitable for practical damage detection in civil engineering structures. The methods listed above are briefly reviewed here.

C.1 Methods Based on Changes in Resonant Frequencies

Reduction in resonant frequencies indicates that damage has taken place. However, in practice, this will identify damage only at Level 1. Cawley and Adams (1979) have shown that by determining the ratio of the changes in any two frequencies, it is possible to identify both the location and severity of the damage. For a practical application of this concept consider the eigenvalue equation given by:

Equation C.1

$$K\phi_i = \lambda_i M\phi_i$$

where K is the stiffness matrix, ϕ_I is the ith mode shape, λ_I is the associated eigenvalue (squared frequency), and M is the mass matrix. Damage in the structure may change both the stiffness and the mass matrices, altering the frequencies as well as the mode shapes. The eigenvalue equation for the damaged structure can be written as:

Equation C.2

$$(K + \delta K)(\phi_i + \delta \phi_i) = (\lambda_i + \delta \lambda_i)(M + \delta M)(\phi_i + \delta \phi_i)$$

Assuming that damage does not alter the mass matrix, δK and δM is small, and neglecting higher order terms, we get:

Equation C.3

$$(K\phi_i - \lambda_i M\phi_i) + (K - \lambda_i M)\delta\phi_i + \delta K\phi_i - \delta\lambda_i M\phi_i = 0$$

The expression in the first set of parentheses is zero because of Equation C.1. Pre-multiplying Equation C.3 by ϕ_i^T and noting that, ϕ_i^T $(\mathbf{K}-\lambda_1\mathbf{M})$ being the transpose of Equation C.1 is also zero, we get:

Equation C.4 $$\delta\lambda_i = \frac{\phi_i^T \delta K \phi_i}{\phi_i^T M \phi_i}$$

We now assume that the first few eigenvalues and mode shapes of the undamaged structure have been determined either by analyzing a finite element model of the undamaged structure, or through modal testing. A modal test must be carried out on the damaged structure to determine the altered eigenvalues for the first few modes. Let $\delta\gamma_I$ represent the difference between the *i*th eigenvalue of the damaged structure, obtained from a modal test, and the corresponding eigenvalue of the undamaged structure as obtained form analysis or testing. Also, let $\delta\gamma_j$ represent the similar value for *j*th mode. Now, select a possible damage site in the structure and assume that a single finite element, say element *r,* represents the site. Damage in the structure has reduced the stiffness of this element rom k^r to α k^r, so that:

Equation C.5 $$\delta K = (\alpha - 1)k^r$$

By inserting the value of $\delta\mathbf{K}$ from Equation C.5 in Equation C.4, we can determine $\delta\lambda_1$, and similarly $\delta\lambda_j$, both in terms of the unknown parameter (a). The ratio $\delta\lambda_1/\delta\lambda_j$ is, however, independent of (a), and is fully determined. If the damage site selected is, in fact, the true site, the ratio $\delta\gamma_i/\delta\gamma_j$ must be equal to or close to the ratio $\delta\lambda_1/\delta\lambda_j$.

As an example of damage detection based on frequency change, consider a simply supported composite steel concrete bridge girder of span L=20 m. The girder has the following properties:

Mass per unit length m = 1290 kg/m

Modulus of elasticity E = 200 x 10^9 N/m^2

Equivalent moment of inertia I = 2760 x 10^6 m^4

A finite element model of the girder is shown in Figure C.1. The girder is divided into 10 beam elements, each 2 m long. The number of nodes is 11. Considering 2 degrees of freedom (d.o.f.) at each node, lateral translation along the *y* axis and rotation about the *z* axis, the total number of d.o.f. is 22. However, lateral translation is prevented at joints 1 and 11, so the number of effective d.o.f. is 20.

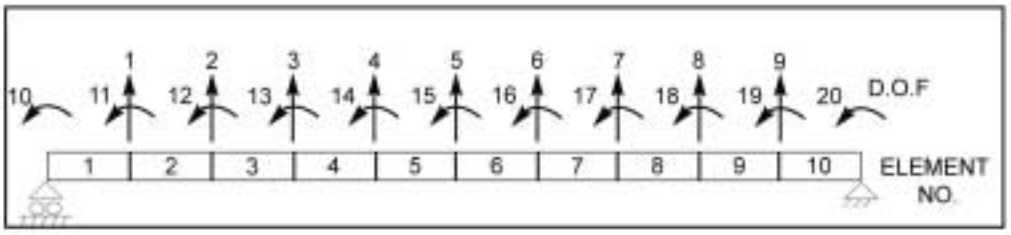

Figure C.1 Finite element model of a composite steel concrete girder

Consider 3 different states for the structure: a healthy structure, a damaged structure in which the stiffness of element 4 has been reduced by 15 percent, and a damaged structure in which the stiffness of element 4 has been reduced by 50 percent. Modal tests on the three structures should give three sets of eigenvalues corresponding to modes 1, 2 and 4, shown in Table C.1, provided there are no errors in the measurements.

Table C.1 - Eigenvalues Obtained from Modal Tests

Mode No.	Healthy		15% Stiffness Reduction in Element 4			50% Stiffness Reduction in Element 4		
	State of the Structure							
	γ	ω rad/s	γ	δγ	ω rad/s	γ	δγ	ω rad/s
1	260.55	16.14	253.4	7.15	15.92	224.8	35.75	14.99
2	4167.2	64.55	4077.0	90.2	63.85	3748.0	419.2	61.22
4	66362.0	257.6	64645.0	1717.0	254.2	58940.0	7422.0	242.8

The ratios of changes in the eigenvalues in any pair of modes can be calculated from the data presented in Table C.1. Equation C.4 shows that these ratios should not vary with the severity of the damage. This is not, however, strictly correct because in deriving Equation C.4 we have neglected the higher order terms. Thus, for a 15 percent reduction in the stiffness of element 4 we get $\delta\gamma_2/\delta\gamma_1 = 12.62$ and $\delta\gamma_4/\delta\gamma_1 = 240.1$. The corresponding values for a 50 percent reduction in the stiffness of element 4 are 11.73 and 207.6.

Using Equation C.4 we can calculate the changes in the eigenvalues of the structure caused by a reduction in the stiffness of a given element of the structure. The changes in the eigenvalues caused by reducing the stiffness of each of the 10 elements, taken one at a time, to zero, are shown in Table C.2 for 5 of the elements and for modes 1, 2, and 4. The values for the other 5 elements can be obtained by noting that the beam is symmetrical about its centreline. Also shown in the table are the ratios $\delta\lambda_2/\delta\lambda_1$ and $\delta\lambda_4/\delta\lambda_1$. We now define parameter (e) as follows:

Equation C.6a $$e_i = \frac{\delta\lambda_i/\delta\lambda_1}{\delta\gamma_i/\delta\gamma_1} \quad \text{for} \quad \delta\lambda_i/\delta\lambda_1 \le \delta\gamma_i/\delta\gamma_1$$

Equation C.6b $$e_i = \frac{\delta\gamma_i/\delta\gamma_1}{\delta\lambda_i/\delta\lambda_1} \quad \text{for} \quad \delta\lambda_i/\delta\lambda_1 > \delta\gamma_i/\delta\gamma_1$$

Table C.2 - Changes in Eigenvalues Caused by Reduction in Element Stiffness

Mode No.	Element No.				
	1	2	3	4	5
1	1.714	10.934	26.056	41.223	50.366
2	102.30	536.98	805.16	536.98	102.30
4	5199.9	10399.0	1981.4	10399.0	5199.9
$\delta\gamma_2 / \delta\gamma_1$	59.68	49.11	30.90	13.03	2.03
$\delta\gamma_2 / \delta\gamma_1$	3033.8	951.07	76.044	252.26	103.30
$\delta\gamma_2 / \delta\gamma_1$	11.69	11.69	11.69	11.69	11.69
$\delta\gamma_2 / \delta\gamma_1$	207.3	207.3	207.3	207.3	207.3
e_2	0.196	0.238	0.378	0.898	0.174
e_4	0.068	0.218	0.367	0.822	0.499

Values of e_i, as defined in Equations C.6a and C.6b, are shown in Table C.2, and plotted in Figure C.2 against the number of elements suffering damage. Elements where (e) is close to 1 are identified as suffering damage. In the present case, both elements 4 and 7 are identified, even though only element 4 was damaged. This result is because of the symmetry in the structure.

Assuming that element 4 is correctly identified as damaged, the severity of the damage can be assessed. The related calculations for five modes are shown in Table C.3, where $\beta=1-\alpha$ measures the severity of the damage. For 15 percent reduction in stiffness, the identified severity is, in each case, quite close to the actual, although somewhat higher. For a 50 percent reduction in stiffness, the calculated severity provides a gross overestimate. This is because the higher order terms were neglected in deriving Equation C.4. This is likely to introduce errors when the damage is substantial.

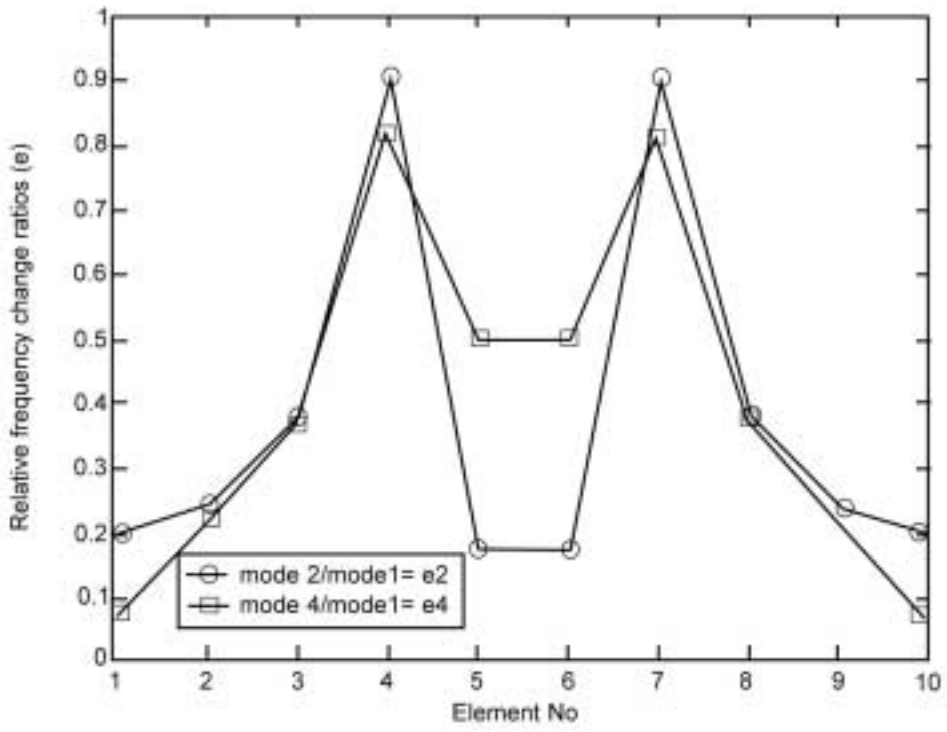

Figure C.2 Relation between frequency change ratios for different damage sites

Table C.3 - Calculation of the Severity of Damage

Mode No.	100% Damage in Element 4	15% Damage in Element 4		50% Damage in Element 4	
	$d\lambda$	$\delta\gamma$	$\beta = \delta\gamma / \delta\gamma$	$\delta\gamma$	$\beta = \delta\gamma / \delta\gamma$
1	41.223	7.15	0.17	35.8	0.868
2	536.98	99.1	0.18	418.7	0.780
3	422.69	74.1	0.175	455.8	0.960
4	10399.0	1717.0	0.165	7423.0	0.714
5	16048.0	2624.0	0.164	11466.0	0.714

The foregoing example highlights the limitations of the damage detection methods that are based on frequency shifts. It is apparent that even a large reduction in the stiffness of an element causes only small changes in the frequencies. In the present example, a reduction of 50 percent in stiffness over a 2 m length of the beam only causes a 7 percent reduction in the fundamental frequency. A 15 percent reduction in stiffness leads to a reduction in the fundamental frequency of only 1.36 percent. Changes of this magnitude are likely to be obscured by noise in the measurements and environmental effects. Farrar et al (1996a, b) reached a similar conclusion with tests on a slab and girder bridge on Interstate Highway 40.

The frequency shift method presented here is able to correctly identify damage only when it is concentrated at a single location; multiple damage sites cannot be identified. In addition, when the structure is symmetrical, ambiguity exists in the identification of the damage site. Finally, estimates of the severity of damage are not accurate for large amounts of damage.

C.2 Damage Detection Based on Modal Residual Vector

This method relies on the measurement of both the frequencies and mode shapes of the damaged structure. The eigenvalue equation for the damaged structure can be written as:

Equation C.7 $$(K + \delta K)\phi_{di} - \lambda_{di} M \phi_{di} = 0$$

Where ϕ_{di} is the ith mode shape of the damaged structure, λ_{di} is the associated eigenvalue, and it is assumed that the damage does not cause a change in the mass.

In Equation C.7 all quantities, other than δK, are known or have been determined through modal test. Equation C.7 can be written in the following alternative form:

Equation C.8 $$K\phi_{di} - \lambda_{di} M \phi_{di} = R_i = -\delta K \phi_{di}$$

Evaluation of the left-hand side of Equation C.8 provides the modal residual vector R_i for the ith mode. Matrix δK will have non-zero terms corresponding to only those degrees of freedom (d.o.f.) that are connected to the damaged elements. Correspondingly, the non-zero terms in R_i will also lie along the same d.o.f. Knowledge of the affected d.o.f., and the connectivity relation between the elements and the d.o.f., will allow determination of the damage location. When more than one mode is determined, an absolute sum of the modal residuals can be used to determine the damage location. When using the absolute sum, the mode shape should be appropriately normalized so that individual elements of the various mode shapes have the same relative order of magnitude. This can be achieved by mass-orthogonalization of the mode shapes.

Having identified the damaged elements, it is possible to express δK as the weighted sum of the stiffness matrices of the damaged elements. The weighting factors, which are the unknowns in the problem, define the severity of damage in the affected elements. For example, if the altered stiffness of element j is expressed as $\alpha_j k_j$, we have:

Equation C.9 $$\delta K = \sum_j k_j (\delta_j - 1)$$

where the summation is carried out over all the damaged elements. Defining $\beta_j = 1 - \alpha_j$ Equation C.8 can be expressed as:

Equation C.10

$$\left(\sum_j \delta_j k_j \right) \ddot{u}_{di} = -R_i$$

When more than one mode is determined, the following equation may be used in place of Equation C.10:

Equation C.11

$$\sum_i \left| \left(\sum_j \delta_j k_j \right) \ddot{u}_{di} \right| = \sum_i \left| R_i \right|$$

Equation C.10 or C.11 can be solved to obtain the values of factors β_j. In general, more than one value will be obtained for each of the factors β_j. The different values can be averaged to obtain the best estimate.

Consider, again, the example beam shown in Figure C.1, and assume that the damage has caused a 50 percent reduction in the stiffness of element 4, and a 25 percent reduction in the stiffness of element 8. Modal testing on the structure provides the eigenvalues and mode shapes for just the first two modes, from which the residuals **R** are determined. The absolute sums of the residuals corresponding to both the displacement and rotation of the degrees of freedom are shown in Table C.4.

Table C.4 - Absolute Sum of the Residuals

Joint No.	Displacement d.o.f.	Rotation d.o.f.
1	0	0
2	0	0
3	0	0
4	0.9146E05	0.4659E06
5	0.9146E05	0.3121E06
6	0	0
7	0	0
8	0.4874E04	0.1385E06
9	0.4674E04	0.1291E06
10	0	0
11	0	0

From the data presented in Table C.4, it is obvious that the elements connecting joints 4 and 5 and 8 and 9 are damaged. Equation C.11 is now utilized for non-zero elements:

Equation C.12

$$\beta_4 \begin{bmatrix} 0.1830\text{E}06 \\ 0.1830\text{E}06 \\ 0.9318\text{E}06 \\ 0.6242\text{E}06 \end{bmatrix} = \begin{bmatrix} 0.9146\text{E}05 \\ 0.9146\text{E}05 \\ 0.4659\text{E}06 \\ 0.3121\text{E}06 \end{bmatrix}$$

and

Equation C.13

$$\beta_8 \begin{bmatrix} 0.1870E05 \\ 0.1870E05 \\ 0.5540E06 \\ 0.5168E06 \end{bmatrix} = \begin{bmatrix} 0.4874E04 \\ 0.4674E04 \\ 0.1385E06 \\ 0.1292E06 \end{bmatrix}$$

Equation C.12 provides four estimates for β_4, each of which is 0.5. In a similar manner, Equation C.13 provides four estimates for β_8, each equal to 0.25. Precise answers have been obtained in this case because in the computer simulation the finite element formulation provides an exact representation of the structure, and there are no experimental errors associated with the measured modes. In a practical case none of this will hold true, and the various estimates of the damage factors will be slightly different. It may also be noted that if a damaged element lies close to the node of a vibration mode shape, the residuals corresponding to that element and mode will be zero, or very small. In other words, a sufficient number of modes should be included so that the damaged elements are located at a distance from at least some of the nodes.

The modal residual method requires that a finite element model of the undamaged structure is available, and that the mode shapes of the damaged structure are measured. In fact, modal displacements need to be measured at all of the d.o.f. in the analytical model including those in the vicinity of the damage. For the example under consideration, rotational degrees of freedom are included, which in practice, are very difficult to measure. The rotations can sometimes be derived from measured translations by using central difference expressions or cubic spline functions.

Upon repeating this example with the damage located in elements 4 and 6, non-zero values for the residuals corresponding to joints 4, 5, 6, and 7 are found. Connectivity of the elements may then lead us to believe that elements 4, 5, and 6 are all damaged, although we cannot be certain about element 5. When Equation C.11 is now used to determine β_4, β_5, and β_6, β_4 will work out to 0.5, β_6 will work out to 0.25, and β_5 will be close to zero.

C.3 Methods Based on Mode Shape Curvature

Changes in the mode shape curvatures can be useful in detecting the location of damage in a structure that deflects primarily in flexure. The curvature is inversely proportional to the flexural rigidity as shown by the following well-known equation:

Equation C.14

$$\frac{\partial^2 u}{\partial x^2} = \frac{M(x)}{EI}$$

where $\partial^2 u / \partial x^2$ is the curvature at location x. Since damage reduces the flexural rigidity in the vicinity of the damage, curvature will increase at that location. Thus, it is possible to detect the location of the damage by comparing the pre- and post-damage curvatures.

The mode shape curvature can be obtained from the measured displacement components of the mode shape by using the following central difference expression:

Equation C.15

$$\frac{\phi_i^{k+1} - 2\phi_i^{k} + \phi_i^{k-1}}{h^2}$$

where k-1, k, and k+1 denote locations of displacement measurements, $X_{k+1} - X_k = X_k - X_{k-1} = h$ and ϕ_i^k is the modal displacement at location k in mode number i. This expression will have to be modified at the beginning of the span, where a corresponding forward difference equation may be used, and at the end of the span where a backward difference expression may be used. As an alternative to the difference expressions, cubic splines can be fitted to the measured displacements. The curvature is then obtained by taking the second differential of the spine curve.

Consider, again, the girder shown in Figure C.1 and assume that the stiffness (EI) of element 4 has been reduced by 50 percent as a result of the damage. The pre- and post-damage curvatures in mode 1 are compared in Figure C.3, which also shows the difference in the two sets of curvatures. The curves in Figure C.3 clearly show that the damage has occurred in element No. 4. The example is repeated with a 50 percent reduction in the stiffness of element 4 and a 25 percent reduction in the stiffness of element 8. The pre- and post-damage curvatures are shown in Figure C.4. Again, it is possible to identify the damage locations, although some judgment is required in interpreting the data.

The mode shape curvature method is useful in identifying the damage location but cannot provide an estimate of the severity of the damage. Also, the usefulness of the method is limited to structures that can be modelled as a set of girders.

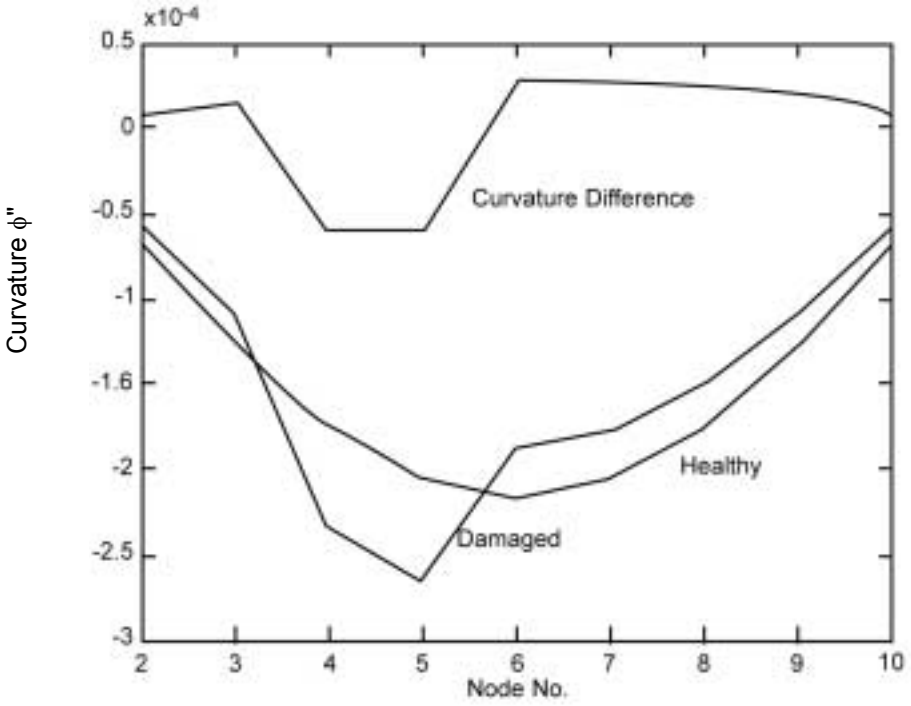

Figure C.3 Mode shape curvature for a bridge girder with damage in element 4

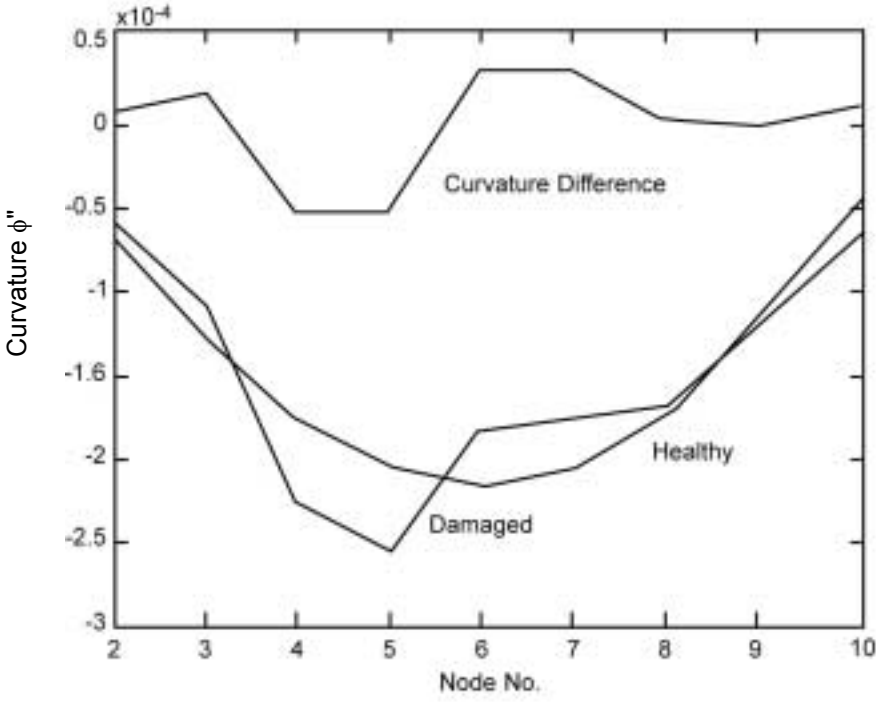

Figure C.4 Mode shape curvature for a bridge girder with damage in elements 4 and 8

C.4 Matrix Update Methods

Matrix update methods constitute the largest class of methods developed for identification of damage from measured vibration properties. The methods are based on the determination of perturbations in the property matrices, such as δK, that will satisfy the eigenvalue Equation C.7. The identified perturbation provides both the location and severity of the damage. In general, the number of unknown parameters in δK is significantly greater than the number of measured frequencies and mode shapes. The problem is, therefore, indeterminate and has an infinite number of solutions. A unique solution can be obtained through the minimization of an objective function, subject to some specified constraints. The matrix update methods can thus be classified on the basis of the objective function selected and the constraints used.

Many different objective functions may be used. This includes the norm of the estimated solution, rank of the perturbation matrix δK, norm of the perturbation matrix, norm of the modal residual vector R_i, and others. The constraints may include satisfaction of the eigenvalue equation, and preservation of the sparsity and connectivity of the property matrices. In addition β_j should be greater than or equal to zero but no greater than 1. Because of the many different ways in which the objective function and constraints can be defined and the different numerical techniques that can be used in the solution of the resulting optimization problem, a large number of methods have been developed. Here we present only one such method for the purpose of illustration.

Assume that the mode shapes of the undamaged structure have been mass orthonormalized. Equation C.4 then reduces to:

Equation C.16 $$\delta\lambda_i = \phi_i^T \delta K \phi_i$$

Equation C.16 gives the sensitivity of the eigenvalue to the change in the stiffness matrix. Now δK can be expressed as:

Equation C.17 $$\delta K = -\sum_{j=1}^{n} \beta_j k_j$$

where n is the number of elements and k_j is the stiffness of the jth element. Substitution of Equation C.17 in C.16 gives:

Equation C.18a $$\delta\lambda_i = -\sum_{j=1}^{n} \phi_i^T k_j \phi_i \beta_j$$

or

Equation C.18b $$D\beta = -\delta\lambda$$

where D is a (m) by (n) matrix whose elements are $d_{ij} = \phi_i^T k_j \phi_1$, β is the n-vector of the unknown changes in element stiffness matrices, and $\delta\lambda$ is the m-vector of measured eigenvalue changes. If m = n, Equation C.18b can be directly solved for β, giving:

Equation C.19 $$\beta = -D^{-1}\delta\lambda$$

In general, however, m will be less than n so that the problem defined by Equation 5.18b is indeterminate and has an infinite number of solutions. In order to obtain a unique solution we may minimize the quadratic norm of the stiffness changes given by:

Equation C.20 $$J = \beta^T\beta$$

with the constraint that Equation C.18b must be satisfied. If these are the only constraints the problem has a closed-form solution given by:

Equation C.21 $$\beta = -D^T\left(DD^T\right)^{-1}\delta\lambda$$

This solution is also useful in refining the analytical model of the undamaged structure to ensure that the analytically determined frequencies and mode shapes match those obtained by modal testing. The refined analytical model then serves as the baseline model in the subsequent determination of damage.

For a damaged structure, the following additional constraint must be placed on the stiffness changes:

Equation C.22 $$0 \le \beta \le 1$$

The problem now becomes a nonlinear optimization problem with the objective function defined by Equation C.19, equality constraints given by Equation C.18b and inequality constraints given by Equation C.22.

As an example, consider again the beam shown in Figure C.1. Suppose the only damage is in element 4, whose stiffness has been reduced by 25 percent. A finite element simulation provides the damaged and undamaged eigenvalues for the first five modes given in Table C.5. In the field application the eigenvalues will be obtained through modal testing. Ignoring the inequality constraint given by Equation C.22, we use Equation C.21 to identify the damage. A comparison of the identified and actual damage is compared in Figure C.5. Because of the symmetry in the structure, the identification method predicts damage in elements 4 as well as 7, each being 15.1 percent. In fact, if the damage in element 7 were constrained to zero, the predicted damage would be 30.2 percent in element 4. This difference between the predicted and actual damage is a result of neglecting the higher order terms in Equation C.16.

Table C.5 - Changes in Eigenvalues Caused by Structural Damage			
Mode No.	Measured Eigenvalues		
	Undamaged Structure	25% Reduction in Stiffness of Element 4	20% and 10% Reduction in Stiffness of Elements 4 and 8
1	260.509	247.454	247.963
2	4167.21	4003.52	3955.79
3	21073.1	20934.4	20747.1
4	66361.8	63298.5	63791.0
5	160465.01	155792.3	155162.4

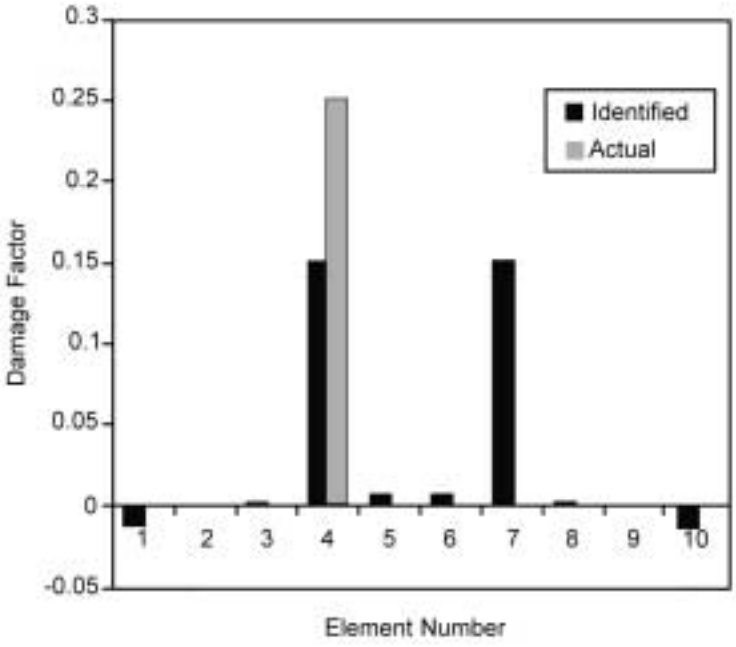

Figure C.5 Identified and actual damage in a girder with damaged element No.4

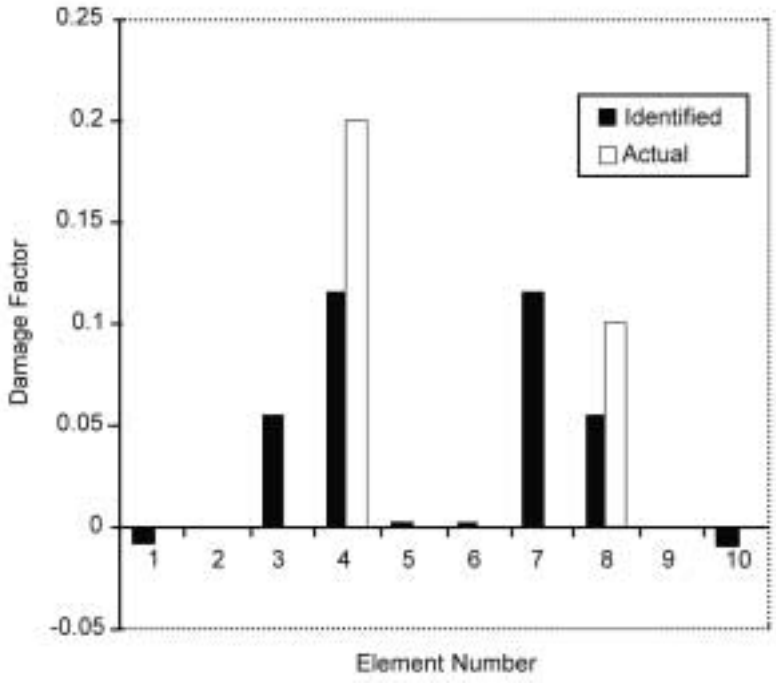

Figure C.6 Identified and actual damage in a girder with damaged elements Nos. 4 and 8

Next, assume that both elements 4 and 8 have suffered damage. As a result the stiffness of element 4 has been reduced by 20 percent and that of element 8 has been reduced by 10 percent. The altered eigenvalues are shown in Table C.5. The damage is identified by ignoring the inequality constraints and using Equation C.21. The predicted and actual damage is compared in Figure C.6. Again, because of symmetry, the identification algorithm predicts damage in elements 4 and 8 as well as elements 3 and 7. The predicted damage in each of elements 4 and 7 is 11.57 percent while that in elements 3 and 8 is 5.48 percent. If elements 3 and 7 were constrained to have zero damage, the predicted damage in element 4 would be 23.14 percent, against the actual value of 20 percent. Similarly, the predicted damage in element 8 would be 10.96, against the actual value of 10 percent.

In this example, we have ignored the inequality constraints placed on β. However, the results obtained show that β is less than 1 in all cases, satisfying one of the constraints. In a few cases, β is negative, implying an increase in the stiffness of the corresponding element. This is, of course, not realistic, but the negative values of β are quite small in magnitude and may be ignored. In many cases better estimates may be obtained by enforcing all of the inequality constraints. This can be achieved by using any one of the many algorithms available for the solution of constrained quadratic nonlinear optimization problems. The computer software, Matlab, offers several routines for this purpose.

ISIS CANADA RESEARCH NETWORK

PUBLICATIONS ORDER FORM

ISIS Canada was created to provide civil engineers with smarter ways to build, repair, and monitor structures using high-strength, non-corroding fibre reinforced polymers and fibre optic sensing systems. It was created by the federal Network of Centres of Excellence (NCE) program and encompasses 14 universities, 30 Project Leaders, 275 researchers, 100 associated organizations and 45 multidisciplinary demonstration projects.

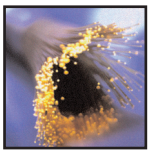

Manual No. 1

Installation, Use and Repair of Fibre Optic Sensors

Prepared as an installation and repair resource primarily for civil engineering applications, this manual covers the use of fibre optic sensing technology in structures. In Canada, innovative remote monitoring field applications have been demonstrated with sensors imbedded in new concrete structures, in reinforcing tendons, and attached to existing structures in composite fibre overwraps. Drawing on expertise gained in the research laboratory and several field installations, the manual provides an overview of basic FOS concepts and goes into the finer details of specific applications in composite laminates, concrete repair and new structures.

Manual No. 2

Guidelines for Structural Health Monitoring

Structural health monitoring (SHM) is used to accurately and efficiently monitor the in-situ behaviour of a structure, to assess its performance under various service loads, to detect damage or deterioration, and to determine the structure's conditions or health. While this manual focuses primarily on bridge applications (case studies of nine bridges and one wharf are covered), the concepts are applicable to civil engineering structures in general. This manual covers the benefits of SHM for those who are not fully initiated. It also serves as a guide for engineers who wish to become more knowledgeable and involved with the various aspects of SHM.

Manual No. 3

Reinforcing Concrete Structures with Fibre Reinforced Polymers (FRPs)

This manual provides guidelines and equations to be used in designing new FRP-reinforced concrete structures. While the equations are not part of national or international codes, they are based on research carried out in Canadian and international university laboratories and institutions and validated in several operational field applications, of which four are described in the manual. An introduction to FRP reinforcing products and their material properties is included for the uninitiated while the detailed design process is covered for those wishing to apply this new technology.

Manual No. 4

FRP Rehabilitation of Reinforced Concrete Structures

FRP rehabilitation projects in Canada have included column and beam strengthening, seismic retrofitting, repairing corrosion-damaged beams and columns, as well as numerous structural components. This manual presents the varied design procedures that have been developed and validated through several field applications. The basic equations and methodology are presented and case studies used to illustrate procedures. Before FRPs become routinely employed as everyday solutions for structural strengthening and repair challenges, codes of practice must be readily available. The guidelines and design equations contained in this manual are the result of extensive investigation, and as such, are a Canadian contribution to the global effort to formulate appropriate codes.

Manual No. 5

Prestressing Concrete Structures with Fibre Reinforced Polymers (FRPs)

Innovative structures based on the use of FRPs will allow new design concepts, and are expected to attain longer service lives than structures built with conventional materials. This manual provides engineers with guidelines that can be used in the design of normal density concrete components prestressed with CFRP, AFRP, and GFRP tendons in buildings and bridges. This document is not a part of a national or international standard, but can be used to assist in the development of such documents. It is based mainly on experimental results of research, analytical work and field applications of FRPs used as prestressed reinforcement which has been carried out in Canadian and other international university laboratories and institutions.

Manual No. 6

Civionics Specifications

Civionics is a new term coined from Civil-Electronics, which is derived from the application of electronics to civil structures. This manual provides guidelines for fibre optic sensors and their ancillaries based on extensive experience gained in numerous field installations. As the design and construction of civil structures continues to evolve, it is becoming imperative that these structures be monitored for their health. The entire structural health monitoring (SHM) process, beginning with system design and concluding with data collection, is addressed in this manual. The Civionics specifications include the technical requirements for the SHM system including fibre optic sensors, cables, conduits, junction boxes and the control room.

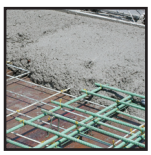

Product Certification

Specifications for FRP Product Certification of FRPs as Internal Reinforcement in Concrete Structures

This manual provides specifications on using fibre reinforced polymers (FRPs) as internal reinforcement in concrete components of structures such as bridges, buildings and marine structures. In the form of bars and grids,the fibres include glass, carbon and aramid fibres, and matrices include isophthalic polyester, vinylester and epoxy resins. Specifications for manufacturing, classification, qualification testing, quality control and assurance tests, manufacturer's quality control tests, reporting and certification and handling and storage are included in the document.

Durability Monograph

Durability of Fibre Reinforced Polymers in Civil Infrastructure

FRPs (fibre reinforced polymers) are becoming more common in replacing steel as a material of choice in both rehabilitation and construction. This set of guidelines was created for the design and construction industry regarding material and bonding selection for various applications to ensure durability of the construction facility. The monograph addresses all the key issues surrounding the use of FRPs for civil applications including numerous production techniques such as filament winding, pultrusion, resin, transfer molding, contact molding, and compression molding, and also addresses the influence of various inert or active additives added to the polymeric phase such as fillers, plasticizers, stabilizers, and sizing and other coatings placed on fibres.

Order Form

Fax to: 204. 474. 7519
Online at: www.isiscanada.com
Email: Charleen Choboter, Financial & Administrative Assistant at **choboter@ms.umanitoba.ca**

Customer Information

Last Name (Please Print) | First Name

Company Name

Address

City | Province/State

Postal Code/ZIP | Country

Phone | Fax | Email

Payment Method

☐ Mastercard ☐ Visa ☐ AMEX ☐ Cheque / Money Order

Card No. | Expiry Date

Order Form

Manuals are $100 per copy for all formats. Price is in Canadian dollars with 5% GST included.
GST #86790-2868

Number and Title		Format		Quantity	Price	Total
No. 1	Installation, Use & Repair of Fibre Optic Sensors	☐ Book	☐ Download*		$100 ea	
No. 2	Guidelines for Structural Health Monitoring	☐ Book	☐ Download*		$100 ea	
No. 3	Reinforcing Concrete Structures with Fibre Reinforced Polymers (FRPs)	☐ Book	☐ Download*		$100 ea	
No. 4	FRP Rehabilitation of Reinforced Concrete Structures	☐ Book	☐ Download*		$100 ea	
No. 5	Prestressing Concrete Structures with FRPs	☐ Book	☐ Download*		$100 ea	
No. 6	Civionics Specifications	☐ Book	☐ Download*		$100 ea	
PC	Specifications for FRP Product Certification of FRPs as Internal Reinforcement in Concrete Structures	☐ Book	☐ Download*		$100 ea	
DM	Durability of Fibre Reinforced Polymers in Civil Infrastructure	☐ Book	☐ Download*		$100 ea	
					Grand Total	

* To purchase an e-book version for downloading, fax order form and payment details to ISIS Canada. Instructions will then be sent to you via email.

Orders will not be shipped until payment is received.

Delivery Options (check one)

- Ship by regular mail (included in manual price) ☐
- Ship by express delivery (not included in manual price. Call or email for quote) ☐

ISIS CANADA RESEARCH NETWORK
Intelligent Sensing for Innovative Structures A Canadian Network of Centres of Excellence
A250 Agricultural & Civil Engineering Building, 96 Dafoe Road, University of Manitoba,
Winnipeg, Manitoba R3T 2N2 Phone: 204. 474. 8506 Fax: 204. 474. 7519
www.isiscanada.com